UNIVERSITY OF PAVIA – IUSS SCHOOL FOR ADVANCED STUDIES PAVIA

Department of Brain and Behavioral Sciences (DBBS)
MSc in Psychology, Neuroscience and Human Sciences

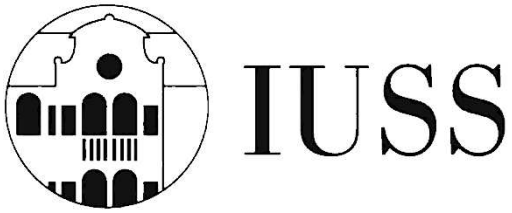

Effective brain connectivity explains causal interactions between the cerebellum and visual areas during a visual-attentive task in developmental dyslexia and typical readers

Supervisors:
Prof. Claudia Gandini Wheeler-Kingshot
Co-supervisors:
Prof. Fulvia Palesi
Dr. Gökçe Korkmaz
Prof. Sara Mascheretti

Thesis written by
Tea Tucić

Academic year 2023/2024

Contents

Table of Figures

Abstract

Developmental dyslexia (DD) is a neurodevelopmental disorder marked by persistent reading difficulties. While previous neuroimaging studies have revealed alterations in the functional connectivity of the ventral attention network (VAN) and cerebellum in DD, the effective brain connectivity of those networks remains understudied in DD.

Dynamic Causal Modelling (DCM), a Bayesian framework, can estimate the direct causal influences (effective connectivity) and the hierarchical organization of activations in different brain regions. Here, for the first time, DCM was employed on functional magnetic resonance imaging (fMRI) data obtained by a visual-attentive tasks to investigate effective connectivity within the cortico-cerebellar visual attention network in typical readers (TR) and individuals with DD. To assess attention networks, twenty participants of TR and twenty participants of DD underwent fMRI while performing full-field sinusoidal grating and coherent motion sensitivity tasks. The investigated visual attention network included: left and right Crus I of the Cerebellum, left and right middle frontal gyrus, left and right middle visual temporal area, and bilateral primary visual cortex. Four different DCM models were specified and estimated to study effective connectivity patterns in two groups. Group-level analysis used Random-Effect Bayesian Model Selection to compare multiple DCM models, aiming to find the best explanation for the neuroimaging data and select the best-fitting model for each group.

Results revealed differential effective connectivity patterns between the two groups, indicating altered organization of the VAN and cerebellar involvement in DD. Specifically, while the TR group exhibited right-lateralized VAN connectivity, the DD group displayed compensatory connectivity patterns.

The present study contributes to our understanding of the neural mechanisms underlying developmental dyslexia and highlights the importance of investigating effective brain connectivity in neurodevelopmental disorders to open new insights for diagnostic and therapeutic approaches.

Keywords: Developmental dyslexia, Dynamical Causal Modeling (DCM), functional magnetic resonance imaging (fMRI), cerebellum, ventral attention network

1 Developmental Dyslexia

Developmental dyslexia (DD) is a neurodevelopmental disorder, and although it has been well-researched it remains challenging to define it due to the lack of consensus on its causes. However, in broad terms,DD can be defined as difficulty in fluent word recognition and spelling despite intact sensory abilities, average intelligence, and educational opportunities (Peterson & Pennington, 2012).

Cases of lost reading abilities and difficulties were described for the first time in the late 1800s by German physician Adolf Kussmaul (Kuerten et al., 2020). He described reading deficits in stroke patients with intact oral and non-verbal reasoning skills. The concept of Dyslexia was introduced a few years after that by Rudolph Berlin to name those deficits (Stein, 2018). Today, these cases would be classified as acquired dyslexia, a reading disorder that occurs due to brain injury or lesions in individuals who previously had normal reading skills (Kuerten et al., 2020). In 1896 Pringle Morgan described a case of "congenital word blindness" in a child who found it impossible to learn to read, despite otherwise normal mental capabilities (Warnke et al., 2012). Therefore, this can be considered a first-described case that aligns with what can now be classified as DD. Moreover, the idea of congenital word blindness as a visual processing problem selectively targeting written words was further developed in the upcoming years. Therefore, until the mid-20th century, DD was considered as an inherited impairment that primarily impacted the visual processing of words, while leaving oral language and non-verbal reasoning abilities relatively unaffected (Stein, 2018).

Unlike spoken language, which most children acquire spontaneously, reading has to be explicitly taught (Stein, 2022). However, around 10% of children experience great difficulties in acquiring reading (Bertoni et al., 2019). Percentages of affected children can vary across languages. For example, it has been estimated that this neurodevelopmental disorder has a higher prevalence in the United States than in Italy (Lindgren et al., 1985). Moreover, twin and family studies suggest a high heritability of dyslexia. In that manner, although there are identified candidate genes associated with DD and replicated in at least one independent sample, such as *DYX1C1*, *DCDC2*, *KIAA0319*, *FOXP2, C2ORF3, MRPL19, ROBO1, GRIN2B,* and *CNTNAP2*(Mascheretti et al., 2017), it is still not possible to identify a single responsible gene (Stein, 2022). In addition, DD has common comorbidities with attention-deficit hyperactivity disorder (ADHD), language impairment, and speech sound disorder (Peterson & Pennington, 2012).

The first theories of causes of DD assumed visual deficits as the main cause, however today it is clear that primary visual functions are not the ruth of the difficulty (Smirni et al. 2020). Morton and Frith (1995) proposed three possible levels of explaining DD that are behavioral, cognitive, and biological. Clinicians mainly use the behavioral level to diagnose dyslexia based on specific behavioral manifestations. On the other side, important understandings come from the cognitive level which links the causes of dyslexia to deficiencies in information-processing mechanisms (Kuerten et al., 2020). Explanation of DD on the cognitive level includes several theories about deficits in short-term or working memory, phonological awareness, incomplete automatization, and slow processing (Kuerten et al., 2020).

Researchers today are more prone to consider DD a multi-componential and complex disorder (Smirni et al. 2020; Pennington, 2006). In recent years, more attention has been put on the biological level and neural processes underlying DD. Many theories of underlying neuronal processes and causes have been proposed incorporating the importance of visual attention, and cerebellum functions for DD. Additionally, even though the cognitive and behavioral levels of clinical evaluations and tests are of great importance for diagnosing DD and understanding some psychological aspects, more is needed to gain the whole picture of the etiology and mechanisms of this reading disorder. For that reason, investigation of the neurobiological basis as well as the functional and effective organization of brain connectivity is crucial for further understanding and treatment of DD. Importantly, all three levels of explanation are equally significant and efforts on understanding the relation and causality between them should be made in future research.

1.1 Neural basis of Developmental dyslexia

Reading is a complex cognitive function unique to humans and in modern societies, it is considered to be a fundamental skill that each individual is expected to acquire. However, written language was invented only around 6000 years ago, much later compared to spoken language (Stain, 2022). Consequently, the human brain did not develop reading-specific regions. Reading is thus processed by various distinct brain areas whose primary roles are other evolutionary older functions. In that sense, several theories have been proposed that attempt to explain the underlying causes and complexity of DD.

According to one of the theories that have been proposed, *the phonological theory*, children with DDstruggle to acquire reading skills due to difficulties in developing phonemic awareness and the skill of separating the sounds within a word and matching them with their corresponding visual letters (Stein, 2018). Indeed, studies commonly show disruption in the left hemisphere language network in DD (Peterson & Pennington, 2012). However, reading is both a linguistic and a visual task (Valdois et al., 2019). Therefore, not only the regions for linguistic or phonological processing are affected in DD, but also visual areas. Moreover, the visual processing of words precedes phonological analysis, and thus often deficient visual processing is the cause of a reading problem. This deficiency extends to other critical visual processes involved in acquiring reading skills, such as sequencing letters, which demands timing or temporal processing (Stain, 2022). One specific type of cell plays animportant role in temporal processing, that is magnocellular (M) cells, large neurons found in the retina and further throughout the brain (Stain, 2018a). These M neurons form one of the two distinct visual pathways, the magnocellular (M) pathway. The second visual pathway, made primarily of Parvocellular (P) neurons, is known as the Parvocellular (P) pathway (Vellutino et al., 2004). M neurons mainly convey information about movement, but they are not involved in color and detail processing (Stain, 2018a). In more detail, as shown in Figure 1.1, from the retina the axons of the M neurons project to the magnocellular layers of the lateral geniculate nucleus (LGN) which is the main relay in the thalamus responsible for the parallel of processing visual information between the retina and the visual cortex (Mascheretti, 2021). On the other hand axons of P neurons project to the parvocellular layer of LGN. Further, from LGN M and P pathways project partially segregated to and beyond the primary visual cortex (V1). From V1 these pathways further separate in dorsal and ventral visual streams. Specifically, M neurons form the dorsal pathway with a key role in directing visual attention

and controlling eye movements during reading, while P neurons constitute the ventral pathway mainly carries information about details and colors (Stain, 2018a).

The dorsal and ventral streams are two major pathways in the visual system, each serving distinct functions in processing visual information. The dorsal stream is primarily associated with tasks involving spatial perception, motion detection, depth perception, and visually guided actions like reaching and saccades. In contrast, the ventral stream is responsible for object recognition and perception (Vidyasagar, 2010). The dorsal stream is also known as the "where" pathway, while the ventral stream is known as the "what" pathway (Stain, 2018b). As the dorsal stream mainly consists of M cells it is considered blind to colors and that it instead processes contrast differences, low spatial frequencies, high temporal frequencies, and both real and illusory motion (Gori et al., 2015). The dorsal pathway projects via the middle temporal or 'motion' area (MT/V5) to the posterior parietal cortex, and then to the prefrontal cortex (Stain, 2018b). Taking into consideration that V5 receives most of its input from M neurons (Vellutino et al., 2004), this brain region is considered to be sensitive to motion. Moreover, functional Magnetic Resonance Imaging (fMRI) studies show decreased activation in V5/MT while watching moving patterns in DD (Stein, 2022). An example of visual pathways and dorsal and ventral visual streams illustration can be seen in Figure 1.1 below.

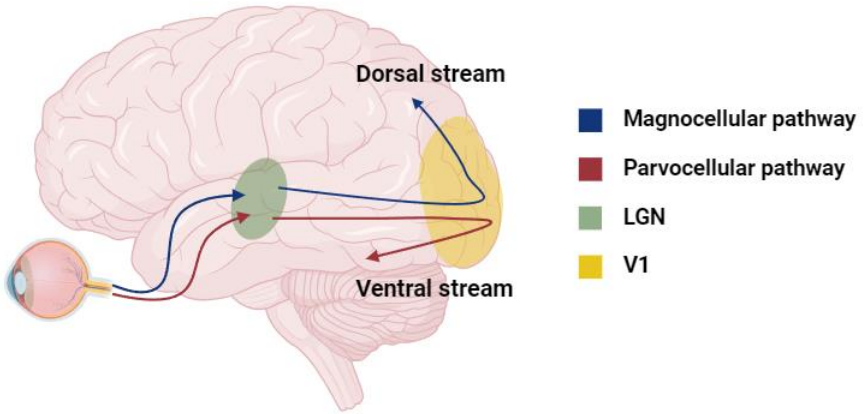

Figure 1.1 Visual pathways. *The Parvocellular and Magnocellular pathways from the retina reach the separate layers of the Lateral Geniculate Nucleus (LGN). Further, they project to the Primary visual cortex (V1) and form there dorsal and ventral visual streamsare formed (Mascheretti et al. 2021).*

While the role of the visual system in dyslexia is still a topic of ongoing research and debate several theories highlight the potential importance of understanding visual processing

differences in individuals with dyslexia. Furthermore, addressing visual processing deficits, particularly those related to the dorsal stream, may be important for developing effective interventions for dyslexia (Pellicano& Gibson, 2008). Indeed, evidence indicates a connection between motion sensitivity and the dorsal visual stream in DD. DD is frequently associated with challenges in visual motion processing, which might be related to abnormalities or impairments in the dorsal visual stream, particularly the magnocellular pathway (Talcott et al., 2000). One's motion sensitivity can be tested by measuring the minimum number of randomly moving dots on a screen that must move in the same direction, for an observer to be able to tell their overall direction of motion. This task is known as a coherent motion sensitivity detection task (Cornelissen et al.,1998). Previous studies showed lower sensitivity to motion in DD, as well as lower activation in V5 (Eden et al., 1996).

Based on the important role and characteristics of the magnocellular system in temporal processing and motion processing, the *magnocellular theory of developmental dyslexia* has been proposed. Particularly, it suggested that poor readers have a weak magnocellular function. Moreover, a connection can be made between poor reading skills and weaker magnocellular sensitivity, while such a relation is not observed with P neurons (Stein, 2018). Also, it has been suggested that in DD, M neurons are smaller compared to typical raiders, thus they sample moving stimuli at a lower spatial resolution and could be the main factor contributing to their reduced sensitivity to motion (Stein, 2003). The visual magnocellular system plays an important role in eye movements, visual search, and directing attention (Démonet et al., 2004). Moreover, M deficiency leads to the slower and less accurate deployment of visual attention (Vidyasagar, 2005). Attention deficits in dyslexia expand beyond the strictly magnocellular pathway and it involves broader attention networks of the brain which will be further addressed in the next section.

1.2 Visual Attention in Developmental Dyslexia

Visual attention can be defined as a filter that limits the number of information that the visual system can process, in other words, it determines which information that reaches the retina can be processed by higher cortical areas involved in visual processing (Steinman et al., 1996). Visual attention relies on the orienting component of the attention system which is composed of both the dorsal attention network (DAN) and ventral attention networks (VAN) (Petersen & Posner, 2012). While reading, rapid orienting of visual attention is necessary to accurately select relevant letters from irrelevant and cluttering letters before the process of letter-to-speech sound integration begins (Franceschini et al. 2012). Hence, visual attention networks may play a significant role in reading (Shaywitz&Shaywitz, 2008). For example, a longitudinal study done by Valdois and colleagues (2019) showed that visual attention span before literacy can predict reading fluency one year later, at the end of the first grade.

The DAN is organized bilaterally, with the intraparietal sulcus and frontal eye field as main nodes (Vossel et al., 2014) and it is mainly responsible for orienting attention in space and helps maintain spatial maps, saccade planning, and visual working memory (Freedman et al., 2020). On the other hand, the VAN is considered more literalized, mainly including regions in the right hemisphere (Vossel et al., 2014). The main regions comprising VAN are the temporoparietal junction (TPJ) and ventral frontal cortex including the middle frontal gyrus (MFG). Moreover, VAN is involved in spatial reorienting of attention to an unattended location, and directing attention to behaviourally relevant sensory stimuli that are outside the focus of processing (Corbetta & Shulman, 2002). Additionally, based on the lesions of the frontal lobes, it has been concluded that these regions have an important role in guiding visual attention (Stein, 2003). Therefore, VAN may play a crucial role in reading by directing attention to external stimuli and then shifting it back to internal processes, such as teasing the meaning from the written words (Freedman et al., 2020). The MFG has been suggested as a region that is involved in this shift and acts as a convergence point by interrupting ongoing internal attentional processes in the dorsal network and redirecting attention toward external stimuli (Japee et al., 2015). In addition, although the cerebellum is traditionally associated with motor coordination, balance, and motor learning, it is increasingly recognized for its role in various cognitive functions, including attention (Brissenden & Somers, 2019). Particularly, findings suggest that the cerebellum plays a role in directing visual attention (Courchesne et

al., 1994), and impairments of this region have been associated with symptoms of DD. The role of the cerebellum in DD will be explained in more detail in the following section.

M cells and magnocellular deficiency can also lead to slower and less accurate deployment of visual attention (Vidyasagar, 2005). For example, Steinman and colleagues (1997) suggested that visual attention is more evoked by luminance contrast stimuli which primarily activate M visual pathways and concluded that activation of the M pathway has an important role in triggering visual attention. Thus, an impaired magnocellular system in DD can contribute to attention deficiencies in DD.

In conclusion, attention could be a vital component in reading and thus in reading difficulties as a result of dysfunctions in VAN, M pathway, and cerebellum. Moreover, the MFG could be one of the regions responsible for attention-shifting deficits observed in DD, and the cerebellum should also be considered as one of the key regions that should be investigated to understand cortico-cerebellar involvement in the guidance of visual attention.

1.3 Cerebellar Involvement in Developmental Dyslexia

For a long time, the cerebellum was considered to have a role mainly in motor functions, however, in more recent years it has been established that the cerebellum has a role in various cognitive functions including attention and language (Schmahmann& Caplan, 2006). Additionally, it is believed now that the main function of the cerebellum is computing "internal models" dependent on inputs not only from motor components but also visual systems (D'Angelo, 2011). In particular, these internal models not only serve the function of motor control and movement but cognitive functions as well (Stein, 2023). Since the role of the cerebellum in dyslexia is still an area of active research, several theories have been proposed to understand the extent of its involvement and its implications for the development and treatment of dyslexia. One of the theories, the *cerebellar deficit theory of developmental dyslexia,* has been proposed by Nicolson and Fawcett (1990). This theory brings to light that behavioral and functional data suggest the majority of dyslexic children suffer from abnormal cerebellar function (Nicolson et al., 2001). Furthermore, it explains the full range of deficits, thus both the problems in reading and additional symptoms of DD like bad handwriting, laborious learning, and visual sequencing.

One of the most prominent symptoms of DD is the failure to acquire and automatize reading and writing (Norton & Wolf, 2012). Further, these impairments of automatization in dyslexia have been associated with cerebellum dysfunction (Démonet et al., 2004). Nicolson, Fawcett, and Dean (2001) proposed a possible causal chain of cerebellar dysfunction on reading and writing skills that is summarised in Figure 1.2. This model links cerebellar dysfunction with phonological processing, motor skills, and problems with automatization. Additionally, attention difficulties in DD can be incorporated into the cerebellar hypothesis due to poor automatization (Démonet et al., 2004). Given that the cerebellum receives input from the magnocellular system for timing and sequencing, it can be said that it is influenced by the broader dysfunction observed in magnocellular processing (Stain 2001). In addition to that, the cerebellum also plays an important role in eye movement control and attention required for reading. Particularly, Allen and colleagues (1997) demonstrated that attention tasks alone are sufficient for the activation of the cerebellum, and thus provided proof of its important role in attention.

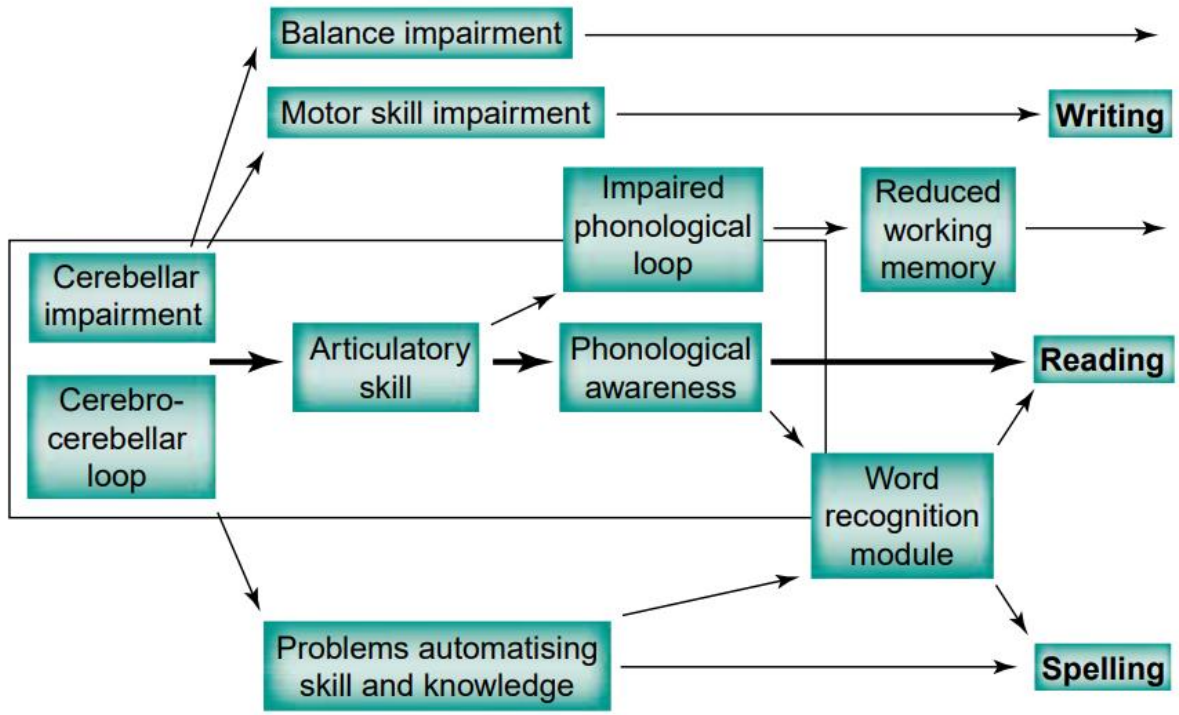

Figure 1.2. Hypothetical chain of cerebellar effect on reading, writing, and spelling skills. *Processes highlighted in the box representabnormalities in the cerebellum present birth resulting in mild motor and articulatory problems. These articulatory challenges lead in turn to a limited representation of the phonological characteristics of speech which subsequently manifests as phonological awareness difficulties around the age of 5 that lead to subsequent problems in learning to read. Outside of the highlighted box are represented other routes that highlight probable problems outside the phonological domain, and indicate that the difficulties in learning to read, spell, and write might be the result of several inter-dependent factors (Nicolson et al., 2021).*

In summary, the cerebellum plays a key role in explaining deficits in DD. It affects the automatization of skills, guidance, and shifting of attention through eye movement control. Moreover, it is frequently found under-activated in DD in both reading and non-reading tasks (Nicolson et al., 2001).

1.4 Brain Connectivity in Developmental Dyslexia

As reading requires multiple distinct brain regions, such as areas within the left hemisphere comprising the temporal, parietal, and frontal lobes (Cattinelli et al., 2013), and DD seems to be a multi-componential reading disorder, brain connectivity should be considered an important aspect for a better understanding of the underlying mechanisms and causes of this disorder.

Studies suggest that functional brain connectivity is altered in DD. For example, Fin (2014) and colleagues found divergent functional connectivity within the visual pathway and between visual association areas and prefrontal attention areas compared to typical readers. Further, Schurz et al. (2015) found reduced functional connectivity between the left posterior temporal areas and the left inferior frontal gyrus as well as different connectivity patternsin the default brain network in dyslexia. Also, effective brain connectivity can also provide us with valuable insights by explaining causal relationships between brain regions. In the last years, increased interest in effective connectivity in dyslexia has occurred, however, more effective connectivity studies are needed to further explore how the dyslexic brain functions compared to the typical reading brain. Morken and colleagues (2017) using Dynamical Causal Modeling (DCM) found differences in connections going to and from the inferior frontal gyrus and the occipitotemporal cortex in theDD group compared to the typical reading group. Additionally, Di Pietro et al. (2023) found altered feedback connectivity between the inferior parietal lobule and the visual word form area in word processing in the DD group compared to both age and reading level matched typical readers group.

Existing effective connectivity studies in DD typically include the arias of the occipitotemporal cortex, parietal regions, and frontal regions such as the inferior frontal gyrus (Cao et al., 2008; Morken et al., 2017; Di Pietro et al., 2023; Turker et al., 2023). However, to our knowledge, no studies have yet explored effective connectivity between the cerebellum and parts of the visual attention network, more specifically the MFG in DD. The present study aims to address this gap.

1.5 Genetic Components of Developmental Dyslexia

DD is a heritable disorder, and family history is one of the most important risk factors (Shaywitz&Shaywitz, 2005). However, considering that reading is, in an evolutionary sense, a relatively new skill humans acquired it is unlikely special genes have evolved for reading. Therefore, DD likely involves the interaction of several genes (Stein, 2019). Moreover, it has been observed that an individual's risk of being affected by DD is increased if other family members are already affected (Scerri & Schulte-Körne, 2010).

Six genes have been proposed as potential contributors to DD (Peterson & Pennington, 2015), four of which are associated with a genetic system crucial for axon growth and neuronal migration during prenatal brain development affecting normal connectivity patterns (Smirni et al., 2020). Those identified genes are *C2Orf3*, *MRPL19* and *DYX1C1*, *KIAA0319*, and *ROBO1* involved in axon growth and neuronal migration. However, identifying the specific genetic variations that impact dyslexia remains challenging (Fisher & DeFries, 2002) considering the high comorbidity of DD with other neurodevelopmental disorders (Scerri & Schulte-Körne, 2010). Additionally, *DCDC2* has also been reported to take part in DD. This gene is related to several deficits in memory and auditory processing, as well as impairments in visual-spatial processing. Thus, *DCDC2* can play an important role in reading abilities such as reading accuracy and speed of reading (Riva et al., 2019).

2 Neuroimaging

2.1 Principles of Magnetic Resonance Imaging

Magnetic Resonance Imaging (MRI) is a powerful non-invasive imaging technique used in both clinical and non-clinical settings. Moreover, it can provide cross-sectional images in any arbitrary plane and give anatomical as well as functional information (Rayan, 1997). The invention of MRI was preceded by two important insights. In 1971 Damadian discovered different proton relaxation properties in normal and tumor tissues. This led to the development of Nuclear Magnetic Resonance (NMR), which allowed the exploitation of different proton relaxations to have better differentiation among tissues than already existing techniques provided. The next breakthrough was made in 1973 when Lauterbur invented spatial encoding. This concept allows the assignment of an NMR signal to a specific spatial position, which was a significant step toward modern MRI. In the following years, many improvements have been made, making MRI widely used and one of the preferred imaging techniques for examining the brain,both for disorders and healthy cases (Cercignani, Dowell & Tofts, 2018).

MRI is sensitive to the amount or density of protons or hydrogen (1H). The human body consists of about 60% water, and for the brain, that percentage goes up to 70, hence human tissue contains a large amount of 1H protons (Sands & Levitin, 2004). More specifically, MRI exploits the magnetic properties of 1H, due to which they act in the manner of compass in the magnetic fields (Rayan, 1997). Unlike other imaging techniques that are based on X-ray technology (e.g. Computed tomography (CT) and positron emission tomography (PET) scanning), MRI does not use ionizing radiation (Caverly, 2015). Ionizing radiation contains levels of electromagnetic energy enough to alter the structures of tissues, which can be dangerous for human health (Zamanian& Hardiman, 2005). Instead, MRI uses specific wavelengths of electromagnetic dynamics that lie in a spectrum of radio wave frequencies that cannot modify and damage tissues (Yoshioka, 2012). As a result, MRI can be considered as a safe method. Today MRI can be considered the gold standard for neurological diagnostic imaging (Bolas, 2016).

2.1.1 Physics of MRI

Magnetic Resonance is sensitive to the properties of 1H protons (Sharma, 2009). Protons are characterized by their positive electric charge and constant spinning around their own axis. Current made by spinning movements generates a magnetic field, making the proton behave in the manner of a small bar magnet (Gibby, 2005).

Magnetic properties of 1H can be described in terms of its intrinsic angular momentum (P) or spin, which explains how a proton behaves in the presence of the magnetic field. This property allows protons to change and react to external magnetic fields. Spin depends on the spin quantum number (I) specific for each nucleus. Further, the spin quantum number depends on the mass number, making the quantum number 0 for all the nuclei with an even number of protons. Additionally, the quantum number is quantized, meaning it can only assume specific desecrate values, and be equal to a number multiple of ½. Given the spin quantum number I for a nucleus, it can have an m number of spin states, which can go from I to $-I$ in steps of 1, as shown in equation 2.1. These number of states are linked to the energy states that a nucleus can assume in a magnetic field.

$$m = I, (I-1), (I-2), \ldots, -I \tag{2.1}$$

The intrinsic angular momentum or spin can therefore be mathematically defined as denoted in equation 2.2. In this equation, P is intrinsic angular momentum, I is the spin quantum number and h stands for Plank constant which indicates the relation between P and I.

$$P = h / 2\pi\sqrt{I(I+1)} \tag{2.2}$$

Further, we can define the dipolar magnetic moment of a nucleus (μ), which is proportional to the intrinsic angular momentum P through the gyromagnetic constant gamma, as indicated in equation 2.3. The gyromagnetic constant gamma defines the behavior of a nucleus in a magnetic field, and it is specific for each nucleus.

$$\mu = \gamma\, P \tag{2.3}$$

However, in MR imaging we are not interested in the spin of the individual proton, but in the average behavior of all protons in the sample. The overall response of the system, for example of the tissue in the brain, is given by the magnetization (M), which represents the sum of all dipolar magnetic moments in the given sample. Magnetization M is the vectorial sum of all dipolar magnetic moments per unitary volume as stated in equation 2.4

$$M = \frac{1}{V}\sum \vec{u_i} = 0$$

2.4

To exploit these properties of protons, an external magnetic force is needed. The external magnetic force used for MRI is usually referred to asB_0. B_0 is constant and it has the magnitude and direction. As already mentioned, 1H electromagnetic properties allow us to think about it as a bar magnet with a north and south pole.

When it is absent the orientation of the dipolar magnetic moment (μ) is random and thus the sum of all spins is zero, making the Magnetization M alsozero. However, when the external magnetic field is present, spins align with the direction of it and start procession. Precession of protons around $B_0$is happening at the specific speed known as Larmor frequency which is directly proportional to the strength of the external magnetic field.

$$\omega_0 = \omega_L = \gamma_0 \cdot B_0$$

2.5

In Larmor frequency equation is indicated above (equation 2.5) which represents Larmor frequency (ω_L), the gyromagnetic ratio (γ_0), a constant specific to a particular proton, and the strength of the external magnetic field (B_0).

In this precession, 1H orients either parallel or anti-parallel to the B_0 as illustrated in Figure 2.1 below. Parallel orientation is described as low energy, thus slightly more protons align parallel to the direction of B_0. This excess of spins in the lower energy state results in the positive magnetization around B_0.

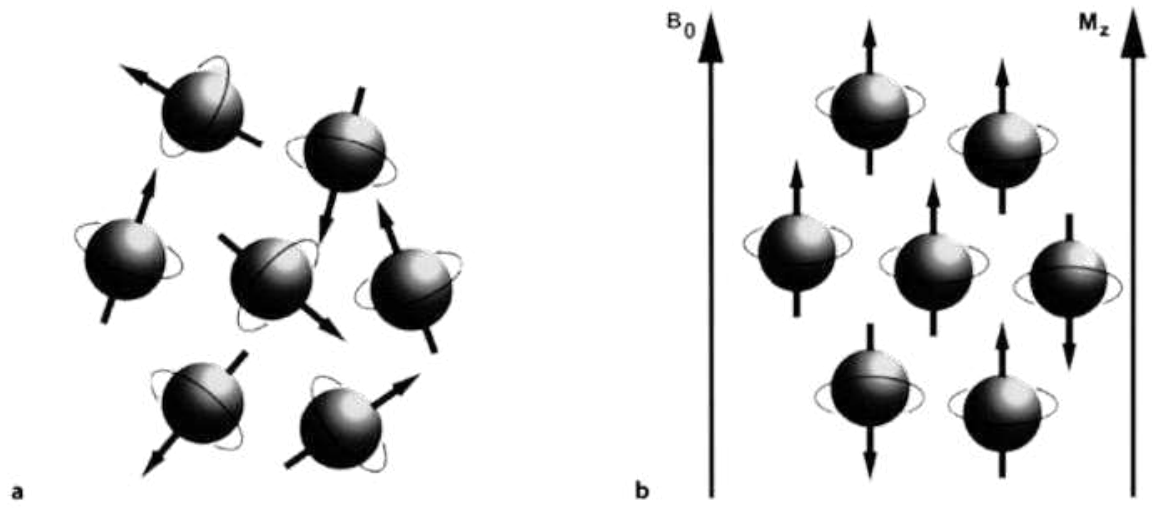

Figure 2.1 Spin axis alignment. ***(a)*** *In the absence of an external magnetic field, protons rotate around their axis in random directions.* ***(b)*** *In the presence of the external magnetic field B_0, there is an excess of spins parallel aligned with the main magnetic field B0, producing M0 (Weishaupt et al. 2006).*

Waiting long enough so that the system reaches its equilibrium, the magnetization reaches its maximum and we refer to it as Mz or M_0. Thus, the magnetization of spins will no longer be 0, since they are no longer randomly oriented, instead, a new value is formed as noted in equation 2.6

$$M = \frac{1}{V}\sum \vec{u_i} = M_0 \qquad 2.6$$

Mo is formed in the z plane, orthogonal to the B_0 magnetic field. In MR imaging the signal is obtained from the net magnetization, however, the magnetic field B_0 is 60,000 times stronger than the resulting magnetization (Weishaupt et al. 2006), making it impossible to measure the signal. To solve this problem, radiofrequency pulse using electromagnetic field B1(t) can be introduced through radiofrequency coils. Electromagnetic field B1(t) must have several important properties to be able to interact with net magnetization: it must oscillate at Larmor frequency, it must be applied orthogonally to B_0, and it must have a certain amplitude and duration that is enough to transfer energy to M0, moving it out of its equilibrium, making it rotate for 90 ° and move to transverse or xy plane as also shown in the figure 2.2 below.

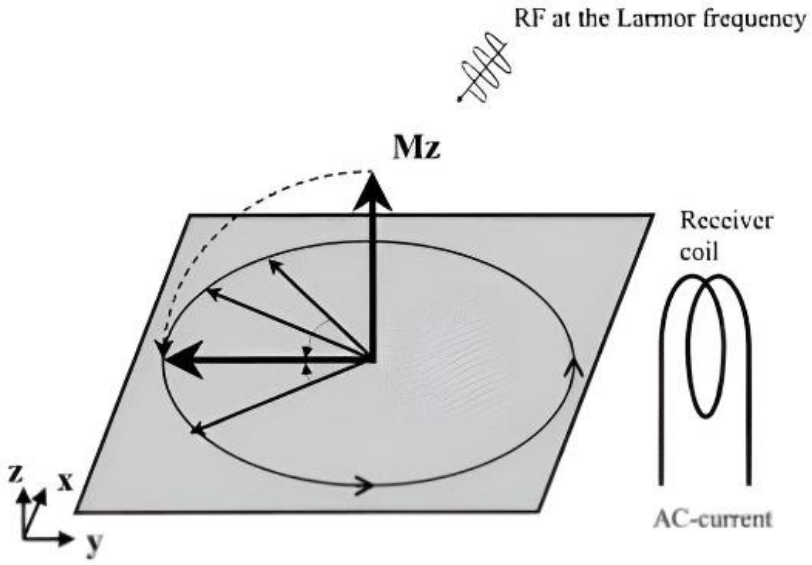

Figure 2.2 Effect of radiofrequency pulse. *When radiofrequency pulse at Larmor frequency is introduced to spins the net Magnetization, Mz flips for 90 ° and spins start precessing around B0 in the xy plane (Van Geuns et al, 1999).*

This process of energy absorption is known as an excitation of the spin system. As a result of excitation Mxy in the transverse plane is not in the perfect equilibrium, therefore over time Mxy goes back to the initial equilibrium of Mo and returns to processing around B_0.

2.1.2 Image reconstruction

The initial MR data acquired is raw data consisting of transversal components of magnetization after excitation sampled over time from receiver coils. The raw data can be represented as a matrix with several frequency components, commonly referred to as k-space. K-space is a mathematical area representing the spatial frequency information in two or three dimensions of the object (Moratal et al., 2008). It consists of two axes, the horizontal kx axis which represents frequency information, and the vertical ky axes with the phase information as represented in figure 2.3 below. Therefore, k-space covers both phase and frequency encoding data.

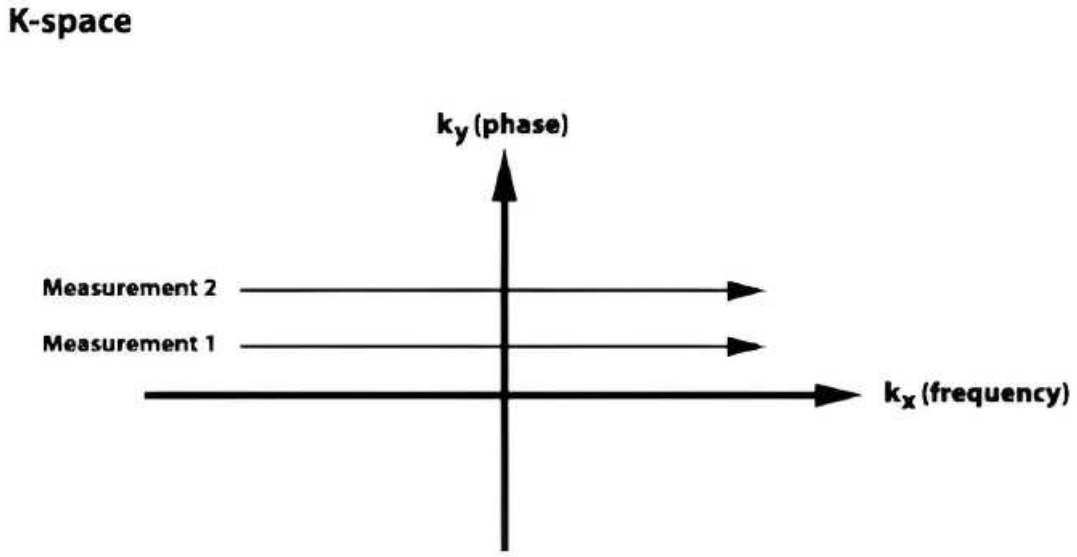

Figure 2.3 Illustration of the K-space.*K-space with two axes: ky axes contain phase information and kx axes contain frequency information. The data from each different measurement fills in the different horizontal lines of the k-space (Weishaupt et al., 2006).*

While the center of the k-space contains information on the borders andcontours of the image, the details are contained in the edges of the k-space. However, this raw data alone is not enough to form an image. To achieve this way to encode the various components of signal coming from different spatial positions is needed. MR provides MR echo, a complicated signal, containing already mentioned frequency and phase-encoded spatial information that contains necessary spatial information to construct an image. Every complicated signal can be rewritten and represented as a sum of a series of simple waves (Gallagher et al., 2008). Fourier transform is performed for these purposes. This

mathematical technique is used to decompose the measured MR signal into its frequency spectrum. It breaks down the MR signal into the sum of the sine waves with different frequencies, phases, and amplitudes (Weishaupt et al., 2006).

Spatial encoding implies three steps: slice selection, frequency encoding, and phase encoding. Three different magnetic field gradients are employed to perform these steps: *Gx* (frequency encoding or readout gradient), *Gy* (phase encoding gradient), and *Gz*(slice selection gradient). These gradients are applied to the main static magnetic field B0 resulting in position-dependent variations in frequencies encoded in the MRI signal. The frequency encoding gradient alters the main magnetic field by slightly changing local frequency causing a spatially specific pattern that allows the encoding of positions along the x-axis. On the other side, phase encoding is performed by briefly turning the phase encoding gradient on and off before the data collection period making some of the spin systems process faster than others depending on the spatial position along the gradient axis. Finally, the slice selection gradient is used to isolate specific slices or planes of image volume by introducing magnetic field variations along the z-axis. This gradient ensures that only the signals from the wanted slices during image reconstruction.

In summary, the grid, also known as k-space, is formed from the raw data by combining frequency, phase, and slice information. Each pixel in this grid corresponds to a specific combination of phase and frequency. Complex signal within k-space can be represented as a sum of simple waves using Fourier transform. This mathematical method is employed to analyze functions or signals by examining their frequency characteristics. It decomposes a function or signal into its fundamental frequencies allowing the creation of the MR image (Gallagher et al., 2008).

2.1.3 Relaxation

As discussed previously, the radiofrequency pulse B1 is a crucial component used to manipulate the spins of atomic nuclei in a magnetic field in order to measure the MR signal. B1 is essentially radiofrequency energy broadcasted at the right frequency so protons can absorb it and form transversal magnetization (Mxy). Transversal magnetization Mxy is not in the perfect equilibrium, after a certain amount of time it starts returning to the initial equilibrium state present before applying a B1 radiofrequency pulse inducing a signal in the receiver coil, known as *Free Induction Decay* (Brown et al., 2014). During this time, the phenomenon of relaxation is taking place. According to Brown and Semeka (2011), relaxation can be defined as a process in which protons release the energy, they absorbed from the radiofrequency pulse while returning to their original state of equilibrium. Two main mechanisms govern this process of return to equilibrium:

- Spin-lattice relaxation, the longitudinal relaxation constant
- Spin-spin relaxation, the traverse relaxation constant

As transverse magnetization decays over time, the longitudinal magnetization along z axes of the main static magnetic field B_0 gradually recovers. Restoration of the longitudinal magnetization is possible due to the exchange of energy between spins and the surrounding matrix or lattice. This process is known as longitudinal relaxation or T1 recovery alternatively referred to as Spin-lattice relaxation, reflecting the characteristic energy exchange mechanism. The time needed for magnetization Mz to return to equilibrium after it was perturbed with the B1 radiofrequency pulse is characterized by time constant T1. The T1 relaxation time is defined as the time needed for the system to recover to 63% of its equilibrium values after the B1 RF pulse (Sharma, 2009). Therefore, T1 can be represented as an exponential curve of the Mz growing back from 0 back to the M0. The T1 relaxation process is shown in Figure 2.4 below

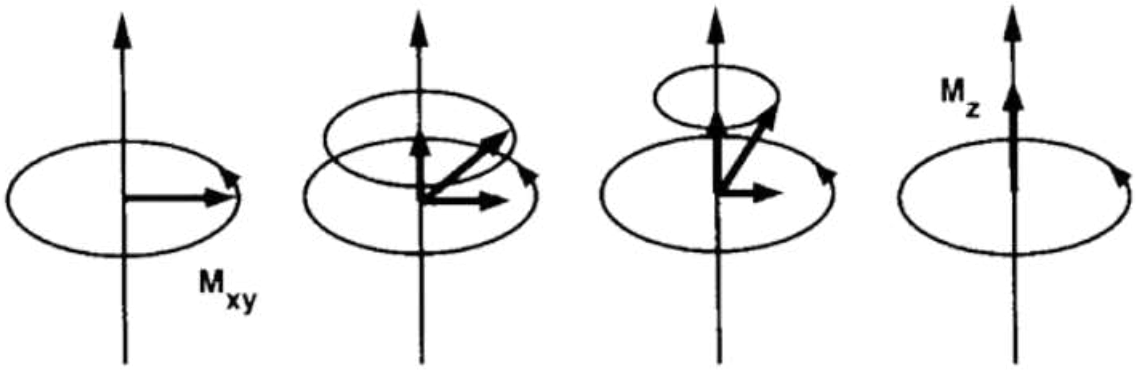

Figure 2.4 T1 relaxation. *Decay of transverse magnetization and regrowth of magnetization along the z-axes. (Weishaupt et al., 2006).*

It is also important to note that the exchange of energy is more efficient if there are more collisions between the spins and lattice, thus making longitudinal relaxation dependent on the microstructure of the tissue. Therefore, different tissue types have different T1 times.

Another process occurring in parallel with longitudinal relaxation is transverse relaxation. Transverse relaxation or T2 is the process of disappearance of transverse relaxation Mxy caused by the loss of phase coherence. This phenomenon is also known as spin-spin relaxation because of the dephasing of the spins caused by their interaction with each other. Unlike in T1, here energy is not exchanged with the surroundings, but among spins themself. Therefore, T2 relaxation can be defined as the time taken by the magnetization Mxy to decay to 37% of its initial value (Sharma, 2009).

When talking about T2, it is important to note that the coherence of spins is lost in two different ways. Dephasing occurs due to the pure spin-spin interaction independent of the strength of the external magnetic field. However, dephasing also occurs due to the inhomogeneities in the B0 caused by local variations of the Larmor frequency. These inhomogeneities contribute to the decay of the Mxy making the free induction decay faster than in the previously described dephasing. Time constant T2* (T2 star) is used to describe this mechanism and it is typically shorter than T2. Although T1 and T2 are independent processes they occur simultaneously. Both of them represent fundamental aspects of MR and are essential mechanisms for different image contrasts (Brown &Semeka, 2011).

2.1.4 Pulse sequences and different image contrasts

Tissues have three intrinsic properties contributing to the signal intensity or brightness on an MR image: proton density, T1, and T2 (Weishaupt et al., 2006). Different types of tissues differ in the mentioned properties, for example. Furthermore, with sequences, it is possible to control the influence of each of those three characteristics on the signal, thus differentiating tissues. Sequence controls radio frequency pulses B1 and magnetic field gradients, and therefore the generation of the signal. Two important sequence parameters dictate the time in which MR images are obtained:

- Repletion time (TR)
- Time Echo (TE)

TR is the interval between successive excitation pulses, and TE is the period between excitation pulse and MR data acquisition. By controlling these two sequence parameters it is possible to form the contrast of the image depending mostly on one of the tissue properties mentioned above (McRobbie, 2005). TR represents the duration of the relaxation period between two excitations and therefore a key component of the T1 weighted images. If the repletion time is short, the image will be mainly affected by the T1, as tissues with short T1 will regain most of the longitudinal during this interval and produce a stronger signal. Therefore tissues with short T1, in this case, would appear as bright in the MR image. In contrast, tissues with longer T1 would appear darker since they would not regain as much of the longitudinal magnetization in a given TR period. On the other hand, selecting a specific TE allows control over the T2 weighting of the image. Long TE ensures differentiating between tissues with short and long T2. Tissues with short T2 in the settings of long TE would appear darker since they already would lose most of their signal. On the contrary, tissues with long T2 would preserve more signal and thus appear brighter. Additionally, short TR provides better contrast and a lower signal-to-noise ratio (SNR), while longer TR results in a lower SNR. SNRis a quantity used to describe the effectiveness of an MRI system, it serves multiple purposes, including image quality assessment, contrast enhancement measurement, comparison of pulse sequences and RF coils, and overall system quality assurance (Dietrich et al., 2007).

Selecting a specific relationship between TE and TR allows obtaining images with different image contrasts, as shown in Figure 2.5 To achieve T1 contrast, meaning that T1 mainly

affects the properties of the image, along with short TR the short TE is also necessary to avoid the T2 effects. T1 weighed images provide excellent contrast between fluids, the gray and white matter of the brain, hence they are often referred to as anatomy scans (McRobbie, 2005). To obtain T2weighted images TR must be longer to avoid T1 weighting, and TE also must be longer to increase the effects of T2 weighting. In these images, fluids appear the brightest and other tissues darker. Therefore, T2 weighted images are often thought of as pathology scans, since they provide very good insight into abnormal fluid collection (McRobbie, 2005).

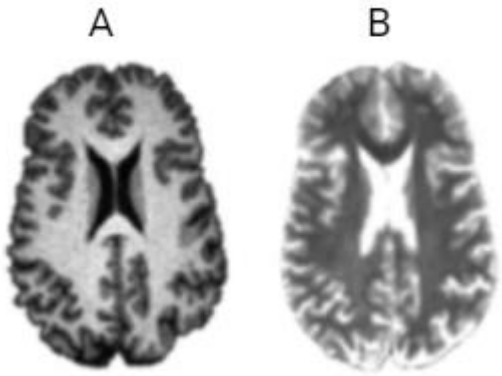

Figure 2.5 T1 weighted and T2 weighted images. *A - T1 weighted image; B - T2 weighted image (Ganzetti et al., 2015)*

2.2 Functional Magnetic Resonance Imaging

In the past, exploring the function of the brain and its regions was mostly out of reach. Although philosophers and scientists of those times had defined some theories and assumptions of a brain with different functions in distinct regions, establishing the function of specific anatomical areas relied mainly on rare cases of particular neural injuries. In recent years MRI has become the dominant imaging technique in neuroscience providing a non-invasive way to study and understand the anatomy of the brain (Lerch, 2017). Moreover, MRI can also provide an insight into the function of the brain relaying on the cerebral blood flow. Even though functional magnetic resonance imaging (fMRI) is a relatively new tool, the idea behind it is quite old, tracing back to the 1800s (Tsougos, 2017). Italian scientist Angelo Mosso was one of the first to make the connection between blood flow and brain activity while observing patients with skull defects (Sandrone et al., 2014). Today, fMRI is widely used in both clinical practice and research.

The fMRI uses MR imaging to map the cerebral hemodynamic changes occurring in the areas of increased brain activity (Bandettini, 2020). It is commonly used in research to trace brain activity caused by experimental stimuli or tasks (Chen&Glover, 2015) Additionally, fMRI can measure brain activity while participants are at rest providing valuable insights into intrinsic brain function that is calledresting-state functional connectivity or resting-state networks (Khanna et al., 2015). Therefore, the fMRI enables the reconstruction of brain activation patterns associated with various mental activities and the mapping of the brain regions in which they occur.

Further, this technique is nowadays commonly used in attempts to understand the mechanisms of brain connectivity and activation patterns in neurodevelopmental disorders such as developmental dyslexia (Vellutino et al., 2004). The fMRI is relatively easy to perform using already existing standard MRI scanners, it does not use exogenous contrasts and more importantly it does not involve ionizing radiation (Glover, 2011). These characteristics make the fMRI more accessible for use and more adequate for studies involving children compared to some other neuroimaging techniques (e.g. positron emission tomography) (Casey et al., 2000).

2.2.1 Principles of fMRI

Increased neural activity creates increased demand for oxygen which is transported through the body by blood. Hence, increased brain activity would result in increased oxygen levels and consequentially increased blood flow. That's why the level of oxygen consumption, althoughit is an indirect measure, can be considered a good measure of brain activity (Goense&Debener, 2010). Furthermore, fMRI relies on this idea, measuring the oxygen level changes over time in response to the energy needs of activated neurons. Blood carries oxygen in hemoglobin, a metalloprotein molecule in red blood cells, which has two states with different magnetic properties: oxygen-bound and oxygen-unbound state (Tsougos, 2017). Oxygen bound state is also known as Oxyhemoglobin and it is diamagnetic, meaning it is weakly repulsed by magnetic fields. On the other hand, the oxygen-unbound state is called deoxyhemoglobin and it has paramagnetic properties thatmake it weakly attracted by magnetic fields (Heeger & Ress, 2002). While oxyhemoglobin does not change the local magnetic properties of the tissues, deoxyhemoglobin paramagnetic properties create the local inhomogeneities of the magnetic field by causing the dephasing and reduction in T2* based signal (Goense&Debener, 2010). When neural activity in a given brain area increases its metabolic rate of oxygen consumption also increases, therefore the decrease of oxyhemoglobin and increase of deoxyhemoglobin will occur resulting in a reduction in MRI signal. However, after this initial dip of oxyhemoglobin, the increase of the blood flow to the active area is triggered so the increased metabolic demand can be met. This increase in oxygen supply results in a higher concentration of oxygen than the activated neurons use and this is a higher concentration of oxyhemoglobin and a lower concentration of deoxyhemoglobin. Further, this leads to a more homogenous magnetic field and increased T2* signal. The concentration of oxyhemoglobin and deoxyhemoglobin depending on neural activation and their effect on MRI signal is illustrated in Figure 2.6.

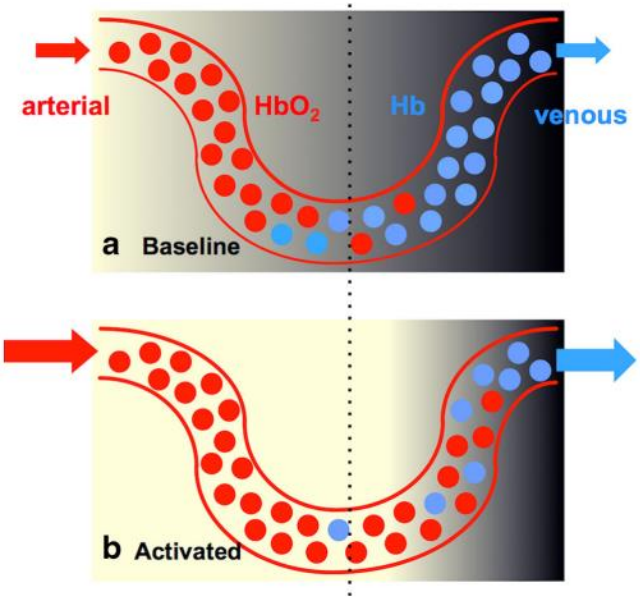

Figure 2.6 Neural activation dependent concentration of oxyhemoglobin and deoxyhemoglobin. *Blood oxygen level-dependent (BOLD) contrast depending on the hemodynamically driven changes in blood oxygen level due to the difference in Oxyhemoglobin (HbO2) and Deoxyhemoglobin (Hb) concentrations. During increased neuronal activation (b) increased blood flow and blood volume cause the reduction in Hb concentration in the blood, increase in the T2* weighted MRI signal, and thus brighter BOLD contrast compared to the baseline state (a)(Chen & Glover, 2015).*

The fMRI exploits described magnetic properties of hemoglobin, for an indirect measure of neuron activity through a blood oxygen level-dependent (BOLD) signal which captures the changes in levels of deoxyhemoglobin and oxyhemoglobin. The main concept behind BOLD is that the hemodynamic response to brain activation is reflected in the decrease in deoxyhemoglobin and an increase in oxyhemoglobin, resulting in increased field homogeneity and a larger MR signal (Deichman, 2016). A Hemodynamic Response Function (HRF) is used to depict the describedvascular response to the stimulus. HRF is a mathematical transfer function modeling neurovascular coupling by connecting neural activity with the BOLD fMRI signal (Rangaprakash et al., 2020). It is important to note that experimental data have suggested that HRF depends on both neural and non-neural factors (Bießmann et al. 2012). Therefore, the shape of HRF can differ across brain regions and individuals (Aguirre et al. 1998). The BOLD effect resulting from stimulus is not a static process, it evolves through a series of stages as illustrated in Figure 2.7. In the first moments of processing the stimulation in the activated brain region an increase in deoxyhemoglobin concentration occurs forming the so-called initial dip in the MR signal (Amaro & Barker, 2006). After this initial dip, there is an increase in oxyhemoglobin levels which eventually

results in the peak of the observable fMRIsignal. Additionally, after the pick of signal activity reaches the plateau slightly under the amplitude of the pick. This usually occurs in prolonged stimulations. When increased neuronal activation stops before the MR signal returns to baseline it decreases below it. This stage of hemodynamic response is known as the undershot. This phenomenon results from a slower rate of blood volume normalization than the changes in blood flow that lead to high deoxyhemoglobin (Amaro & Barker, 2006).

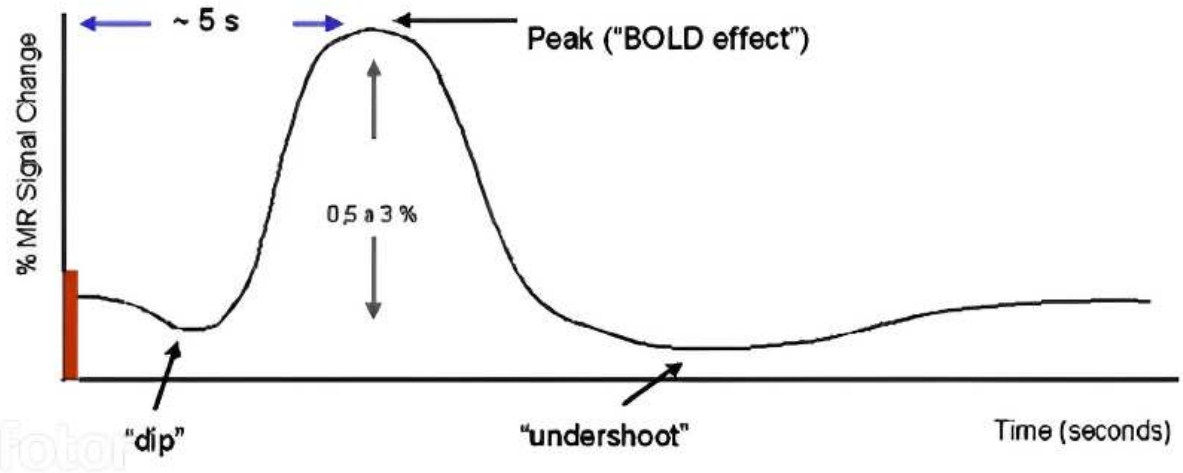

Figure 2.7Hemodynamic response function for a short-duration stimulus. *In a specific brain region, the initial processing of stimuli triggers a temporary rise in deoxyhemoglobin concentration known as the initial dip. Subsequently, the MR signal undergoes changes reflecting neural activity, with an increase in the oxy/deoxyhemoglobin ratio resulting in a positive BOLD effect proportional to neural activity reaching the peak in the BOLD effect. This signal eventually stabilizes during sustained stimuli and returns to baseline levels post-stimulus, often accompanied by an undershoot effect attributed to slower normalization of blood volume compared to blood flow (Amaro & Barker, 2006).*

2.2.2 Experimental Study Designs

Designing an fMRI experiment requires careful consideration of multiple factors to ensure efficient capturing of the brain activation behind certain mental processes. The decision to use one of the possible fMRI paradigms will mainly depend on the specific research question and objective.

The block design, initially adopted from PET studies, represents one of the earliest and simplest experimental designs employed in fMRI research. This approach consists of a series of periods in which the subject is either exposed to the stimuli or tasks or is at rest. These periods are referred to as epochs (Tsougos, 2017). Blocks of tasks or rest can vary in time,

with the usual average length between 10 and 30 seconds (Christidis& Reynolds, 2004). According to Tsougos (2017), the advantages of this method are reflected in the robustness of results and increased statistical power. Additionally, block design offers another advantage: the power of detection due to the repetitive stimuli that create additive effects on brain activation (Dimoka, 2012). However, block design also has noticeable shortcomings. For example, it cannot differentiate between correct and error trials (Tsougos, 2017). Further, the repetitive nature of tasks and rest can be predicted by participants, resulting in habituation and anticipation of the stimuli. According to Christidis and Reynolds (2004), block design also doesn't provide information regarding activation response time courses because individual responses are lost within the block. Finally, certain pathological conditions rule out the application of this design approach altogether.

In event-related design, stimuli are presented in arbitrary sequences, rather than in blocks, where stimuli are separated by the so-called inter-stimulus interval (ISI) (Tsougos, 2017). This design can overcome some of the downsides of the block design. It allows analyses related to individual responses to stimuli (Amaro & Barker, 2006), and it is useful for avoiding cognitive adaptation because of the randomization of the order of conditions presented (Tsougos, 2017). In addition, it provides greater flexibility for determining responses to novel or periodically presented stimuli or exploring changes over time (Christidis& Reynolds 2004). One major disadvantage of the event-related design is that the timing of single events results in a lower signal-to-nice ratio (Tsougos, 2017).

To maximize the advantages of the two previously mentioned designs it is possible to combine them and perform mixed design. Here, subjects are presented with stimuli that are grouped as blocks, but the time (ISI), conditions between them, or both are randomized. The advantage of a mixed approach is the possibility of extracting brain regions exhibiting an item-related pattern of information processing (transient), or task-related information processing (sustained) (Amaro & Barker, 2006). On the other hand, this design involves more assumptions than other described designs, as well as a poorer estimation of HRF (Donaldson, 2004). All three described experiential designs in fMRI research are represented in Figure 2.8.

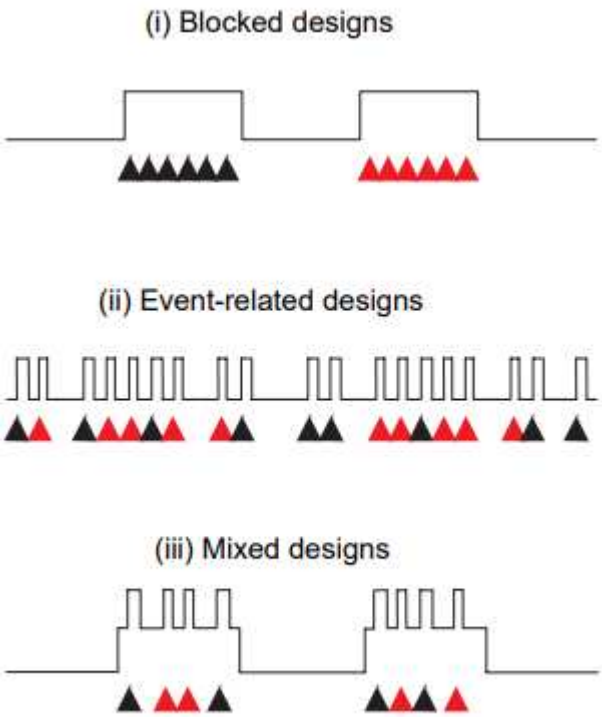

Figure 2.8 Different experimental designs in fMRI studies (Donaldson, 2004).

Every brain region is characterized by basal activity even when a person is not performing any specific task or exposed to stimuli. This provides an opportunity for the exploration of different functional connectivity patterns of the brain. Another possible experimental paradigm, resting state fMRI is employed for these proposes. Furthermore, the fMRI represents an analysis of the spontaneous BOLD signal in the absence of any explicit task (Smitha et al., 2017). It has a simple acquisition protocol, a participant is simply lying in the scanner with instructions to try not to think about anything in particular (Tsougos, 2017). By using correlation analysis between the fluctuation of the signal of different brain regions fMRI allowed the exploration of many resting state networks that exhibit a stronger coherence of signal fluctuations between their parts compared to the rest of the brain. Examples of some of the resting state networks are shown in Figure 2.9.

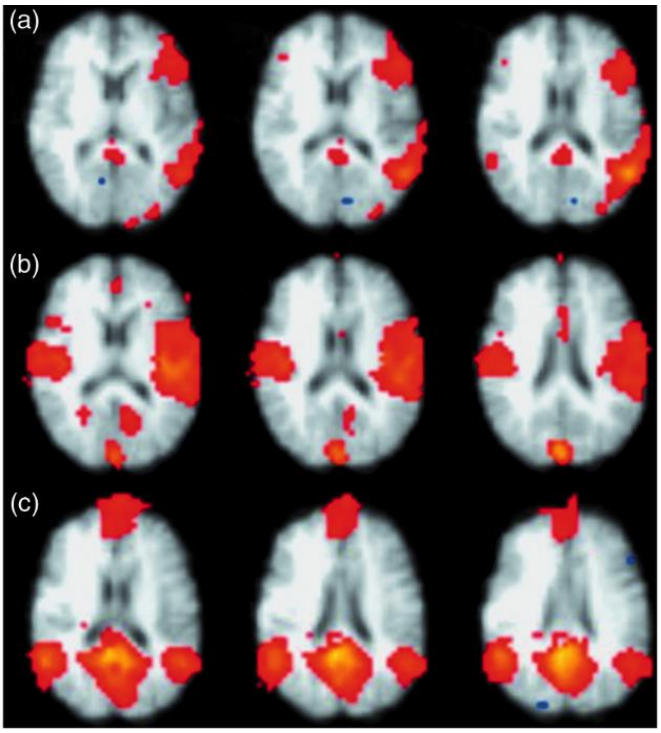

Figure 2.9 Resting state networks. *a - language network; b - auditory network; c - default mode network (Smitha et al., 2017)*

3 Dynamical Causal Modeling

3.1 Brain Connectivity

Understanding brain networks and interconnections is essential for comprehending the brain's complex functions and roles in various mental processes. Furthermore, in the past few decades, technological improvementshave provided non-invasive ways to explore those complicated patterns of brain connectivity in the healthy brain and observe changes in pathologies (Rubinov&Sporns, 2010). Links between distinct neuronal systems can be described through three different types of connections: anatomical links or anatomical connections, statistical dependency or functional connections, and causal interactions or effective connectivity (Sporns, 2007).

Anatomical, also known as structural connectivity, can be defined as the presence of white fiber tracts that directly connect different brain regions (Rykhlevskaia et al., 2008). For instance, Diffusion tensor imaging (DTI) can provide an opportunity for non-invasive investigation of structural connections of the human brain (Sporns et al., 2005). Moreover, DTI can also allow estimation of the dominant orientation of axons in a specific section of the white matter tract (Rykhlevskaia et al., 2008).

Friston (1994) defined functional connectivity as temporal correlations between spatially remote neurophysiological events. He also pointed out that functional connectivity is an observed correlation and it does not provide any direct insights into how those correlations are mediated. Functional connectivity can be measured with several techniques including functional magnetic resonance imaging (fMRI), positron emission tomography (PET), electroencephalography (EEG), magnetoencephalography (MEG), and the event-related optical signal (Rykhlevskaia et al., 2008).

However, more than functional connectivity is needed to explain how regions communicate and interact with one another (Rajapakse & Zhou, 2007). Thus, to fully understand how information is processed in the brain it is important also to consider effective connectivity. Effective connectivity can be defined as the influence one neural system exerts over another, either at a synaptic or cortical level (Friston, 1994). Friston and colleagues (2003) developed a new method for estimating effective connectivity called dynamical causal modeling (DCM), which represents the generalization of the proposed “covariance structural equation modeling” technique that assigns effective connection strengths to anatomical pathways that

best match observed covariances in a given task.DCM utilizes a Bayesian framework to estimate and draw inferences regarding directed influences among variables (Sporns, 2007). This method will be described in more detail in the following parts of this chapter.

The relation between structural, functional, and effective brain connectivity is still not fully known. However, two mechanisms to explain the link betweenthese different types of brain connectivity have been proposed: segregation and integration (Tononi et al., 1994). In particular, segregation involves specialized neurons and brain regions organized into distinct groups, forming segregated cortical areas. On the other hand, integration facilitates coordinated activation among distributedneuronal populations, allowing for coherent cognitive and behavioral states to emerge. The interaction between segregation and integration in brain networks produces information that is both diverse and integrated, resulting in complex patterns (Sprons, 2007). Models of structural, functional, and effective brain connectivity are illustrated in Figure 3.1.

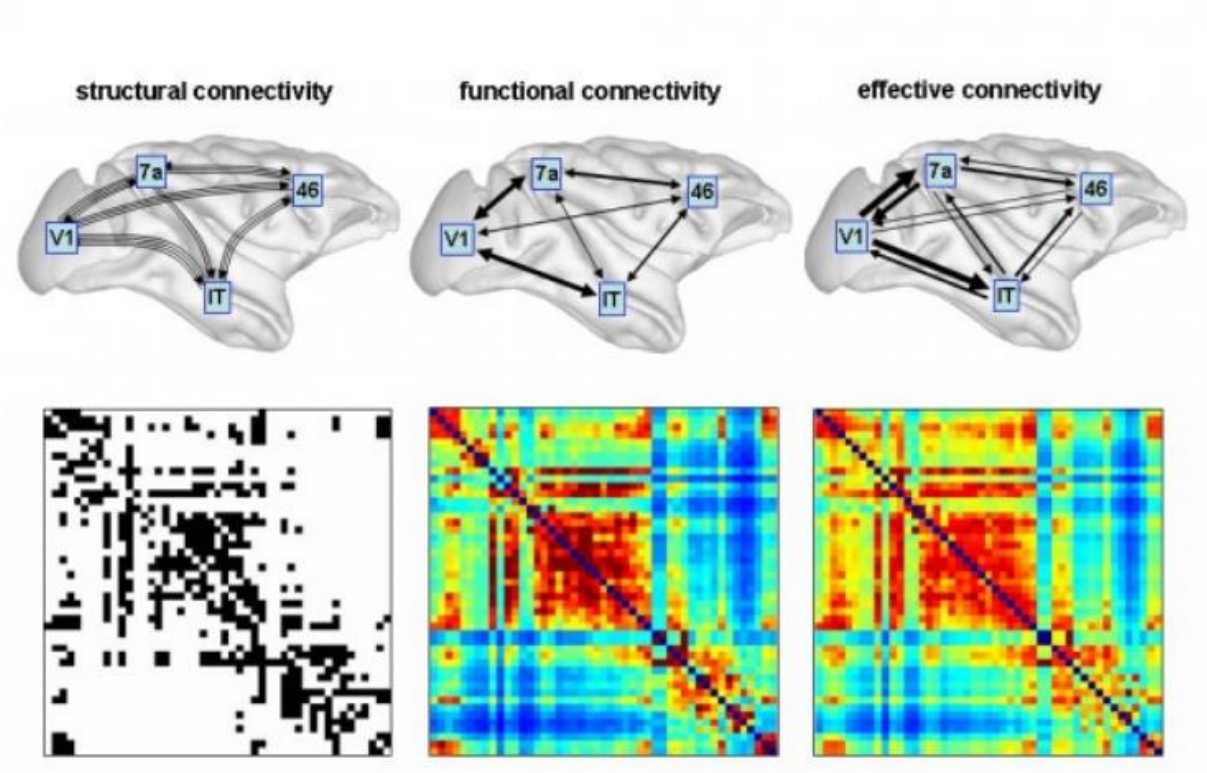

Figure 3.1 Modes of brain connectivity.*Sketches at the top illustrate structural connectivity (fiber pathways), functional connectivity (correlations), and effective connectivity (information flow) among four brain regions in the macaque cortex. Matrices at the bottom show binary structural connections (left), symmetric mutual information (middle), and non-symmetric transfer entropy (right) (Honey et al., 2007).*

3.2 Conceptual Basis of Dynamical Causal Modeling

Dynamical Causal Modeling (DCM) is the Bayesian framework for inferring hidden neural states from measured brain activity (Stephan et al., 2010). It was developed to estimate coupling among brain regions and how that coupling is influenced by experimental changes (Marreiros et al., 2010). Since its introduction in 2003 by Friston and colleagues, it became a widely used method in various branches of cognitive neuroscience such as motor processing, memory, language, perception decision-making, and most importantly for the present study visual attention (Stephan et al., 2010). DCM can be exploited on different techniques including electroencephalography (EEG), magnetoencephalography (MEG), and local field potentials (LFPs) (Kahan, &Foltynie, 2013). However, here the focus will be on DCM for fMRI.

The main idea behind the DCM is to look at the brain as a non-linear dynamic system susceptible to inputs and in return produce outputs (Friston et al., 2003). It tries to estimate the parameters of a reasonably realistic neuronal system model that can accurately predict how changes in neural activity would affect the BOLD signal, which is measured using fMRI. In the context of DCM, the BOLD signal can be considered a dependent, measurable variable (y) of the underlying neural activity (z) that cannot be measured with fMRI, and thus, the neural activity is referred to as the "hidden state variable" (Kahan, &Foltynie, 2013). The causal interactions among these hidden state variables, such as specific aspects of neuronal population activity, are represented by differential equations that describe how the current state of one neuronal population influences the dynamics, or rate of change, of another neuronal population through synaptic connections and how these interactions change under the influence of external experimental manipulations or intrinsic brain activity (Stephan et al., 2010). Therefore, DCM models how neural activity is influenced by external factors that are controlled in experiments. These external influences, referred to as perturbations, are represented by inputs "u" that can affect the neural activity in two main ways: through *driving inputs* that can elicit responses through direct influences on specific regions or they can change the strength of coupling among regions through *modulatory inputs* (Ashburner et al., 2014).

Mathematically, neuronal responses can be written as shown in equation 3.1 below:

$$\dot{z} = \frac{dz}{dt} = f(z, u)$$

3.1

where $\dot{z}$ is the rate of change in each brain region or neural response, vector z is the state or level of activity in each region and f is a function describing the change in brain activity in response to experimental inputs u (Zeidman et al., 2019a). When accounting for the changes derived due to experimental manipulation neuronal state equation can be written as

$$\dot{z} = \frac{dz}{dt} = f(z, u, \theta^n)$$

3.2

This equation describes changes in neural activity resulting from experimental manipulations. Encoded within a vector z, neural activity across all modeled brain regions represents hidden states, not directly observable via fMRI. The function f embodies the neural model, describing neuronal dynamics and specifying how changes in neural activity (z) over time arise from experimental stimuli (u), current state (z), and connectivity parameters (θ^n).

According to Ashburner and colleagues (2014) in DCM $f$has a bilinear form, thus an effective connectivity model can be represented as

$$\dot{z} = Az + \sum_{j=1}^{m} u_j B_j z + Cu$$

3.3

Further, parameters A, B, and C from this bilinear neural state equation can also be expressed as partial derivatives of:

$$A = \frac{\partial}{\partial z} | \, u = 0$$

$$B^{(j)} = \frac{\partial^2}{\partial z \partial u_j}$$

$$C = \frac{\partial}{\partial u} | \, z = 0$$

3.4

These parameter matrices, measured in hertz (Hz), describe three key causal components that drive neural dynamics: parameter matrix A specifies the average or baseline effective connectivity, matrix B specifies the modulation of effective connectivity due to experimental condition k, and parameter matrix C represents the sensitivity of each region to driving inputs. In other words, Matrix A is the rate of change in neural response due to neural activity z, i.e. the effective connectivity. Matrix Bj is the rate of change in the effective connectivity (matrix A) due to the modulatory inputs. and matrix C is the rate of change of the neural response due to the driving inputs (Zeidman et al., 2019a).

In essence, this equation describes how the interactions between different brain regions change over time based on both their inherent connections (matrix A) and external inputs (matrix B) while also considering any external perturbations (matrix C).

Further, it is also crucial to take into account and incorporate the inhibitory self-connection properties. These parameters, determined by the elements along the main diagonal of the average connectivity matrix A and modulatory input matrices B(k), regulate the self-inhibition within each region. In other words, they control the region's gain or responsiveness to input stimuli. Additionally, these parameters are typically negative, to prevent runaway excitation within the network. To achieve this, the average connectivity matrix A and modulatory input matrices B(k) are divided into two components: intrinsic self-inhibition within regions and extrinsic connectivity between regions and in this way (Zeidman et al., 2019). This can be represented by equation 3.2.5:

$$J \; = \; -0.5 \cdot exp(A_I) \cdot exp(\textstyle\sum_k B_I^{(k)} u_k \, (t)) + (A_E + \; \textstyle\sum_k B_I^{(k)} u_k \, (t))$$

3.2.5

where 0.5Hz is the default strength of the self-connections. Matrices AI and B(k)I represent the self-connections expressed as unitless log scaling parameters and matrices AE and B(k)E represent between-region connections, measured in units of Hz.

Experimental stimulation invoices the neuronal activation in specific regions causing changes in volume and deoxyhemoglobin and therefore the observable BOLD response (Friston et al., 2003). DCM combines neural dynamics models with hemodynamic models which are experimentally validated and biologically probable to explain how neuronal activity translates into a BOLD response (Ashburner et al., 2014). The Ballon model was developed by Buxton and colleagues (1998) for this purpose, and it explains the process of changes in blood oxygenation that are measured with fMRI caused by changes in neural activation (Penny et al., 2007). This model consists of a set of differential equations. The hemodynamic model can be written as follows:

$$y=h(x,u,\theta)+X\beta+\epsilon \tag{3.5}$$

This function specifies biophysical processes that transform neural activity z into the BOLD response y using parameters θ (Zeidman et al., 2019).

The summary of the Conceptual basis of Dynamical Causal Modeling is illustrated in Figure 3.2.

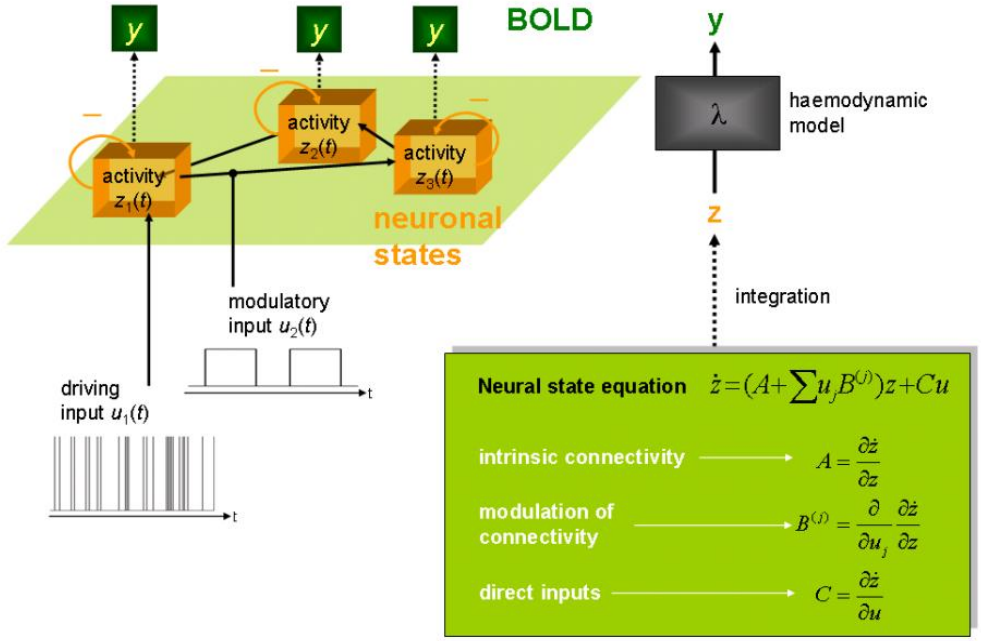

Figure 3.2 *Schematic summary of the conceptual basis of DCM. (Ashburner et al., 2014)*

In addition to the described parameter matrices and hemodynamic model, DCM also incorporates the General Linear Model (GLM) similar to standard GLM analysis. However, GLM used by DCM differs in one key concept: it allows an experimenter to additionally consider the effects of other regions on their neural model (Kahan, & Foltynie, 2013). Neural states (z) causing BOLD data (y) in DCM are sensitive to both exogenous inputs (as in the standard GLM analyses), and also to inputs from other regions. Additionally, convolution models in DCM are nonlinear (Kahan, & Foltynie, 2013). Friston and colleagues (2003) highlighted that the GLMs used in typical data analyses are just cases of bilinear models that embody more assumptions.

In summary, DCM provides a framework for defining models that describe the effective connectivity between different brain regions, estimating their parameters, and evaluating hypotheses (Zeidman et al., 2019a). DCMs are dynamic, employing differential equations to describe neuronal dynamics and they are causal, illustrating how the dynamics of one neuronal population influence another, and how those interactions are modulated by experimental manipulations or endogenous brain activity (Stephan et al., 2010). Although DCM is a complex framework Statistical Parametric Mapping (SPM) run through MatLab (The MathWorks Inc., Version R2022b) provides a relatively easy way of performing DCM in a user-friendly interface.

3.3 Bayesian Model Selection and Estimation

Every modeling approach encounters the challenge of model selection, which involves determining the best model among several alternatives based on observed data (Ashburner et al., 2014). DCM utilizes the Bayesian model selection (BMS) for this issue (Stephan et al., 2010). BMS in DCM refers to the process of comparing multiple DCM models and determining the most appropriate model among a set of candidate models that describe the connectivity among brain regions. This comparison is based on Bayesian principles, where each model is assigned a probability or "evidence" based on how well it fits the data and how complex it is. It balances the trade-off between model fit and complexity to determine the most plausible model given the data. Further, it allows us to compare different hypotheses or models about how brain regions interact and are influenced by experimental manipulations (Stephan et al., 2009).

In more detail, BMS is a statistical procedure that computes the probability of the data y, given some model m, also known as model evidence p($y|m$) (Stephan et al., 2010). The model evidence can be used to compare a series of models and determine which of them is the most likely to have generated the observed data. The model evidence is obtained by integrating out dependencies on the model parameters as denoted in equation 3.6:

$$p(y|m) = \int p(y|\theta,m)p(\theta|m)d\theta \tag{3.6}$$

Furthermore, the model evidence also serves as a measure of generalizability (Stephan et al., 2010). This emphasizes the importance of considering model complexity when selecting the model. This can be considered a crucial step because there is a trade-off between model fit and generalizability. In the Bayesian context, models are usually compared through the Bayes factor to determine which model represents the optimal balance between fit and complexity (Ashburner et al., 2014) as shown in equation 3.7:

$$p(y,m) = \frac{p(y|\theta,m)p(\theta|m)}{p(y|m)} \tag{3.7}$$

This equation is an application of Bayes' theorem, where we update our beliefs about the model parameters (θ) based on the observed data (y) and prior beliefs about the model parameters. Where $p(\theta|y, m)$ represents the posterior probability of the model parameters (θ) given the observed data (y) and the model (m); $p(y|\theta, m)$ is the likelihood function, representing the probability of observing the data (y) given the model parameters (θ) and the model (m). It measures how well the model with specific parameters explains the observed data; $p(\theta|m)$ is the prior probability distribution of the model parameters (θ) under the model (m). It represents our beliefs about the model parameters before observing any data; $p(y|m)$ is the marginal likelihood or evidence of the model (m). It represents the probability of observing the data (y) under the model (m), integrating all possible values of the model parameters. It measures how well the model, on average, explains the observed data across all possible parameter values. In the context of model selection, comparing the evidence ($p(y|m)$) of different models allows us to evaluate the trade-off between model fit (how well the model explains the data) and model complexity (the number of parameters or complexity of the model) (Stephan et al., 2007).

According to Stephan and colleagues (2010), BMS is the first and essential step of every DCM analysis regarding whether it relies on inference on model space or inference on parameter space. Inference on model space is used when the main interest is aspects of the model structure. In this case, either fixed effects BMS (FFX BMS) or random effects BMS (RFX BMS) can be used. FFX BMS is typically used when we assume that the optimal model structure is identical across subjects, on the other hand, RFX is applied when that is not the case (Stephan et al., 2010). Further, RFX can compute the likelihood that a particular model generated the data of a randomly selected subject as well as the probability that one model is more likely than any other model, given the group data (Stephan et al., 2010). Therefore, RFX assumes heterogeneity of model structure across subjects. Furthermore, the usage of BMS has been extended to compare models in group studies and compare different families of similar models allowing DCM studies to use model comparison for insights into pathological mechanisms (Kahan, & Foltynie, 2013).

On the other hand, if one wants to understand the neurophysiological mechanisms represented by specific parameters of the given model, then inference on the parameter space is needed. Here, the further type of analysis depends on whether one is interested in inferences on the optimal model or parameters of all models. If the first is the case, then FFX analysis of parameter estimates should be performed if the optimal model structure is assumed to be

identical across subjects, more specifically Bayesian model averaging can be used (BPA) (Stephan et al., 2010). BPA is The routine that generates a new DCM by averaging parameters from multiple fitted DCMs. These DCMs can be averaged across sessions or subjects. The averaged model can then be analyzed using standard DCM review options to examine parameter contrasts. The resulting inferences represent a Bayesian Fixed Effects analysis.BPA can be performed in MatLab through the implemented spm_dcm_bpa function. If an identical structure is not assumed RFX analysis of parameter estimates should be used (Stephan et al., 2007).

On the contrary, if one is interested in inference on parameters of all models Bayesian model averaging (BMA) should be performed which considers the entire model space and computes weighted averages of each model parameter. These weights are determined by the posterior probability associated with each model. BMA is often used when no single model outperforms the others. Additionally, it can be used for comparing parameter estimates across groups, such as patients versus controls, particularly when BMS indicates a group difference regarding the optimal model (Stephan et al., 2010). Similarly, as in the case of BPA, MatLab has implemented the spm_dcm_bma function for performing this analysis.

The decision between different approaches in specifying and estimating DCM models depends on the specific research question and formed hypothesis. All described techniques are summarised in Figure 3.3.

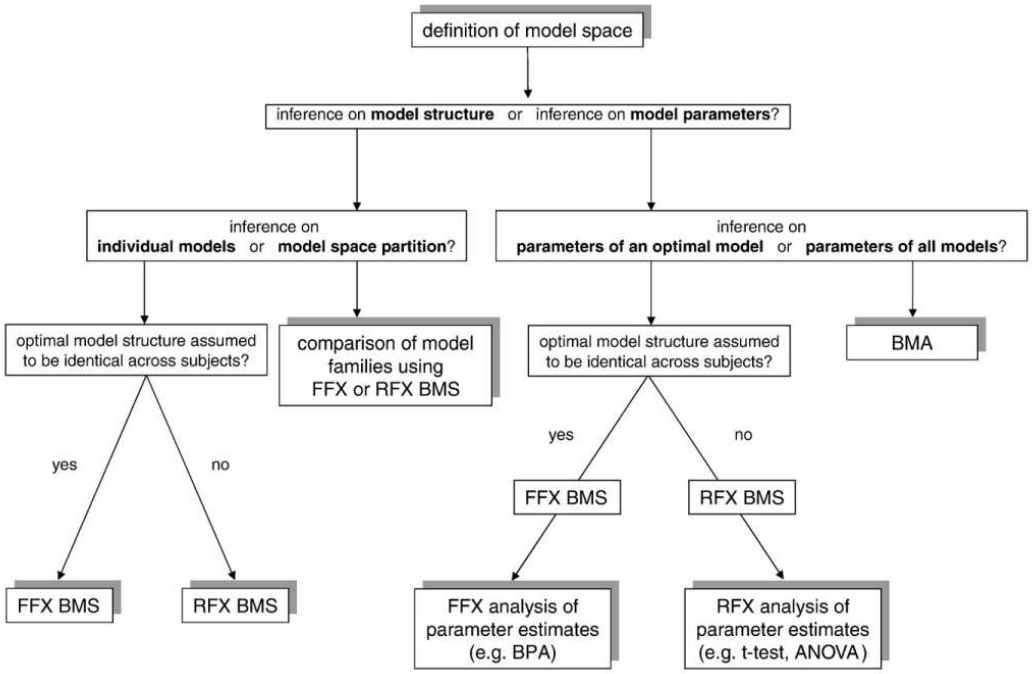

Figure 3.3 Different approaches for specifying and estimating DCM models. *FFX - Fixed effects; RFX - Random effects; BMS - Bayesian model selection; BPA - Bayesian parameter averaging; BMA - Bayesian model averaging (Stephan et al., 2010).*

3.4 First and Second Level Analysis

First-level analysis refers to the within-subject level. DCM forward or generative model is used to generate neuroimaging time series from the underlying causes, such as neural fluctuations and connection strengths (Zeidman et al., 2019a). Specifying the DCM forward model further allows the simulation of the data under different models and determining which simulation matches the observed data the best. This process typically includes two steps: Bayesian model inversion and comparison. Model inversion refers to finding the best balance of trade-offs between the accuracy and complexity of the model through the model evidence described in the previous section. The balance between complexity and accuracy is important to avoid "overfitting" where increasingly complex models may begin to incorporate noise that is unique to a particular dataset and therefore become less generalizable (Ashburner et al., 2014). Further, in the Bayesian model, the comparison hypothesis is tested by comparing the model evidence of different specified models.

After determining the connectivity strengths for each subject, the next task is to measure the similarities and variations across subjects. This allows testing differences between groups, for example, one could test if certain connections are altered by pathology compared to the healthy control group. Thus, second-level analysis refers to inter-subject variability in effective connectivity. After the DCM is specified and estimated for each subject the parameters of interest are then gathered and analyzed collectively at the second level using a General Linear Model (GLM), therefore individual differences in connection strengths are decomposed into the hypothesized group-level effects (Zeidman et al., 2019b). The process of first and second-level analysis is shown in Figure 3.4.

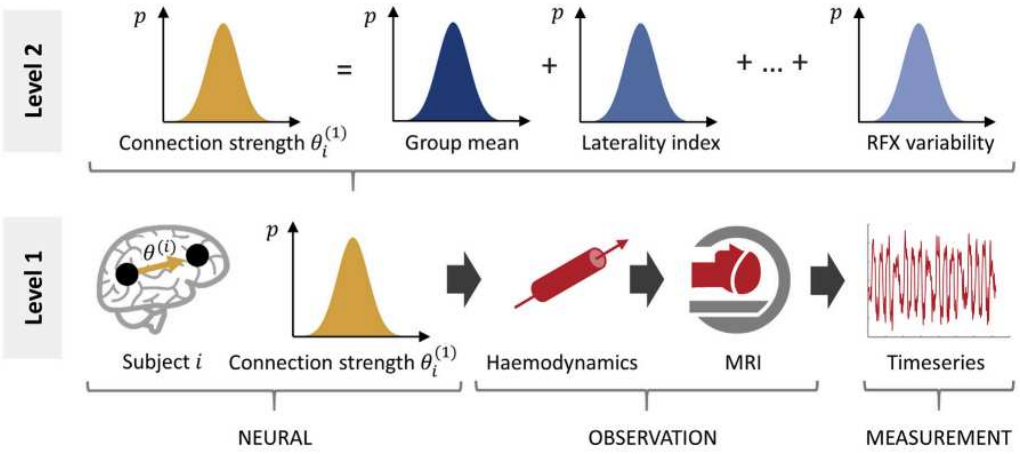

Figure 3.4 First and second level analysis. *The neural model is driven by experimental stimuli. The resulting neural activity causes a change in hemodynamics, mediated by neurovascular coupling, and consequently the generation of the BOLD signal. The addition of observation noise gives the fMRI time series (Zeidman et al., 2019a). In the first level analysis forward DCM modeldescribes how neural activity causes the fMRI time series of each subject (second row). The parameters from the neural part of the model are then taken to the group level (Zeidman et al., 2019b).*

In summary, DCM analysis consists of two main steps First and Second level analysis. First level analysis focuses on modeling and estimating DCM parameters at the individual subject level, while second-level analysis involves taking and comparing results across multiple subjects to make population-level inferences about the underlying neural dynamics.

Both First and Second level analysis demand DCM specification and estimation. Specifying a DCM involves defining the structural and dynamical properties of the model while estimating a DCM consists of fitting the model to observed data to infer the values of its parameters. Estimation of DCM is assessing how well the model fits the observed data to evaluate its validity. DCMs can be specified with the *spm_dcm_specify* function implemented in MatLab (2002-2017 Wellcome Trust Centre for Neuroimaging). This function is used to specify the DCM structure, including the neural model, experimental inputs, and priors on model parameters. For DCM estimation, the *spm_dcm_estimte* function (2002-2012 Wellcome Trust Centre for Neuroimaging) which implements Bayesian inference to estimate the posterior distribution is used.

4 Materials & Methods

4.1 Participants

Data used in this study was acquired from the previously published study by Mascheretti et al., 2021. The original sample size contains 90 participants, 45 with DD and 45 with TR participants. However, for both groups, the overall participant cohort was adjusted to the occurrence of the DCDC2 genetic mutation in the general population, based on the study by Mascheretti et al.,2021, with two participants for each group included with genetic involvement. Additionally, two participants from the DD and two from the TR group were excluded from the study due to the challenges in detecting a significant activation (i.e., the number of active voxels) in the VOI extraction procedure. Therefore, the current study includes the final number of participants of twenty children with the clinical diagnosis of DD (age = 14.08 ± 1.55; 6 females) and twenty TR children (age = 13.53 ± 1.8; 7 females). All participants belonged to Caucasian families and were native Italian speakers with no certified neurological, neurodevelopmental, visual, hearing, intellectual, or motor disabilities. Further, for all participants written informed consent was signed by both parents.

4.2 Neuropsychological Assessment

All the children underwent the following neuropsychological assessment that was administered by the previously published study by Mascheretti et al.,2021:

1. *IQ*: Estimated using the vocabulary and block design subscales of the WISC-III (Wechsler, 2006)
2. *Reading*: Evaluated through text reading (Cornoldi & Colpo, 1995; Cornoldi & Colpo, 1998), single unrelated words, and pseudo-words reading tests (Sartori et al., 1995; Arina et al., 2013).
3. V*erbal Working Memory (VWM)*: Assessed using the Single Digit Forward Span, Single Digit Backward Span, Single Letter Forward Span, and Single Letter Backward Span tasks (Reynolds & Bigler, 1994).
4. *Phonological Skills*: Measured by the nonword repetition test (NWR) (Bertelli & Bilancia, 2006).
5. *Hand Preference*: Determined using the Briggs and Nebes Inventory (BNI) (Briggs & Nebes, 1975).

6. *ADHD Traits*: Assessed with the Conners' Parent Rating Scales–Revised: Long version (CPRS-R) (Conners, 1990; Conners et al., 1998; Nobile et al., 2007), focusing on two subscales: DSM-IV-inattention (DSM-IV-I) and DSM-IV-hyperactivity/impulsivity (DSM-IV-HI).

Scores of the neuropsychological assessment are shown in the Appendix.

4.3 MRI Acquisition Protocol

A 3T Philips Achieva d-Stream scanner with a 32-channel head coil was used by Mascheretti et al. (2021) for acquiring fMRI data. Visual stimuli were developed with Presentation® software created by Neurobehavioral System Inc., Berkeley, CA, US, and presented via a VisuaStim digital device for fMRI (Resonance Technology Inc., Northridge, CA, USA). A two-display MRI-compatible goggles with a 60 Hz frame rate and 800 x 600 spatial resolution (4/3 aspect ratio) subtending a horizontal visual angle of 30◦ were used. Additionally, an MRI-compatible pad was used for recording participants' answers and reaction times.

MRI protocol contained:

1. Anatomical images acquisition: T1-weighted (T1W) performed with 3D Turbo Field Echo sequence for obtaining high-contrast structural images with Field Of View (FOV) = 256 × 256 × 175 mm3, voxel size 1 × 1 × 1 mm^3, Time of Repetition (TR) = shortest (~8.1 ms), Time of Echo (TE) = shortest (~3.7 ms), Flip Angle (FA) = 8◦.

2. fMRI acquisition: T2*- weighted Gradient Echo planar sequence with FOV = 240 × 240 mm^2 , voxel size = 3 × 3 mm^2 , slice thickness = 3 mm, slice gap = 0.5 mm, slice number = 39, TR = 2 s, TE = 26 ms, FA = 90◦.

4.4 fMRI task design

All participants performed two tasks: the coherent motion sensitivity detection task and the full field sinusoidal grating task (Mascheretti et al.,2021).

Coherent Motion Sensitivity Detection Task

Motion coherence sensitivity was assessed by the Coherent Motion Sensitivity Detection task with radial motion pattern (expansion and contraction). Stimuli included 50 small black dots and 50 small white dots with dimensions of 20 arc mins presented on a mean luminance gray background for 250 ms. A portion of the presented dots moved coherently at a rate of 10 degrees per second with a restricted lifetime of 8 frames at a frame rate of 60 Hz moving either towards the center (contraction), or away from the center (expansion). Meanwhile, the rest of the dots appeared randomly positioned in each frame. Stimuli were presented in three different levels of coherent motion of the dots: 6%, 15%, and 40%. The protocol included 8 repetitions for each combination of coherence level and motion direction, hence 48 blocks of stimuli. Stimuli were presented in pseudorandom order with the condition that the same coherence would not appear in more than two consecutive blocks regardless of the direction of motion. At the beginning of each block, the fixation point subtending 0.2◦ visual angle was presented at the center of the screen for 0.5s. After the stimulus participants were given 4s to answer whether the dots were expanding or contracting by pressing an adequate button on the response pad. Participants were instructed to maintain fixation throughout the run and to provide a response even if they were unable to detect the direction of coherent motion. In between every stimulus block, there was a 4.25s inter-stimulus waiting period. The protocol is summarised in Figure 4.1.

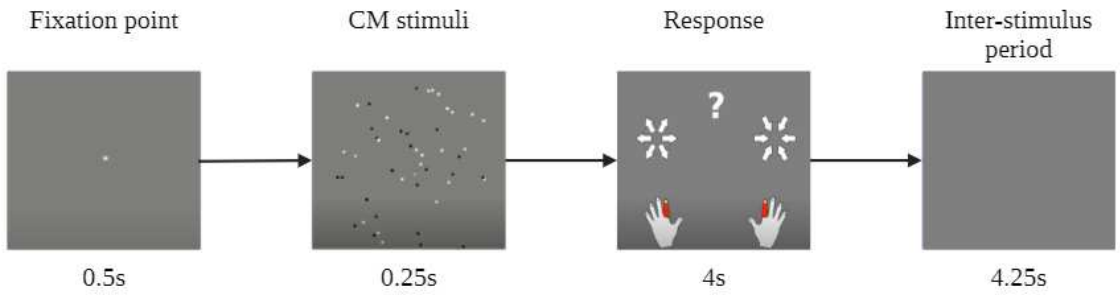

Figure 4.1 Coherent motion detection task protocol. *CM stimuli = Coherent Motion stimuli(adapted from Mascheretti et al.,2021).*

Full Field Sinusoidal Grating Task

The Field Sinusoidal Grating task is designed to differentiate BOLD signals from magnocellular and parvocellular visual pathways (Mascheretti et al.,2021). The task consisted of two different types of stimuli: Magnocellular (M) and Parvocellular (P) stimuli. The M stimulus consisted of a monochrome, low spatial frequency, high temporal frequency, high luminance contrast, and full-field sinusoidal grating featuring sinusoidal counterphase flicker. Additionally, it consisted of a 100% luminance contrast, black-white grating with a spatial frequency of 0.5 cycles per degree (cpd), and a flicker frequency of 15 Hz. On the other hand, The P stimulus was a high color contrast, high spatial frequency, low temporal frequency, and low luminance contrast full-field sinusoidal grating with sinusoidal counterphase flicker. More specifically, the P stimulus featured a low luminance contrast, high color contrast, and red-green grating with a spatial frequency of 2 cycles per degree (cpd) and a flicker frequency of 5 Hz. Color levels in the P stimulus were adjusted to be near-isoluminant, with the red luminance set to the maximum level and the green set to 39% of the maximum level. Both gratings were displayed at one of six orientations (0°, 30°, 60°, 90°, 120°, and 150°) and transitioned to the next orientation every 2.33 seconds. In addition to M and P stimuli blank stimuli consisting of gray screen of mean luminance were also presented. The outer edges of each stimulus gradually transitioned into gray to prevent sharp visual edges at the boundaries of the stimulus. Examples of stimuli in the full field sinusoidal grating task are represented in Figure 4.2.

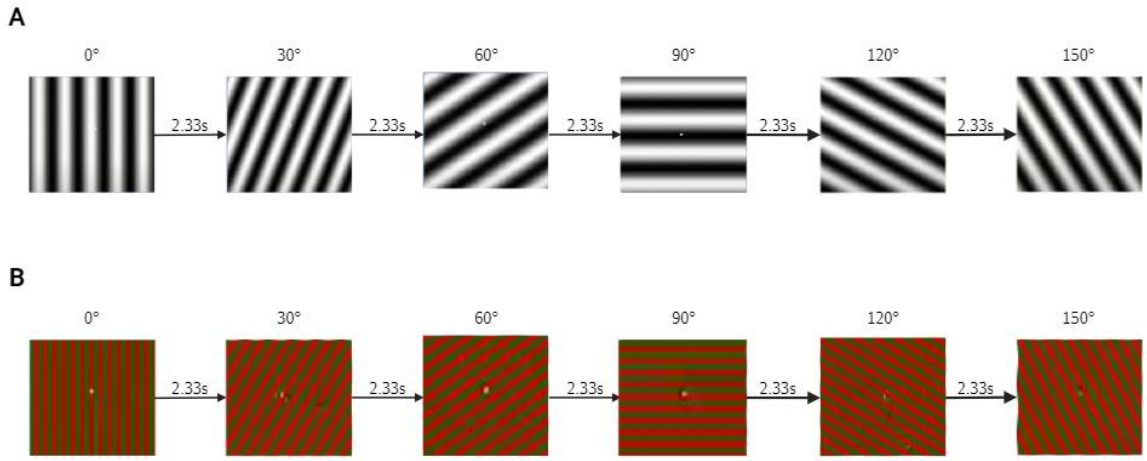

Figure 4.2 The full field sinusoidal grating´s task M and P stimuli. *A. Magnocellular (M) stimuli in different orientations change from one to another every 2.33 seconds. B. Parvocellular (P) stimuli presented in six different orientations changing every 2.33 seconds (adapted from Mascheretti et al.,2021).*

The protocol included 28 blocks, consisting of 8 M blocks, 8 P blocks, and 12 blank blocks, presented in a pseudorandom order. To minimize adaptation to the stimuli, the same type of stimulus could not appear in subsequent blocks. A white fixation point, subtending 0.2 degrees of visual angle, remained at the center of the screen throughout the stimulus blocks. The inter-stimulus waiting period between stimulus blocks was 2s. Participants were instructed to maintain fixation throughout the experiment. Additionally, during the M and P stimulus blocks, participants performed an irrelevant target detection task to encourage the maintenance of fixation. The target consisted of a bi-dimensional Gaussian contrast reduction patch, with its size linearly scaled based on the distance from the fixation point. It appeared randomly for 300 ms and in random positions during the second half of each stimulus block at 50% of the time. After each stimulus block, the screen turned gray, prompting subjects to indicate whether the target appeared by pressing the corresponding button on the response pad. Participants had 4s to answer. The protocol of the full field sinusoidal grating task is illustrated in figure 4.3.

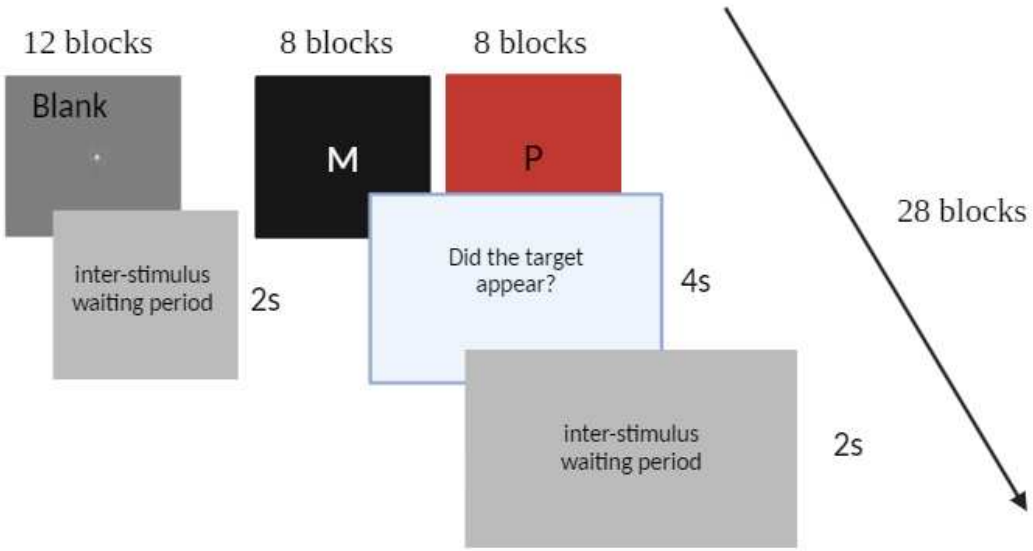

Figure 4.3 *Three stimuli were presented in pseudorandom order: 12 blocks of Blank stimuli, 8 blocks of M stimuli, and 8 blocks of P stimuli. After each block of stimuli, participants had 4 seconds to respond if the target, presented 50% of the time, appeared or not. Additionally, between blocks of stimuli, there was a 2-second inter-stimuli waiting period (adapted from Mascheretti et al.,2021).*

4.5 fMRI analysis

4.5.1 Pre-processing

When acquiring MRI and fMRI images not only brain tissue is captured but also these anatomical and functional images include non-brain tissues like the skull, neck, soft tissues, and background images. However, non-brain tissues can cause some processing difficulties in further analyses. Therefore, a series of steps are needed to "clean" and prepare raw fMRI data before conducting any further steps of research. This process is often referred to as pre-processing (Smith, 2004). In the case of functional MRI, these steps can be divided into two large groups: structural pre-processing and functional pre-processing. As the data used in the present study was already partially preprocessed by the authors of the original study from which the data was obtained (Mascheretti et al., 2021), the pre-processing procedure was completed and also done for one subject for demonstration purposes.

Structural Pre-processing

BET extraction

Brain Extraction Tool (BET) is an automated method for removing non-brain tissue from a whole head image (Smith, 2002). This tool implemented in the FMRIB Software Library (FSL) package (Woolrich et al., 2009, Smith et al., 2004, Jenkinson et al., 2012) is often used as one of the first steps of pre-processing MRI images. FSL is a software tool that is used in structural, functional, and diffusion MRI brain image analysis (Jenkinson et al. 2012). FSLs BET is used to extract brain tissue from other noisy non-brain aspects in T1 images. When using BET one should specify the input image, the label for the output image, and options. The output provided is a result of performing defined options on an input image. The standard pseudo-code used for BET extraction is:

bet <input> <output> [options]

Several options can be used based on specific needs for the images and research settings. Some of the most commonly used options are:

- -f, fractional intensity threshold. Values range from 0 to 1 and the default value of this option is 0.5, smaller values give larger brain outline estimates.
- -g, vertical gradient in fractional intensity threshold. Values go from -1 to 1, and the default value is 0. Smaller values give larger brain outlines at the bottom and smaller ones at the top.
- -B, this option is considered to be advanced, but it is commonly used to reduce neck voxels.

After this procedure is done, the user should have an output image from a raw T1 image containing only brain tissues. Output can be viewed and inspected in FSLeyes. The output image is presented below in Figure 4.4.

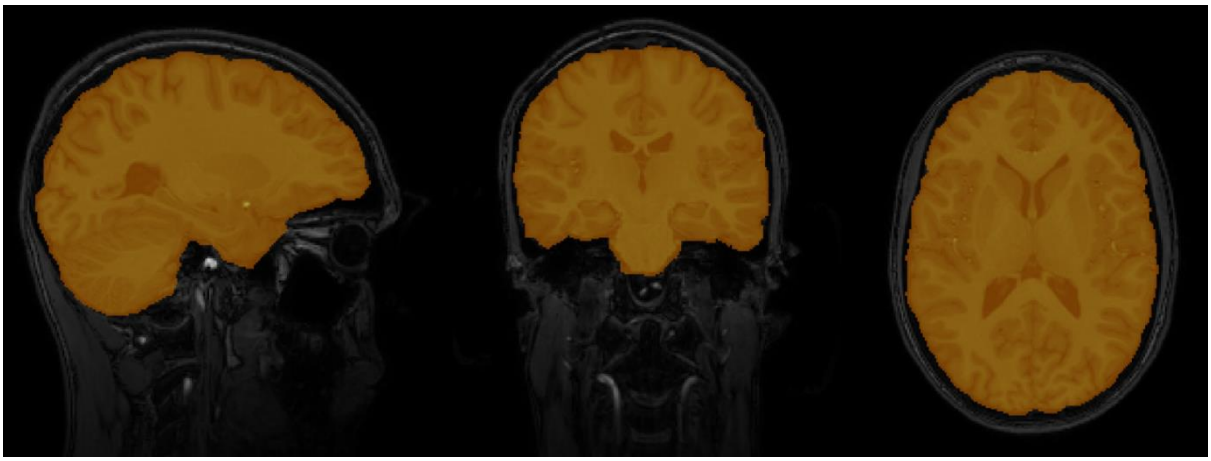

Figure 4.4 Raw anatomical image of randomly selected participants with overlaid BET extracted image in orange color.

Segmentation

Segmentation is used to classify and identify different brain tissue types, such as gray matter, white matter, and cerebrospinal fluid (CSF). This procedure provides a way to eliminate unwanted artifacts and transform data into the standard format adequate for further analysis. For instance, gray matter is one of the most important tissue types for the detection of activity in fMRI compared to white matter and CSF, thus segmentation can be used to segregate those different brain tissues and perform analysis on the specific tissue of interest. One way of performing segmentation is by using FSL FAST (FMRIB's Automated Segmentation Tool) (Zhang et al., 2001). This approach is based on a hidden Markov random field model and

allows completely automated and reliable segmentation of 3D images of the brain into different tissue types (Zhang et al., 2001). Pseudo code for FSL FAST is:

fast<input><output> -o fast_segm

The BET-extracted image is usually used as an input image for FAST. –o is used to indicate the base name of output images. When using FSL FAST one can also specify the number of segmented types of tissues. The standard number is 3 (White matter, Gray matter, CSF), but in some cases, if there is inferior grey/white matter contrast this option can be reduced to 2. This can be done by adding the following option:

-n <number_of_classes>

The output file names created by FSL FAST indicate the type of matter. Pve_0 implies CSF, pve_1 gray matter, and pve_2 implies white matter. For example, if the file has the name indicated below, it designates the gray matter segment:

fast_segm_pve_1.nii.gz

An illustration of a segmented brain with 3 types of matter is shown below in Figure 4.5.

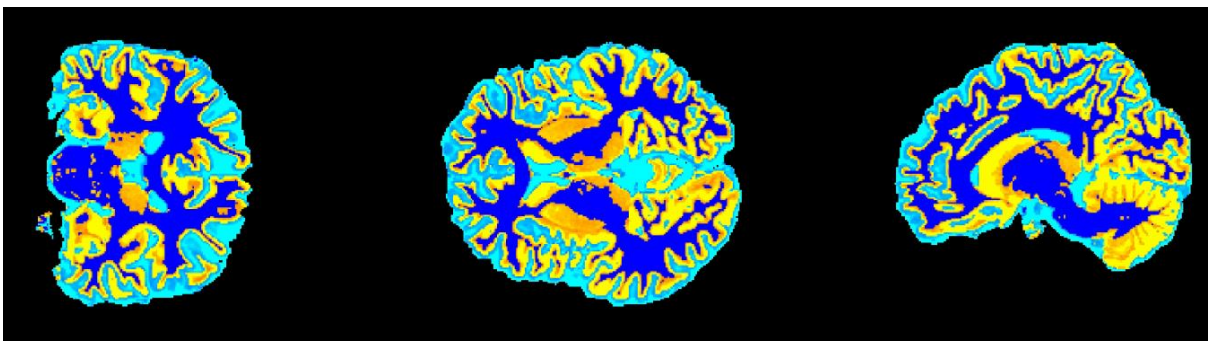

Figure 4.5 Segmented brain tissue for one randomly selected subject. *CSF is represented with light blue, gray matter with yellow, and white matter with dark blue color.*

Functional pre-processing

The BOLD signal measured by fMRI is often influenced by non-neural sources of variability such as system-related noise, intrinsic physiological fluctuations, and movement-related effects. Therefore functional preprocessing steps are needed to identify these sources and reduce their impact on the data (Caballero-Gaudes& Reynolds, 2017). Furthermore, functional preprocessing enables the better anatomical localization of signals ensuring accurate interpretations of neuroimaging data (Esteban et al., 2019). Specific procedures used in functional pre-processing will be explained in more detail in further text.

MP-PCA

Marčenko-PasturPrincipal Component Analysis (MP-PCA) is used for deleting the noise from the raw functional images. It uses principal component analysis across different time points and in that way separates signal from noise, thus improving signal-to-noise ratio.

Slice timing

The next step is slice timing correction. To create 3D images in fMRI acquisition 2D slices are rapidly acquired over hundreds of milliseconds and stacked together, but each of the slices is not obtained simultaneously, thus they are not temporally aligned (Parker &Razlighi, 2019). Slice timing correction is a temporal correction used to resolve the mentioned phenomena and problems that it can cause in further analysis. This procedure corrects the temporal offsets between slices by shifting the time series of each slice to temporally align all slices to a reference time point (Parker & Razlighi, 2019).

Realignment

During the scanning process, the head movements of the subject can significantly impact the data collected, therefore addressing the movement correction is necessary as well. Without movement correction the signal from a particular voxel in one position can change in the case of movement, for example, it can originate from outside the brain (Zafar, et al. 2015). The realignment allows spatial alignment of all functional images with the first functional image and in that way removes unwanted movement of participants in the scanner. Thus, this procedure aims to align all images to maintain consistency in the positioning of the brain across all frames and therefore ensure that the signal from a particular voxel always corresponds to the physical location (Zafar, et al. 2015).

Coregistration

After completing all the previous steps in structural and functional pre-processing it's necessary to register functional images with anatomical ones.The process of coregistration involves aligning these functional and structural MRI images spatially. In addition to aligning functional MRI (fMRI) data with structural MRI data, coregistration often involves aligning these images to a standardized anatomical space, such as the Montreal Neurological Institute (MNI) space (Mazziotta et al.,1995) One way of performing coregistration is by using FSL's FLIRT (Jenkinson & Smith et al. 2001; Jenkinson et al., 2002) which is a program performing affine registration. The main options in this program are input, an image to transform, and reference volume, the image with which the input should be aligned. Thus, the input is usually a functional image and the reference is a T1-weighted anatomical image.

The examples of structural and functional images after the pre-processing are illustrated in Figure 4.6.

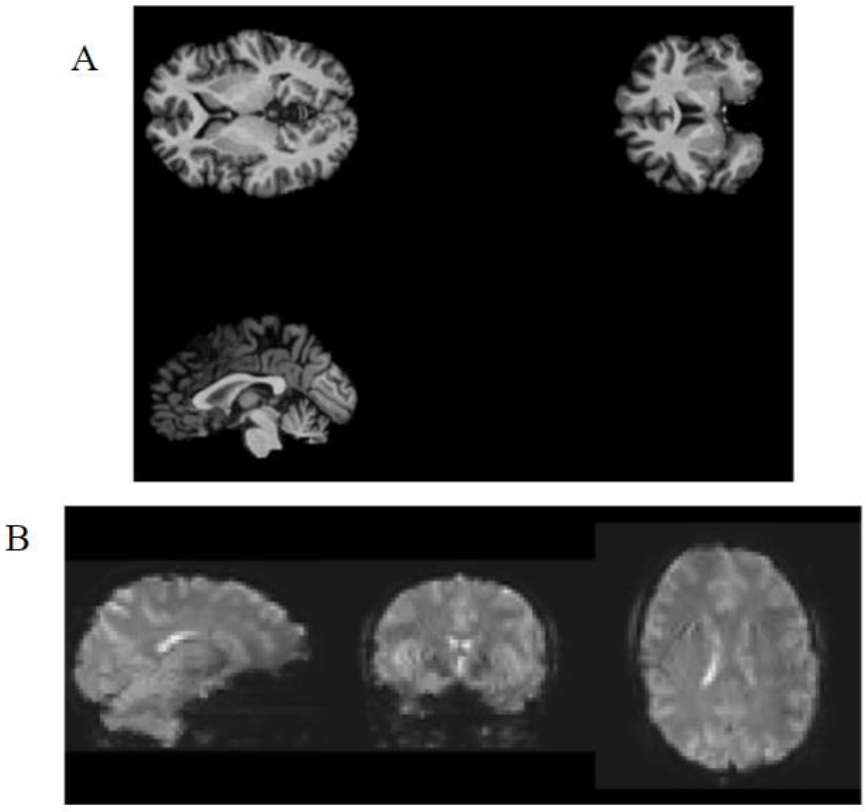

Figure 4.6Example of pre-processed images.*A - T1-weighted image after pre-processing; B - The fMRI image after pre-processing (Courtesy of Gökçe Korkmaz).*

Quality control with SPM's CheckReg Tool

CheckReg is a tool implemented in the SPM that can be used for checking the coregistration of multiple images. It can be used to evaluate the correspondence between a structural image and the mean of functional images acquired with fMRI (Ashburner et al., 2012). Therefore, this tool can be used as a quality control after the coregistration procedure to ensure that images are properly aligned and in the same anatomical positions without large errors or mismatches (Peelle, 2019). An example of the output of the ChekReg tool for one randomly selected participant is shown below in Figure 4.7.

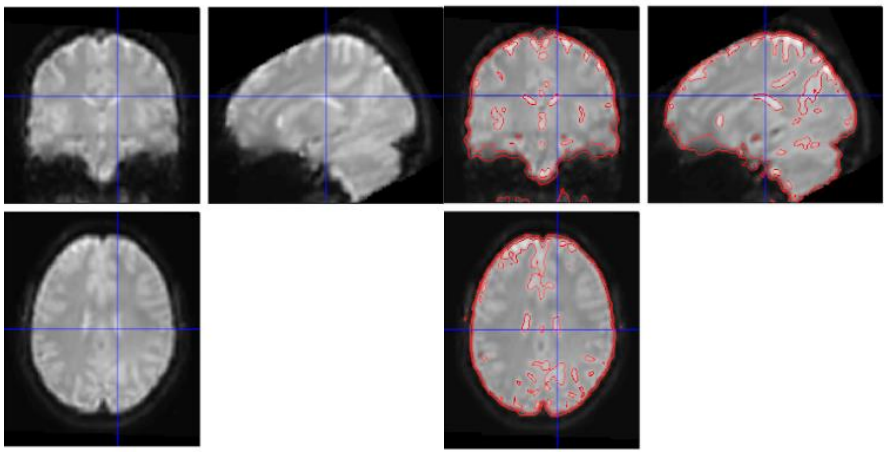

Figure 4.7*An example of the evaluation of the correspondence between a structural and the mean of the functional images for one randomly selected subject.*

Additionally, the pipeline of the described pre-processing procedure is illustrated in Figure 4.8.

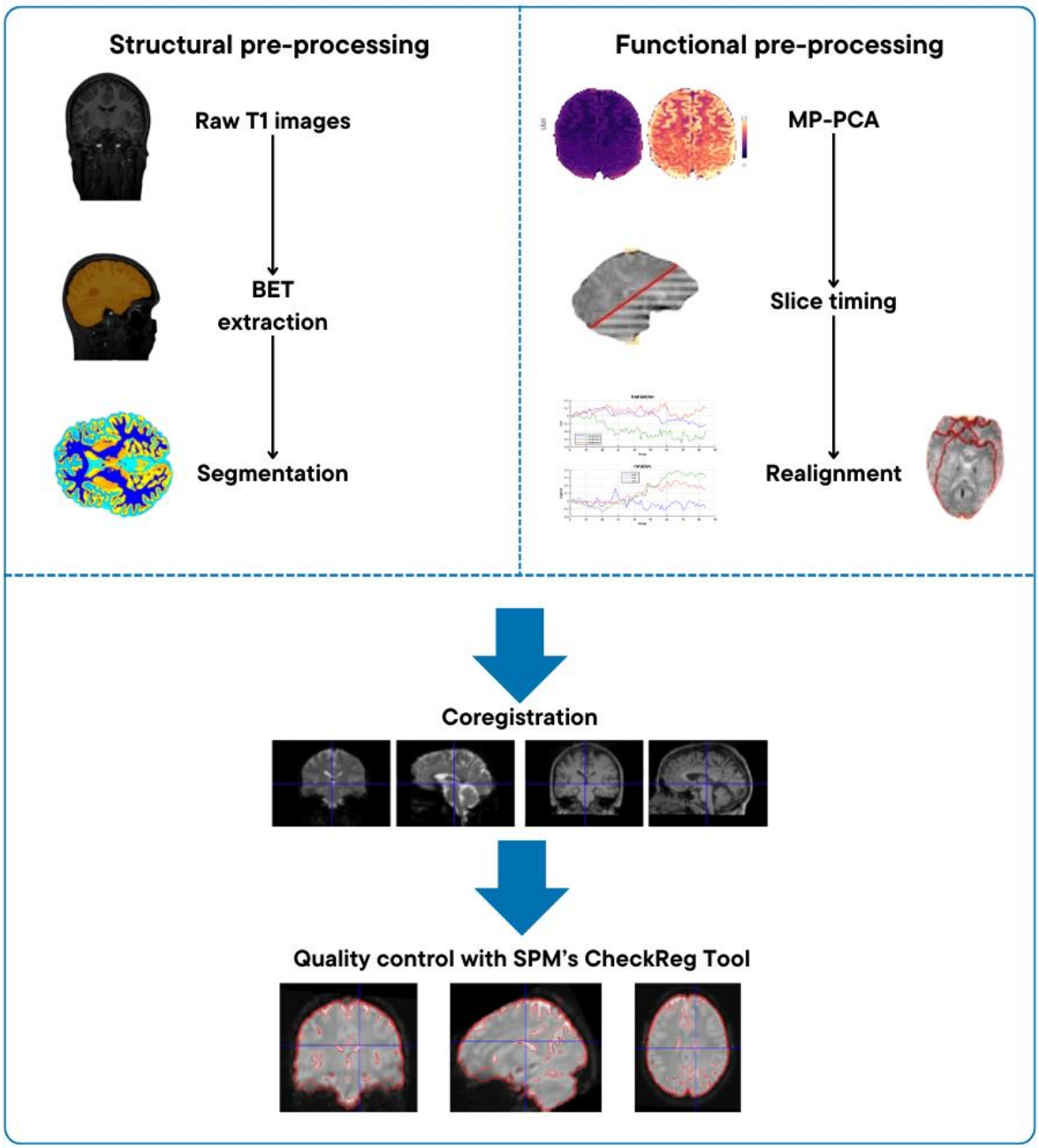

Figure 4.8 The pipeline of the pre-processing procedure.

4.5.2 Subject Level Analysis

Analysis of fMRI data typically consists of two stages: first-level or subject level and second-level or group level (Ashburner et al. 2014). Subject-level analysis, also known as first-level analysis, is a critical step involving analyzing individual subjects' brain activity by modeling the measured BOLD signal over time. The goal of this procedure is to determine how different experimental conditions influence brain activity in each participant (Poldrack et al., 2011).

The analysis of fMRI data employs the method grounded on General Linear Models (GLMs). GLMs model the measured BOLD signal from a single voxel over time (Y) as the sum of a number of experimental predictor variables (X) each multiplied by the weighting parameter (β), plus the error (ε), where the aim is to explain as much of the variance of Y as possible with X and thus make the error as low as possible (Monti, 2011). Mathematically GLM can be denoted as shown in equation 4.4.2.1:

$$Y = X\beta + \sum$$

4.4.2.1

Statistical analysis of fMRI data using GLM involves steps such as specifying the GLM design matrix, estimating parameters, and generating statistical maps. The design matrix, which outlines the experimental design and hypothesis testing, includes rows for each scan and columns for each effect or explanatory variable and can be built with session-specific partitions.

In subject-level analysis parameters of the model are specified and estimated for each participant, thus the activation is averaged across multiple scans for each subject. Therefore, the number of first-level models corresponds to the number of subjects. The specifications of the models can be performed through an SPM batch editor implemented in MATLAB (The MathWorks Inc., Version R2022b). The SPM batch and necessary options that have to be specified are shown in Figure 4.9.

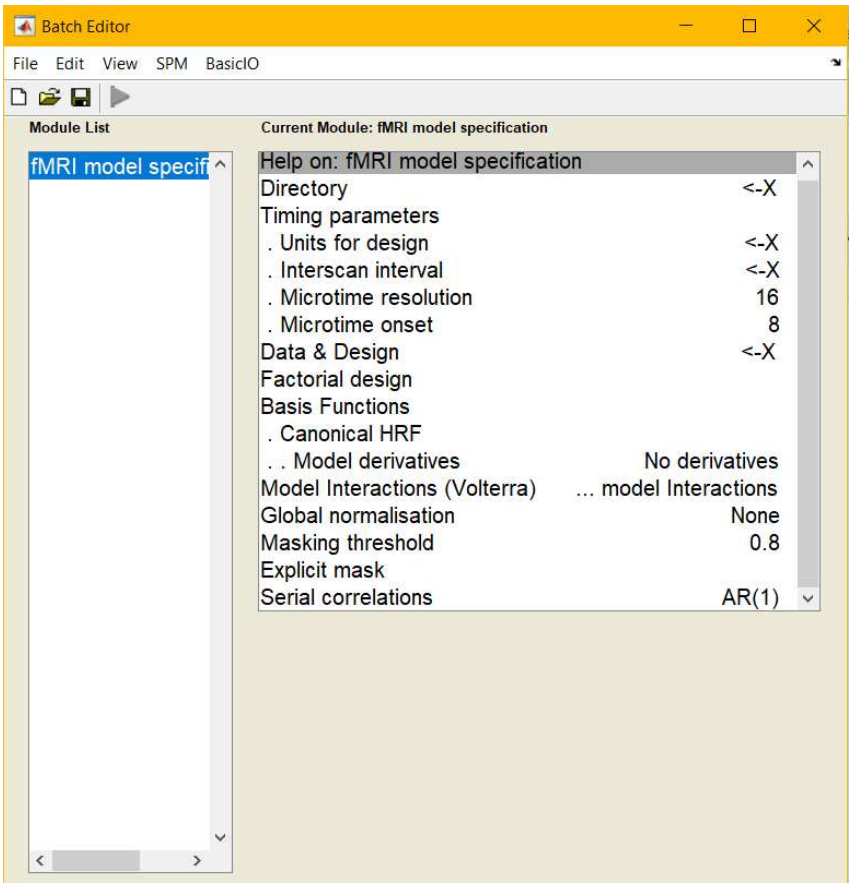

Figure 4.9 SPM batch editor for GLM specification.

Timing parameters specify timing properties such as units of design, interscan interval, microtome resolution, and microtome onset necessary for design matrix creation. In the present study units of design were set to seconds for both tasks due to the event-related design of the study. Further, the interscan interval corresponds to TR expressed in seconds and it was set to 2 seconds according to fMRI acquisition properties in Mascheretti et al., 2021. Microtime resolution and onset were kept on default values.

After the GLM is specified it is also necessary to perform model estimation. In this process, the model parameters are estimated using classical or Bayesian algorithms (Ashburner et al. 2014). Estimation can be performed through the SPM batch editor as well, and once it is performed one can further specify contrasts. Contrasts are used to compare the different conditions in an experiment. Moreover, two types of contrast can be differentiated: F contrast or effect of interest and T contrast. F contrast is used to test multiple linear hypotheses, including main effects and interactions. However, F contrast does not specify whichparameter is driving the effect or the direction of the difference. On the other hand, T contrast assesses

the effect of one parameter or compares specific combinations of parameters (Penny et al., 2011). In the present study, two T contrasts were created:

- *Coherence 15* - refers to the coherent motion detection task and the condition where the level of coherent motion of the dots is 15% versus the baseline blank stimuli. This condition is specifically chosen due to its reported better discriminating accuracy between TR and DD subjects compared to the 6% and 30% conditions (Mascheretti et al. 2021).
- *Magnocellular* - represents the magnocellular condition of the full field sinusoidal grating task versus the baseline blank stimuli. The magnocellular condition was used as previous studies have reported different functioning of the magnocellular visual pathway in DD compared to TR, but the same was not found in the parvocellular pathway (Stein, 2018).

The ending output of the first level analysis was obtained as contrast images, containing the information of the defined contrast, necessary for the second level or group level analysis which will be described in the following subsection.

4.5.3 Group Level Analysis

To draw conclusions about group activation the second-level or group-level analysis has to be performed. This process, like the first level analysis, comprises model specification and estimation. This method uses contrast images from each subject as summary measures of their responses and then enters them as data into a "second-level" model (Ashburner et al. 2014).

This study used the full factorial design for group-level GLM, including two factors with two levels. One factor represents the group with levels DD and TR, while the other factor represents a task with two levels the full field sinusoidal grating task and the coherent motion detection task. Factorial design is represented in the table 4.4.3.1. The ending output of group-level GLM estimation is the group SPM.mat file that contains all necessary information for further analysis including the VOI extraction. Some of the files contained in the SPM.mat file are:

- SPM.xX.X - Containing information about the design matrix
- SPM.xX.name – Containing labels for each column of the design matrix
- SPM.xY.P – Containing input files
- SPM.xCon - Containing information on contrast definitions

	CM	GR
DD	DD_CM	DD_GR
TR	TR_CM	TR_GR

Table 4.4.3.1. The factorial design used in group-level GLM specification. DD: developmental dyslexia group, TR: typical readers group, CM: coherent motion detection task, GR: full field sinusoidal grating task.

4.6 Conjunction Analysis

The initial intention of this study was to compare not only DD and TR groups on one task but also to compare effective connectivity between the two described tasks, the Full Field Sinusoidal Grating task, and the Coherent Motion Detection task. To be able to make these comparisons it is necessary to define the same Volumes of Interest (VOI) for both tasks. One way to select the same VOIs in different tasks is to perform the Conjunction analysis (Price & Friston, 1997; LaBar et al., 1999), used in this study.

Conjunction analysis was performed with a full factorial design, combining two tasks and two groups. Full factorial design refers to an experimental design with several experimental factors, each represented by multiple levels (Henson & Penny, 2003), where all of the main effects and interactions are intended to be tested (Ashburner et al. 2014). The design matrix is shown in Figure 4.10. below.

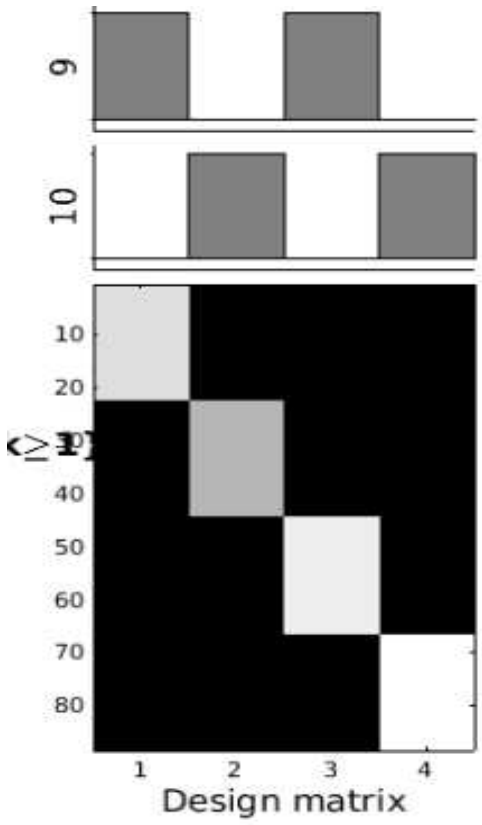

***Figure 4.10* Conjunction analysis design matrix.** *9 - Coherent motion detection task contrast. 10 - Full-field sinusoidal grating task contrast. 1 and 3 - DD group. 2 and 4 - TR group.*

This approach allowed us to identify voxels activated in each task and group, highlighting the common regions of activation.

4.7 Volumes of Interest Definition and Extraction

In defining the volume of interest (VOI) definition, several key factors were considered. First, the study's aim to investigate cerebellar and attentional visual network deficits in DD was crucial. Second, existing literature on the involvement of specific regions in visual attention in DD was thoroughly reviewed. Finally, areas showing significant activation overlap between DD and TR groups, as well as between Coherent Motion Sensitivity and Full Field Sinusoidal Grating tasks were considered.

After careful reasoning, we identified seven VOIs for our further analysis with the stated reasons for selection :

- *Bilateral Primary Visual Cortex (V1)* given the visual nature of used tasks;
- *Right and left Middle Temporal Cortex (V5_R and V5_L)* - Selected for their involvement in movement processing (Stein, 2022), magnocellular pathway function (Vellutino et al., 2004), and previous associations with DD (Stein, 2022).
- *Right and left Middle Frontal Gyrus (MFG_R and MFG_L)* - Known to be a part of VAN and crucial for attention reorienting, making them one of the key regions involved in proficient reading (Corbetta & Shulman, 2002, Freedman et al., 2020);
- *Right and left Crus I of Cerebellum (CRUSI_R and CRUSI_L)* - Chosen to test the cerebellar deficit theory, with Crus I specifically targeted due to its cognitive functions and reported role in language processing (Mariën & Borgatti, 2018).

Additionally, when deciding on the number of VOIs, DCM limitations were considered. Previous research has demonstrated that, in the absence of prior hypotheses regarding inter-regional connectivity, DCM can reliably infer effective connectivity for models involving fewer than eight regions of interest (Seghier & Friston, 2013).

After determining VOIs the anatomical mask extraction was performed to obtain information deriving from anatomical atlases. Anatomical mask extraction refers to extracting binary images that outline specific brain regions of interest which serve as templates that define the spatial boundaries of ROIs. Anatomical information obtained from these masks further provides a basis for the selection of subject-specific coordinates guided by group maxima. In other words, group-level activation peaks are used to pinpoint the most relevant coordinates within each subject's brain. VOI activity can then be summarized by extracting combined

anatomical and group-level constraints for each subject, ensuring that both anatomical accuracy and functional relevance were maintained in the analysis. The present study used three anatomical atlases implemented in the FSL for this purpose: the Jülich histological brain atlas (Amunts et al., 2020) and the Harvard-Oxford atlas (Desikan et al., 2006; Frazier et al., 2005; Goldstein et al., 2007; Makris et al.,2006), and Probabilistic cerebellar atlas (Diedrichsen et al., 2009). Atlases visualized in FSLeyes(McCarthy, 2024) are illustrated in Figures 4.11, 4.12, and 4.13.

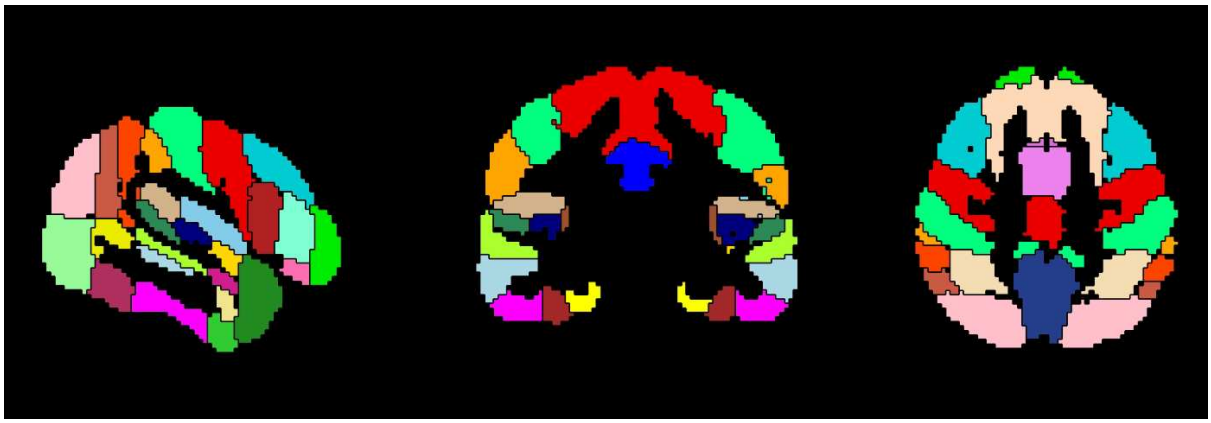

Figure 4.11 Harvard-Oxford atlas vi sualized in the FSLeyes

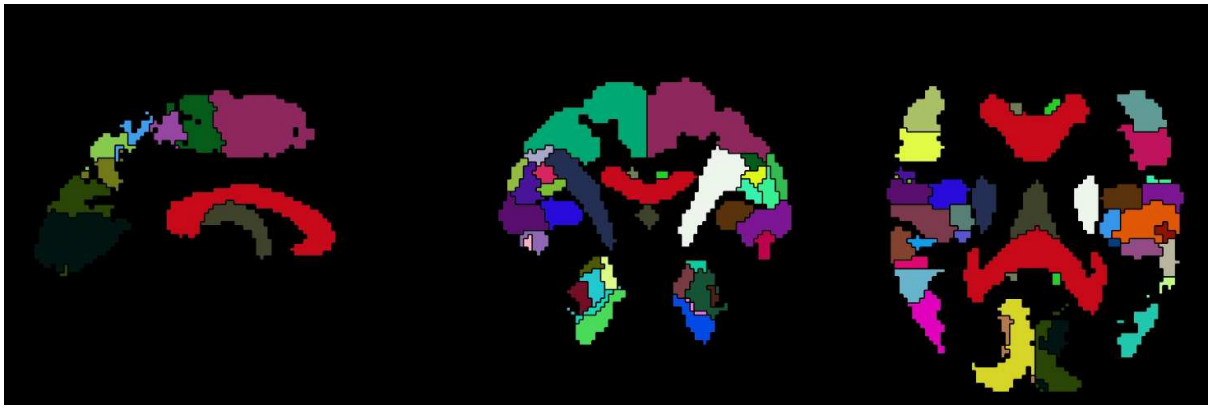

Figure 4.12 Jülich histological brain atlas visualiezed in the FSLeyes

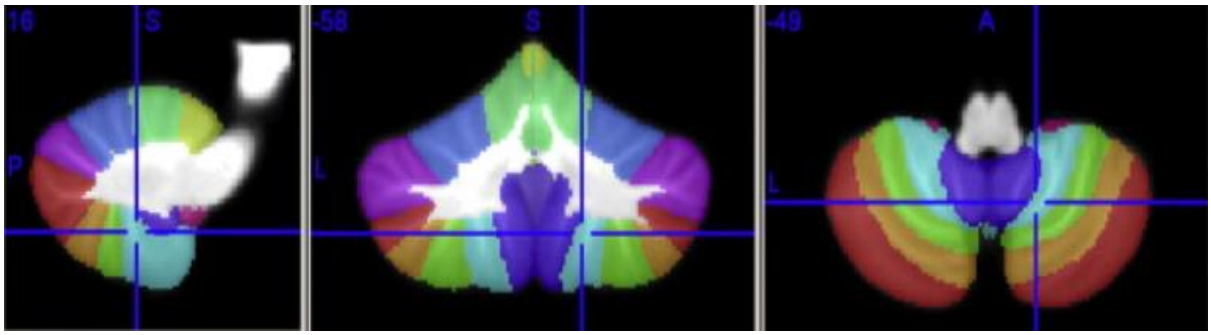

Figure 4.13 Probabilistic cerebellar atlas (Diedrichsen et al., 2009).

The next step consisted of VOI extraction based on group activation. VOI extraction implies extracting the representative time series from the selected brain regions, taking into account previously created contrast. Therefore, time series are extracted only from the selected conditions. In this process, it is necessary to specify the geometry, dimensions, and thresholds of the contrast for each corresponding VOI. This information, as well as the coordinates of VOI on the group level, are shown in Table 4.6.1.

Region	Geometry	Coordinates	Threshold
MFG_R	Sphere, 15mm	[45.71; 10.99; 30.99]	0.005 Uncorrected
MFG_L	Sphere, 15mm	[-44.03; 4.81; 35.87]	0.005 Uncorrected
V5_R	Sphere, 15mm	[44.87; -66.83; 3.492]	0.005 Uncorrected
V5_L	Sphere, 15mm	[-41.17; -74.15; 4.95]	0.005 Uncorrected
CRUSI_R	Sphere, 10mm	[25.67; -75.48; -19.94]	0.005 Uncorrected
CRUSI_L	Sphere, 10mm	[-25.68; -72.01; -20.32]	0.005 Uncorrected
V1_BIL	Box, [50x50x50] mm3	[6.99; -78.34; 4.51]	0.005 Uncorrected

Table 4.7.1. Geometry selection of each ROI. *MFG_R - right middle frontal gyrus, MFG_L - left middle frontal gyrus, V5_R - right middle temporal region, V5_L - left middle temporal region, CRUSI_R - right crus I of the cerebellum, CRUSI_L - left crus I of the cerebellum, V1_BIL - bilateral primary visual cortex.*

The result of VOI extraction on the group level is the group-level mask images in the NIfTI format and the VOI.mat files containing the information about extracted masks. An example of an extracted time series for one VOI is shown in Figure 4.14.

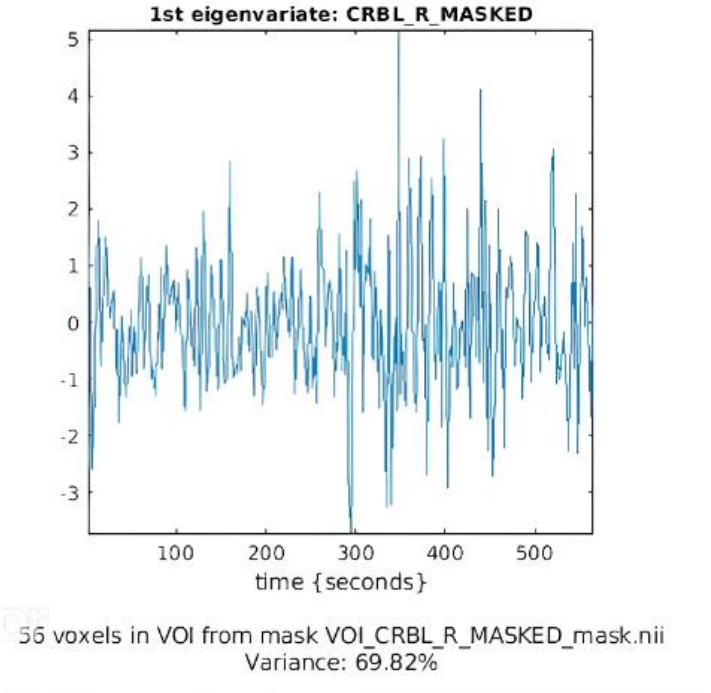

Figure 4.14. Extracted time series from the right Crus I of the cerebellum.

After the VOIs based on the group-level activation are extracted, the next step is the subject-specific VOI extraction. Figure 4.15 of a randomly selected subject illustrates the extracted MFG_L and MFG_R using the defined pipeline.

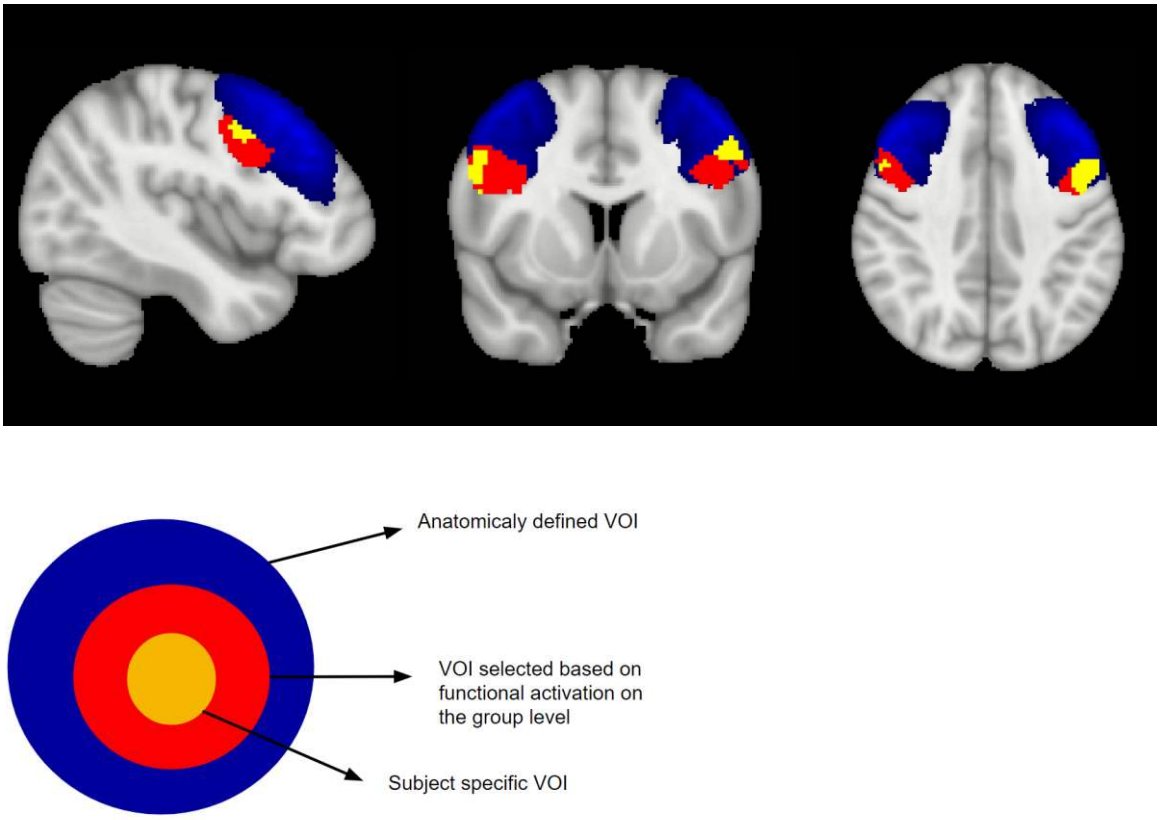

Figure 4.15Extracted VOI of MFG for the randomly selected subject. *The blue color represents the anatomically restricted region based on the Hardvard-Oxford atlas. The red color indicates the group-level activation obtained from the group-level SPM.mat file. The yellow color indicates the region selected from subject-specific activation of the randomly selected subject.*

While performing VOI extraction based on the subject-specific activation in the Full-field sinusoidal grating task, we encountered some difficulties, most likely due to the passive nature of the task. This resulted in the "empty" voxels with no significant activation in the ROIs in most participants. Therefore, we decided to proceed with further analysis only on the coherent motion detection task. Additionally, four subjects (S11, S18, S30, S37), two in each group, exhibited the same difficulties, thus we excluded them from the study.

4.8 Dynamical Casual Modeling

Testing models

The present study used Dynamical Casual Modeling (DCM) on fMRI data to investigate patterns of effective brain connectivity in the visual attention network in DD and TR. To compare the DD group with the TR group, the 7 nodes of volume of interest were kept constant across all models. The selected nodes included: V1_BIL, V5_R, V5_L, MFG_R, MFG_L, CRUSI_R, CRUSI_L. The selected nodes for DCM analysis are illustrated in Figure 4.16.

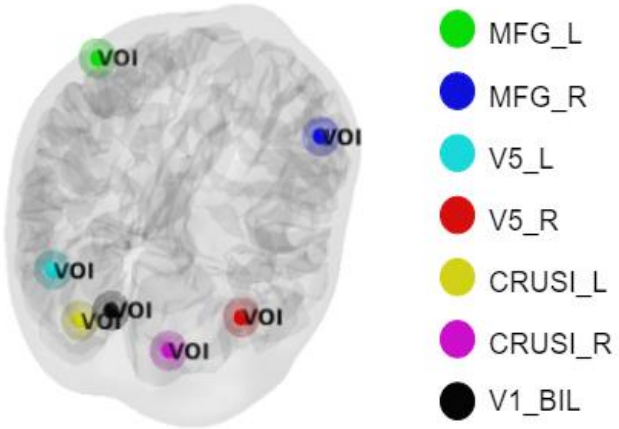

Figure 4.16 VOI selected for DCM analysis. *MFG_L: Left Middle Frontal Gyrus, MFG_R: Right Middle Frontal Gyrus, V5_L: Left Middle Temporal Cortex, V5_R: Right Middle Temporal Cortex, V1_BIL: Bilateral Primary Visual Cortex, CRUSI_L: Left Crus I of Cerebellum, CRUSI_R: Right Crus I of the Cerebellum.*

Specifically, this study employed Random Effects Bayesian Model Selection (RFX BMS) to determine the best-fitting model from a set of models for each group given the observed data. The same set of models was tested for both groups to ensure valid comparisons.

In DCM studies, a prevalent approach involves defining models starting from a fully connected model, subsequently pruning connections, and developing reduced models based on current literature, existing knowledge, and hypotheses. A fully connected model refers to a model with an interconnected architecture among all nodes of interest, which does not reflect any prior knowledge or assumptions. This study employed the same strategy. However, the fully connected model was excluded from the final analysis due to the inherent bias in DCM towards such models (Stephan et al., 2007). Fully connected models, particularly those with

numerous regions and connections, tend to become overly complex. This complexity arises from the large number of parameters that need to be estimated, increasing the risk of the model being excessively influenced by noise and thus overfitted. Consequently, while the model may appear to be the best fit, its generalization capability is often limited (Stephan et al., 2007).

Four reduced models were developed, each representing a different hypothesis regarding potential effective connectivity patterns based on the nature of the task and current understandings of visual attention networks. For each model, the driving input of Matrix C was configured to enter V1_BIL, consistent with the visual nature of the task. Furthermore, the anatomical contralateral connectivity between the cerebellum and cerebrum was considered for all models (Roostaei et al., 2014). Specified models are the following:

Model 1 emphasizes bidirectional connections among visual areas and visual areas (V1_BIL, V5_L, and V5_R) and the cerebellum (CRUSI_L and CRUSI_R) with frontal regions (MFG_L and MFG_R) receiving inputs through V5. Specifically, it models the bidirectional connectivity between V1_BIL and V5_L and V5_R as well as with CRUSI_L and CRUSI_R. Furthermore, bidirectional connectivity of V5_R with the CRUSI_L and between V5_L and CRUSI_R are included in this model. Family, connections from V5_R to MFG_R and V5_L and MFG_L are included in Model 1.

Model 2 highlights connections between visual areas and MFG_L and MFG_R, while the CRUSI_L and CRUSI_R receive inputs through V5_R and V5_L respectively. This model contains bidirectional connections between V1_BIL and V5_R and V5_L, as well as between V1_BIL and MFG_L and MFG_R. Further, MFG_L and MFG_R have bidirectional connections with both V5_R and V5_L. Moreover, unidirectional connections from V5_L to CRUSI_R and from V5_R to CRUSI_L are modeled here. Lastly, the direct bidirectional connections between MFG_L and MFG_R with CRUSI_R and CRUSI_L, respectively, are implemented in Model 2.

Model 3 considers the right-lateralized nature of VAN, thus excluding MFG_L from the model. Here, V1_BIL has bidirectional connections with MFG_R, CRUSI_R and CRUSI_L, as well as with V5_R and V5_L. Additionally, bidirectional connections between V5_R and V5_L with MFG_R are modeled in the Model 3. Furthermore, a bidirectional connection between MFG_R and CRUSI_L is included. Connections from V5_R to CUSI_L and from V5_L to CRUSI_R are modeled as well.

Model 4 combines the connectivity of visual areas with both cerebellar areas and frontal areas comprising a more complex architecture compared to the rest of the defined models. It highlights the bidirectional connectivity between MFG_L and MFG_R as well as between MFG_L and CRUSI_R and between MFG_R and CRUSI_L.

All described models are illustrated in Figure 4.17.

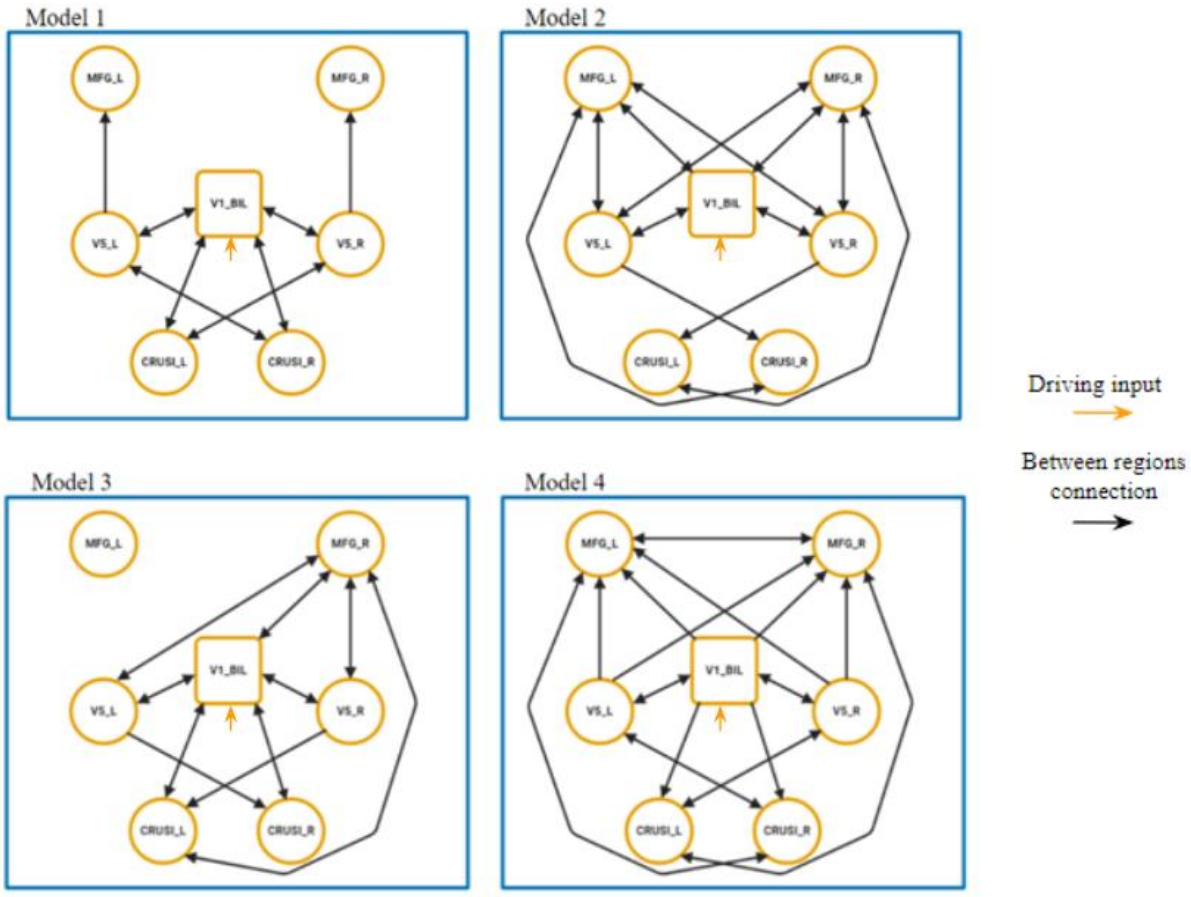

Figure 4.17 **Tested DCM models.** *MFG_R – right middle frontal gyrus; MFG_L – left middle frontal gyrus; V5_R – right middle temporal visual area; V5_L – left middle temporal visual area; CRUSI_R – right crus I of the cerebellum; CRUSI_L – left crus I of the cerebellum; V1_BIL – bilateral primary visual cortex.*

After obtaining the best-fitting model for both groups, the Bayesian Model Averaging (BMA) was used to further explore the nature of patterns of connectivity in selected models.

5 Results

5.1. Group level Analysis Results

GLM estimation for the group analysis with the Coherence-15 contrast revealed significant task-dependent activation ($p < 0.001$ uncorrected) in several brain regions of the visual attention network in the cerebrum and cerebellum in both DD and TR groups. The results of this group analysis for the TR and DD groups are visualized with xjview (https://www.alivelearn.net/xjview) in Figure 5.1. The regions with significant activation included the left and right middle frontal gyrus (MFG_L and MFG_R), left and right middle temporal cortex (V5_L and V5_R), left and right crus I of the cerebellum (CRUSI_L and CRUSI_R), and bilateral primary visual cortex (V1_BIL) as shown in Figure 5.2.

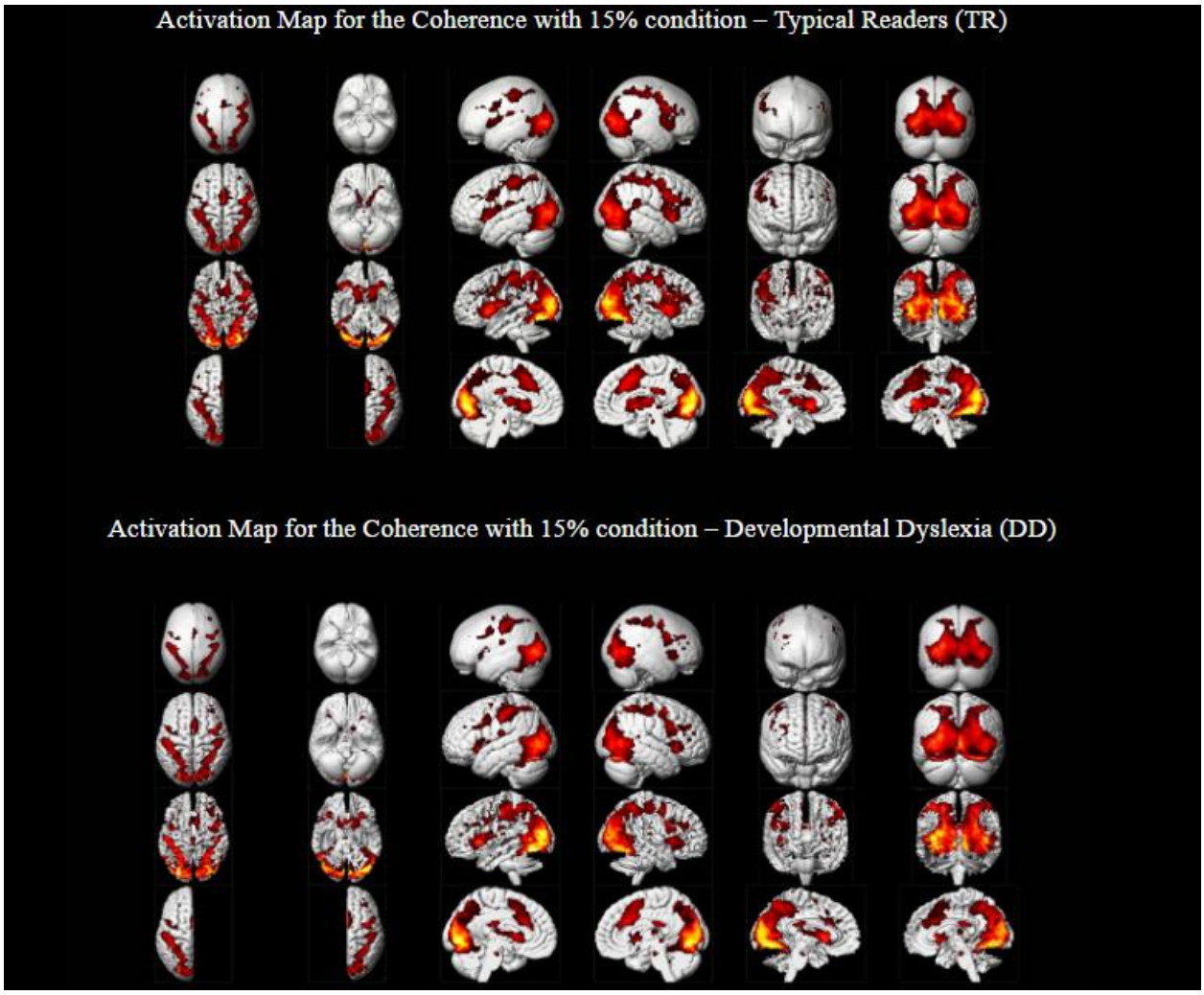

Figure 5.1 Activation map of the estimated GLM with the contrast Coherence- 15 in the TR and DD group. *The p<0.001 activation maps of overall activation of TR and DD groups on Coherence 15 condition visualized using xjview toolbox.*

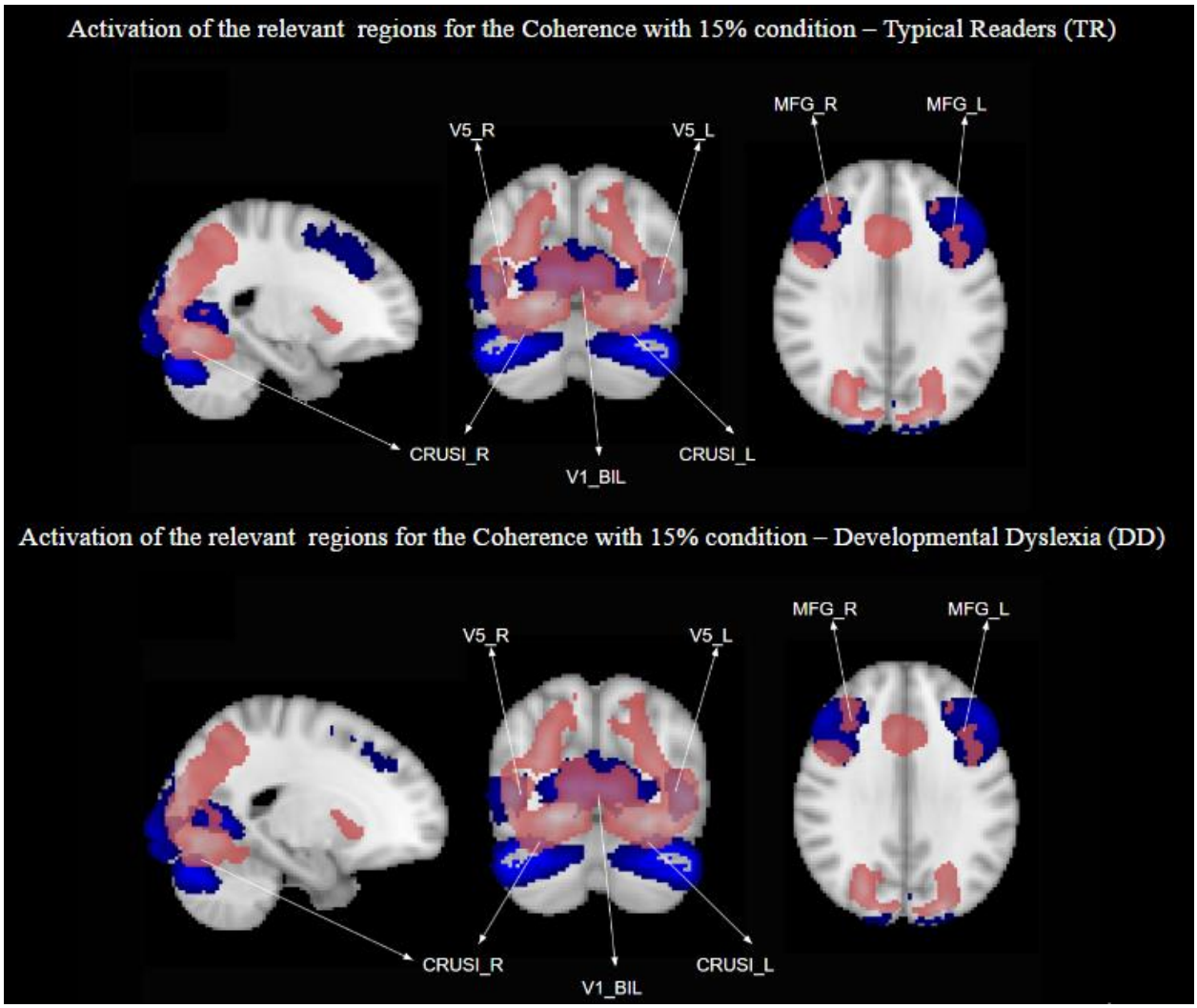

Figure 5.2 Activation of the relevant regions of the visual attention network with the Coherence - 15 contrast in TR and DD groups. *Group-level activation ($p<0.001$) (pink color) was overlaid on the anatomical masks of the relevant VOIs.*

These results were further used to establish ROIs and perform VOI extraction and DCM analysis.

5.2. Conjunction Analysis Results

An implemented fully factorial design with two experimental tasks (coherent motion detection and full-field sinusoidal grating) across two groups (DD and TR) to compare the activations showed activity in several brain regions involved in visual attention. In particular, the included design showed significant overlap ($p>0.001$ uncorrected) between task type and group activation in: MFG_L, MFG_R, V5_L, V5_R, CRUSI_L, CRUSI_R, and V1_BIL. Figure 5.3 presents illustrations of a conjunction analysis at $p>0.001$ uncorrected, visualized with xjview.

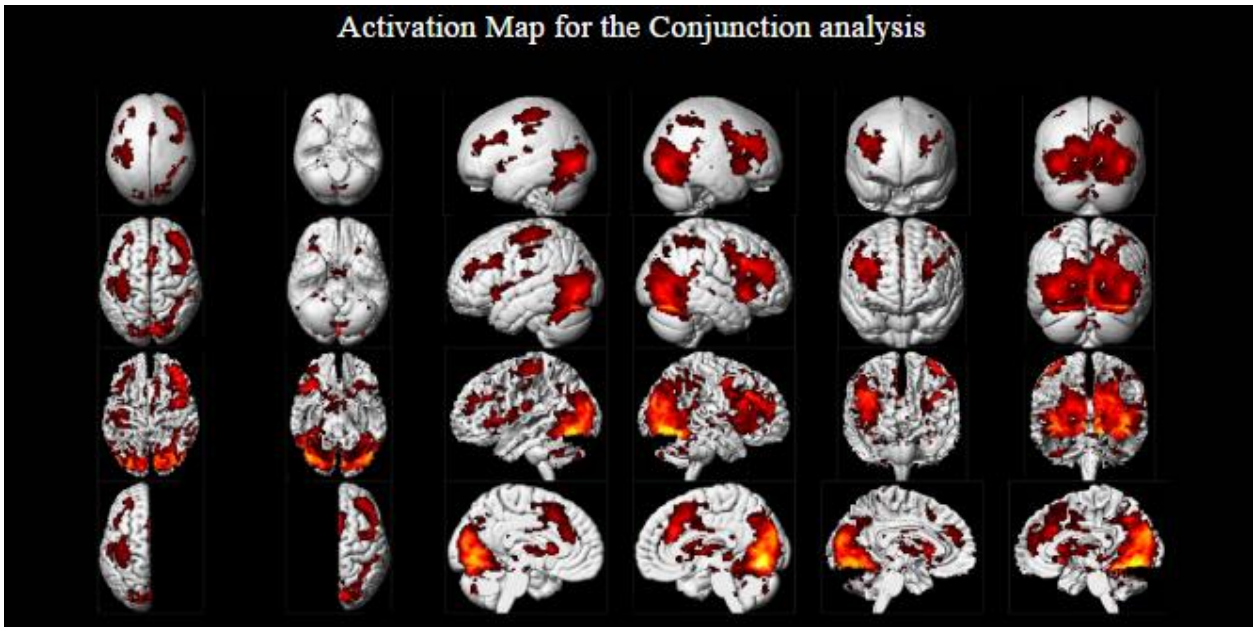

Figure 5.3. Activation on the group level was obtained from the conjunction analysis and used for selecting ROIs.

Furthermore, to gain a better insight into the active regions revealed by the conjunction analysis, the results of this procedure were overlaid on the anatomical masks of the relevant brain regions involved in visual attention obtained from the Harvard-Oxford atlas (Desikan et al., 2006; Frazier et al., 2005; Goldstein et al., 2007; Makris et al.,2006). These results confirmed that the main regions of interest have significant activation ($p < 0.001$ uncorrected) in each condition and, therefore, are suitable for further inclusion in the study as represented in Figure 5.4.

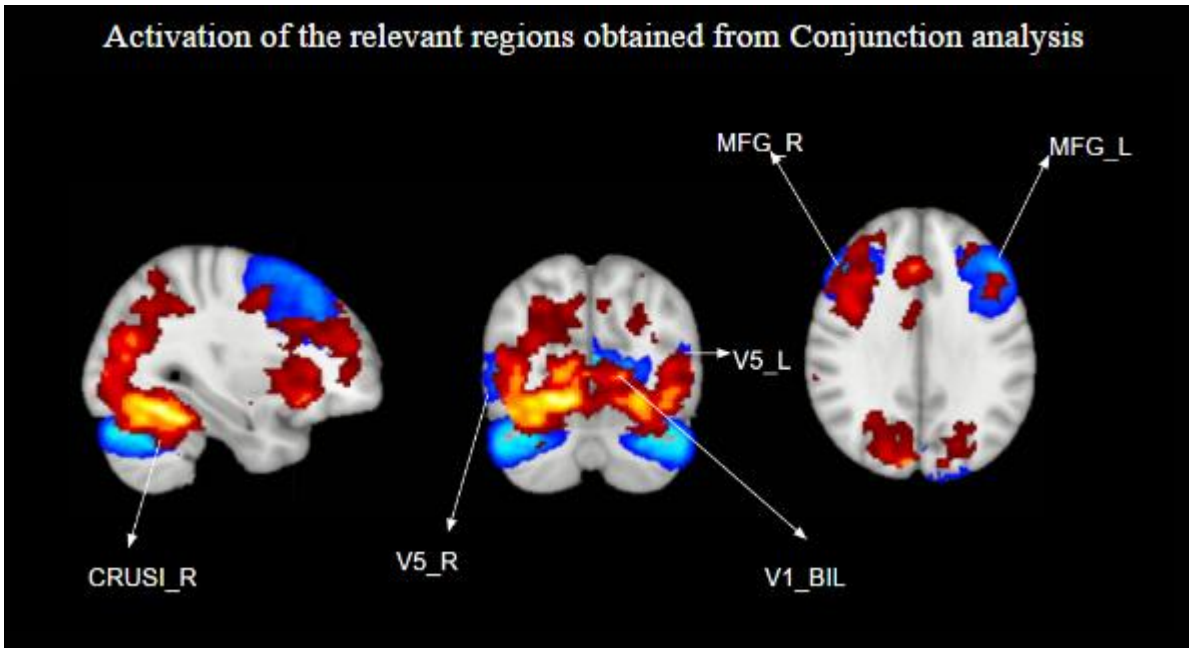

Figure 5.4 Activation obtained from conjunction analysis (red color) overlaid over anatomical masks of the determined VOIs (blue color).

5.3. Dynamical Casual Modeling Results

Dynamic Causal Modelling results after specification and the estimation of multiple models for each subject were used for the Bayesian Model Selection (RFX- BMS) in the further analysis. The result of the estimated time series of the DCM models was obtained for each participant, as the examples subject was shown in Figure 5.5. Further subject-specific exploration was conducted, and the results from t he randomly selected subject's SPM DCM are discussed in the following text.

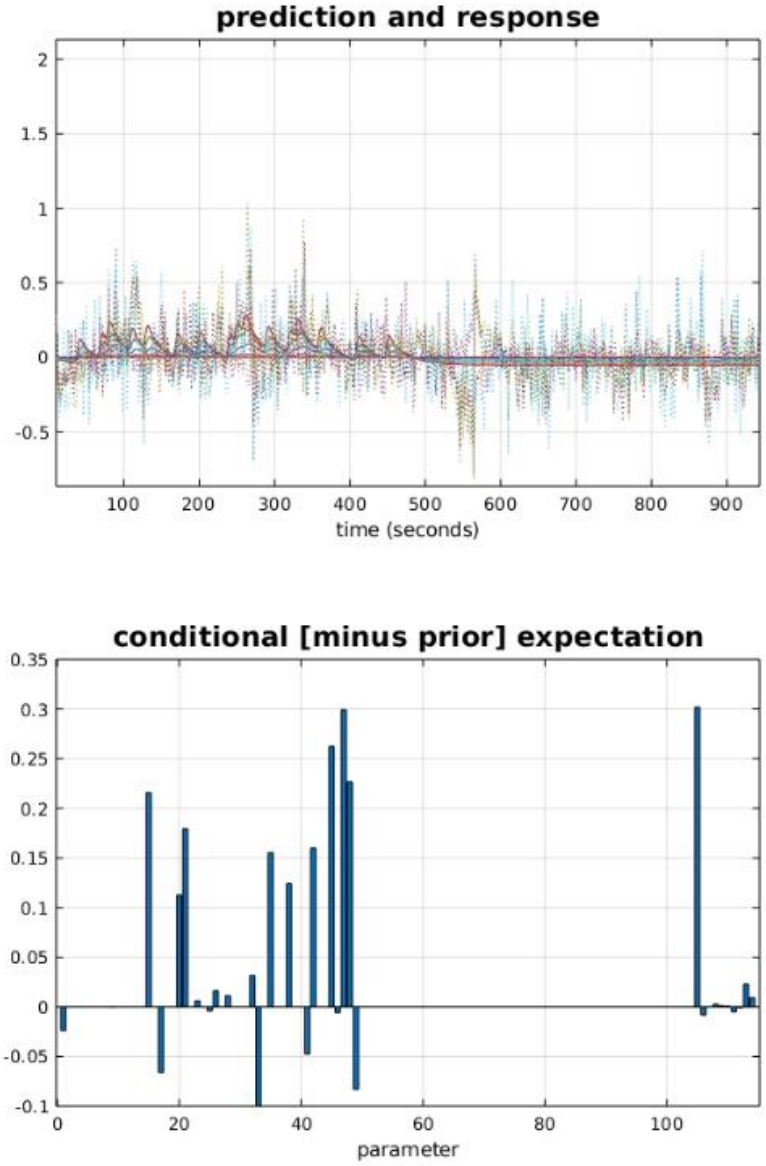

Figure 5.5 Estimated time series of the DCM model for one randomly selected participant. The upper row represents the predicted and observed time series with each line representing one brain region. The lower row represents the expectation of the connectivity parameters, where the empty parameters represent Matrix B that is not included in the current study.

Figure 5.6 illustrates an example of the output signal (Hz) for both the predicted response (blue line) and the observed response (red dots) across each ROI over time (seconds).

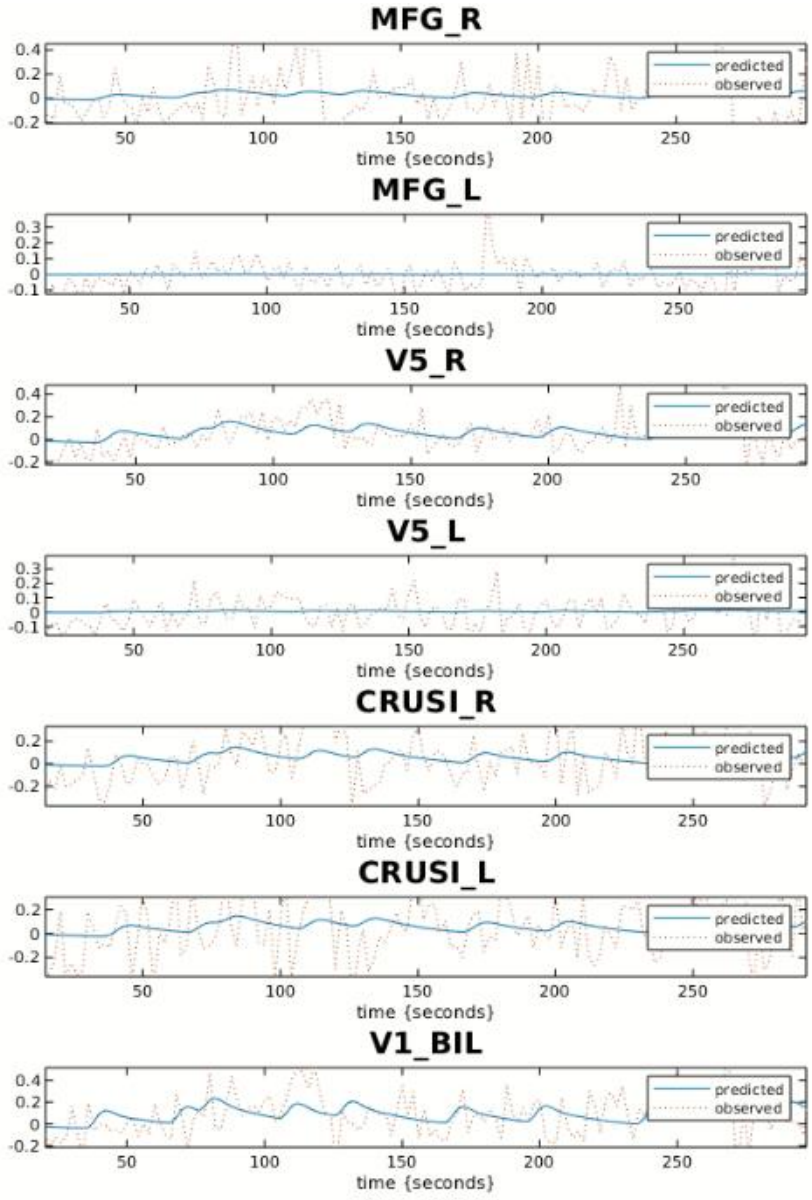

Figure 5.6 Plot of randomly selected subject's predicted and observed response of each VOI on Model 1.

Additionally, Figure 5.7. displays the fixed connection probabilities (A) and strengths (B) for the randomly selected subject. Each color bar represents the signals from VOIs that have reached the target region of interest.

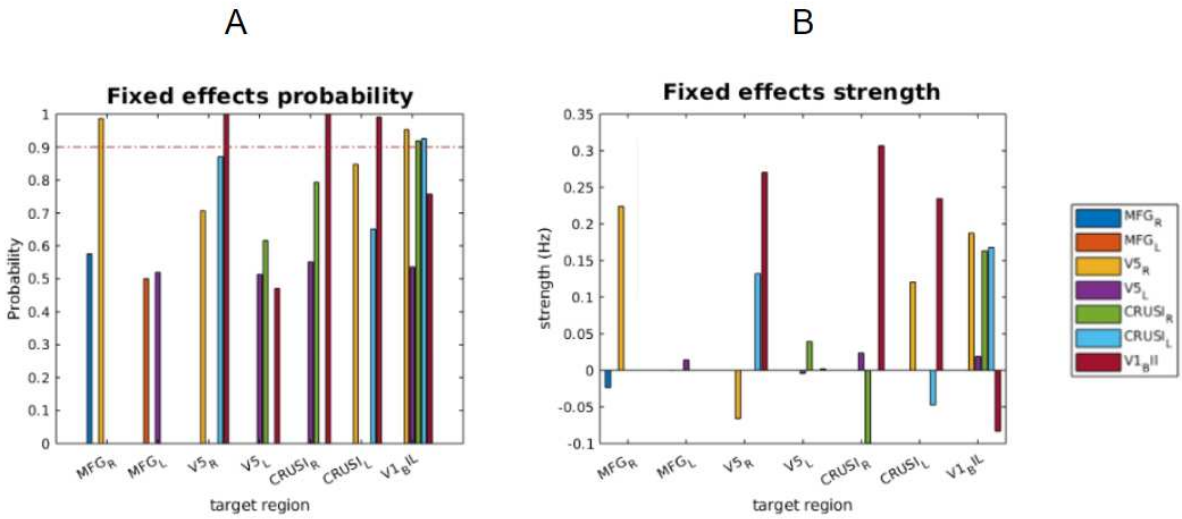

Figure 5.7 **Fixed connections probabilities (A) and strength (B) for one randomly selected participant.** *MFG_R – right middle frontal gyrus; MFG_L – left middle frontal gyrus; V5_R – right middle temporal visual area; V5_L – left middle temporal visual area; CRUSI_R – right crus I of the cerebellum; CRUSI_L – left crus I of the cerebellum; V1_BIL – bilateral primary visual cortex.*

Figure 5.7. illustrated the nature of the fixed connection (Matrix A), where positive strengths reflect facilitation and negative parameters suggest inhibition of neural activity. For instance, CRUSI_R has the strongest facilitating connection coming from V1. Further, only a few inhibiting connections can be observed and their strength is low. The posterior probability of the majority of connections is higher than 0.5, while connections coming from V1 to V5_R, CRUSI_R, and CRUSI_L, and from V5_R coming to MFG_R and V1_ BIL are somewhat larger, reaching above a value of 0.9.

Additionally, the MATLAB function <spm_dcm_fmri_check(GCM)> was utilized to perform diagnostics on the DCM models for a randomly selected subject, offering insights into the percentage of explained variance. Figure 5.8 illustrates these findings, where the upper part displays the predicted time series with solid lines, while the observed data is represented by dotted lines. The estimated parameters from matrix A are shown in the lower part of the figure.

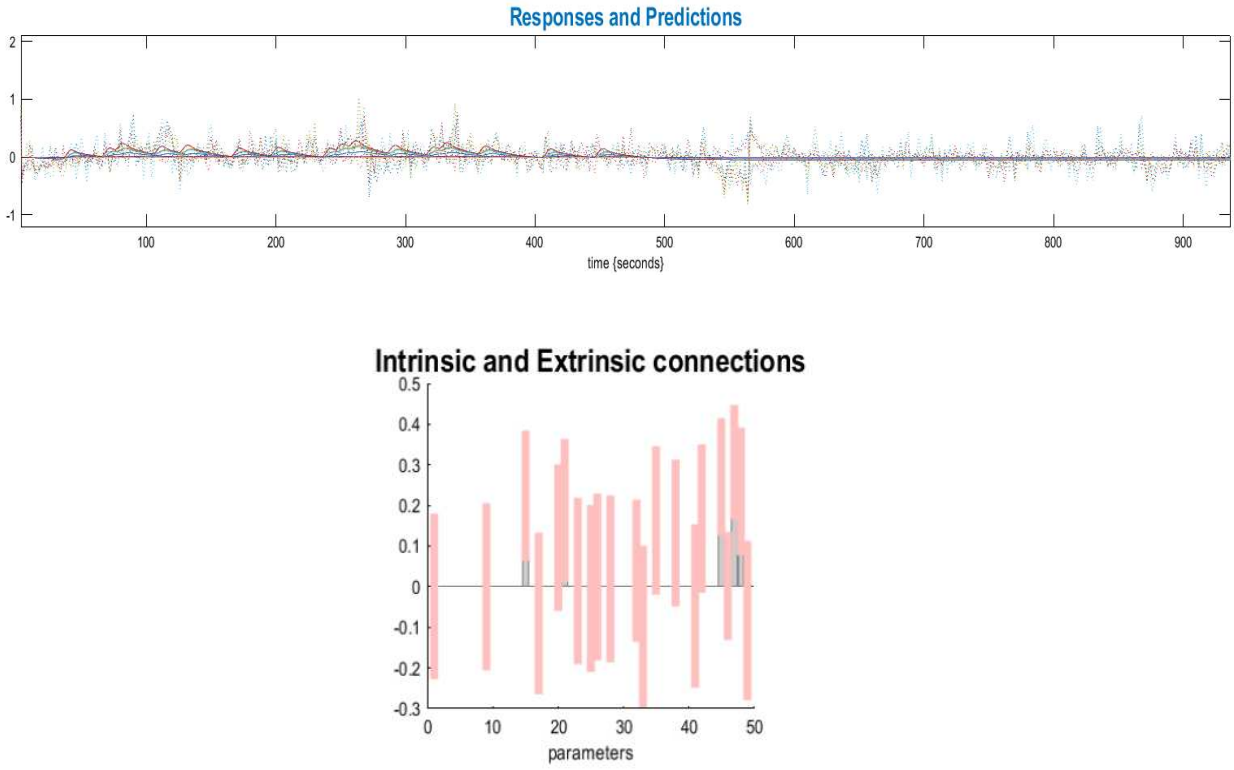

Figure 5.8 **DCM diagnostics for one randomly selected subject on one model.**

Bayesian Model Selection

The optimal model architecture was determined from four specified models for both the DD and TR groups using Random Effects Bayesian Model Selection (RFX BMS). The selection process for the TR group is illustrated in Figure 5.9, while for the DD group, it is represented in Figure 5.10. The results indicate that, among the four tested models, Model 3, representing the right-lateralized VAN, most effectively explains the observed data in the TR group. Conversely, Model 1, which emphasizes bidirectional connections between visual and cerebellar areas, best accounts for the observed data in the DD group. Moreover, a greater heterogeneity among participants in the DD group can be observed, as evidenced by the posterior probabilities. The winning model in the DD group does not dominate as clearly as in the TR group, and there is significant evidence supporting other models.

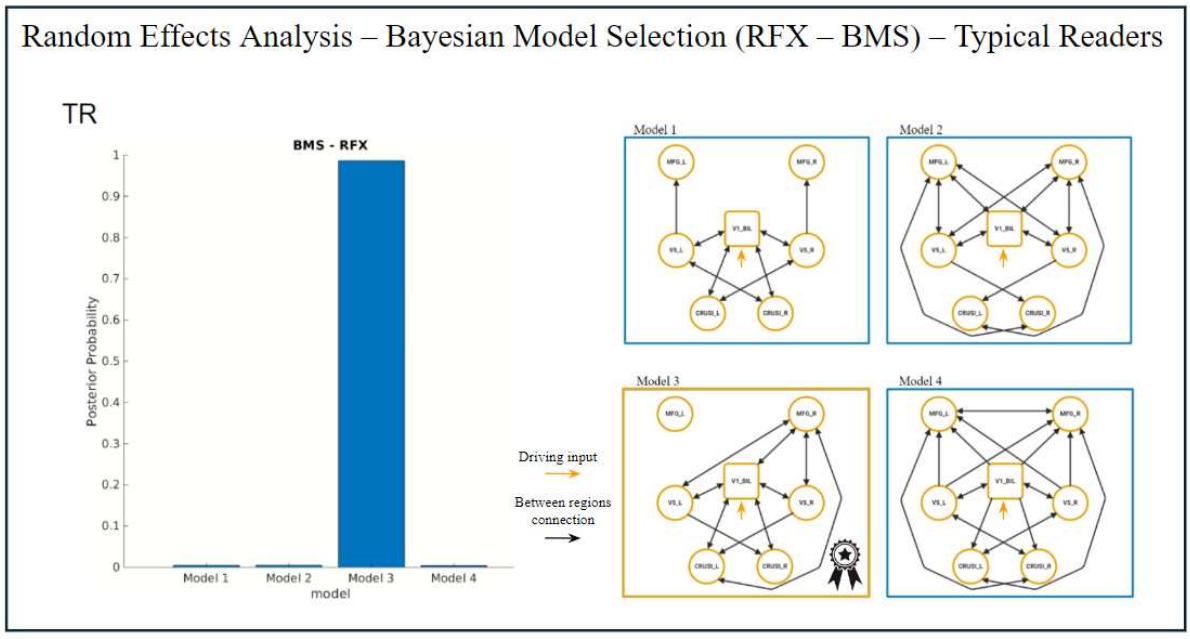

Figure 5.9 RFX BMS results for the TR group. *RFX-BMS results identified model 3 as the winning model in the TR group with the probability of >90%. MFG_R – right middle frontal gyrus; MFG_L – left middle frontal gyrus; V5_R – right middle temporal visual area; V5_L – left middle temporal visual area; CRUSI_R – right crus I of the cerebellum; CRUSI_L – left crus I of the cerebellum; V1_BIL – bilateral primary visual cortex.*

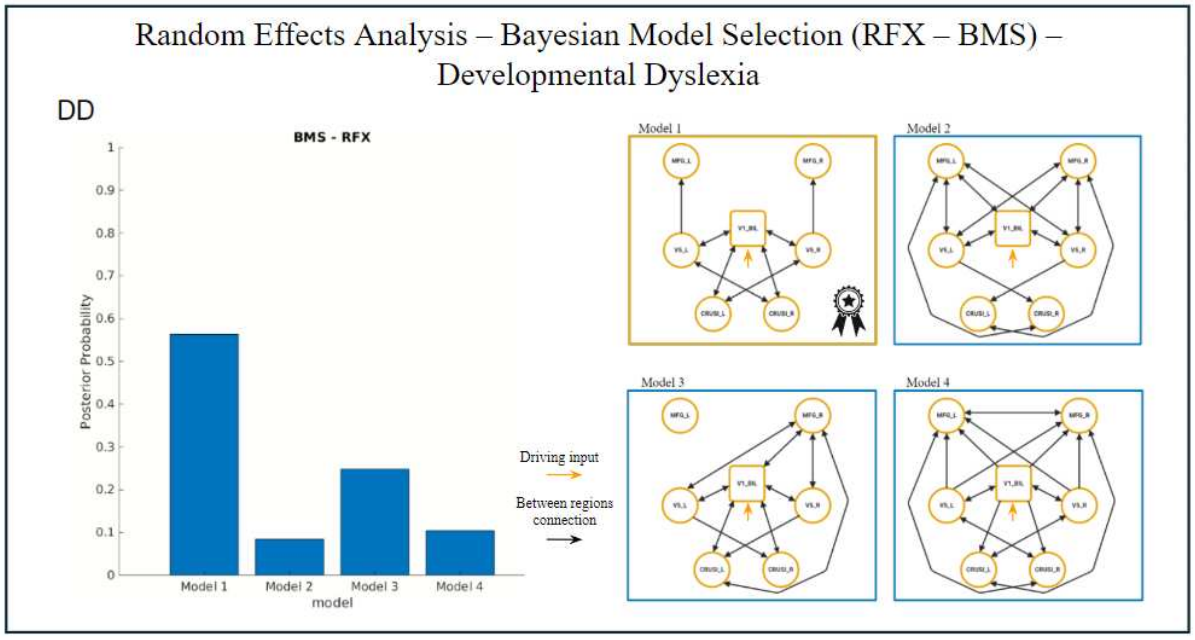

Figure 5.10 RFX BMS results for DD group. *RFX-BMS results identified model 1 as the winning model in the DD group with the probability of >50%. MFG_R – right middle frontal gyrus; MFG_L – left middle frontal gyrus; V5_R – right middle temporal visual area; V5_L – left middle temporal visual area; CRUSI_R – right crus I of the cerebellum; CRUSI_L – left crus I of the cerebellum; V1_BIL – bilateral primary visual cortex.*

Bayesian Model Averaging

For further inspection of the nature of the optimal models, we used BMA to look into the strength of the connection between regions and possible differences between groups. BMA results for Model 3 (the BMS winning model in the TR group) in each group are shown in Figure 5.11, whilethe results for Model 1 (the BMS winning model in the DD group), are represented in Figure 5.12.

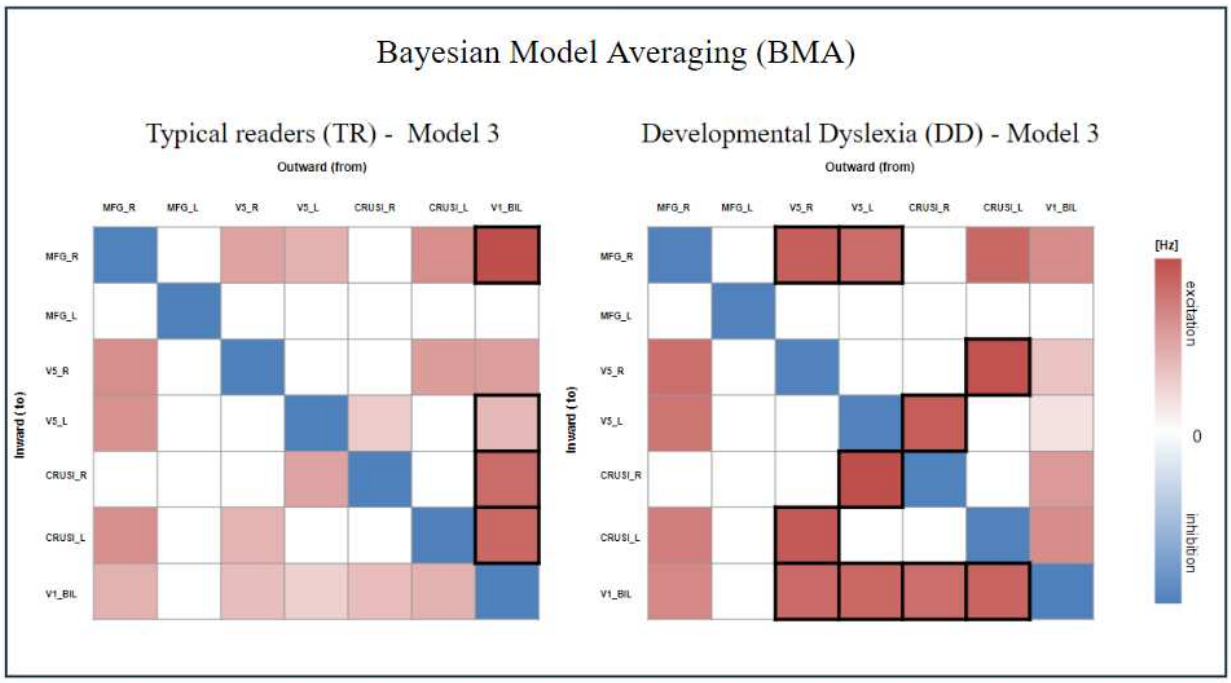

Figure 5.11BMA results of Model 3 (winning model for the TR group) for both TR and DD groups. *Changes in the strength of connections between groups are labelled with a black frame, connections that are stronger in the TR group are marked in the TR graph (left), while the connections that are stronger in the DD group are indicated in the DD graph (right).*

Results of the BMA of Model 3 in Figure 5.3.8. show changes in the strength of the connection between several regions across groups. Connections from V1_BIL have weaker strength in the DD group compared to the TR group. On the other hand, the majority of the other connections are stronger in the DD group. More specifically observable differences can be seen in connections:

- From V5_Rto MFG_R, from V5_R to CRUSI_L, from V5_R to V1_BIL;
- From V5_L to MFG_R, from V5_L to CRUSI_R, from V5_L to V1_BIL;
- From CRUSI_R to V5_L, from CRUSI_R to V1_BIL, from CRUSI_L to V5_R, from CRUSI_L to V1_BIL.

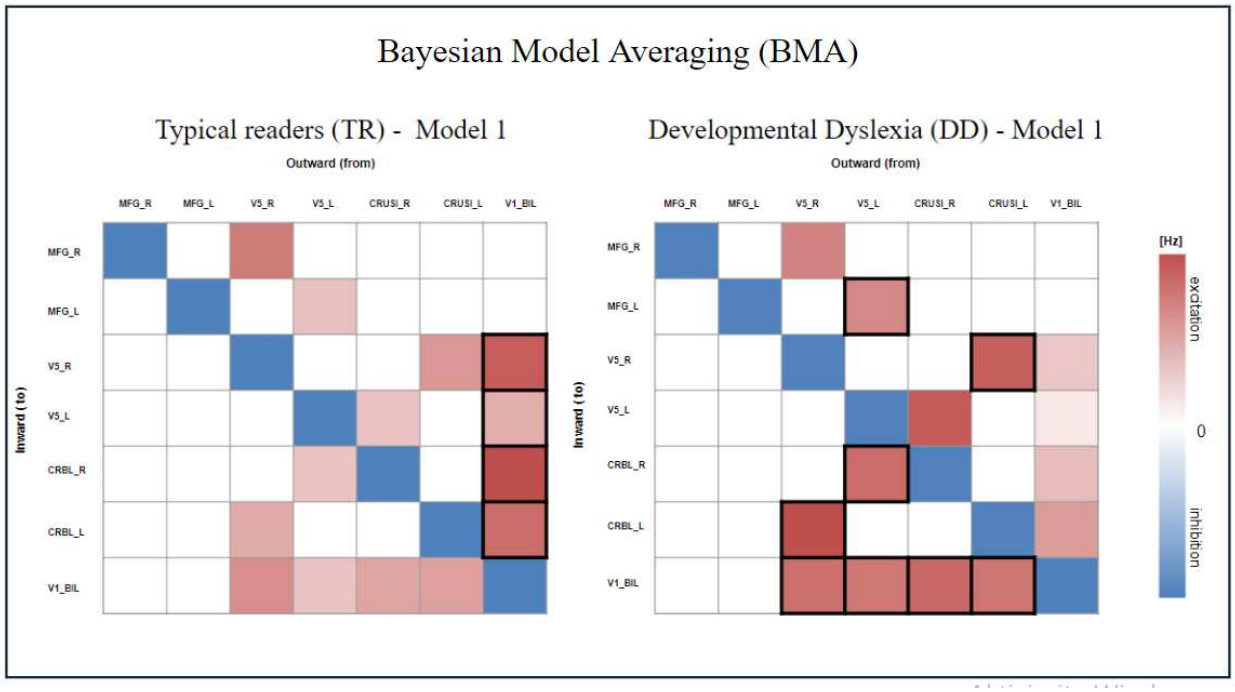

Figure 5.12. BMA results of Model 1 (winning model for the DD group) for both TR and DD groups. *Changes in the strength of connections between groups are labelled with a black frame, connections that are stronger in the TR group are marked in the TR graph (left), while the connections that are stronger in the DD group are indicated in the DD graph (right).*

Results of the BMA of Model 1 in Figure 5.3.9. show changes in the strength of the connection between several regions across groups. Similarly, with Model 3, connections from V1_BIL have weaker strength in the DD group compared to the TR group in Model 1. Other connections show higher strength in the DD group. More specifically observable differences can be seen in connections:

- From V5_R to CRUSI_L and from V5_R to V1_BIL
- From V5_L to CMFG_L, from V5_L to CRUSI_R, and from V5_L to V1_BIL
- From CRUSI_R to V5_L, and from CRUSI_R to V1_BIL
- From CRUSI_L to V5_R, and to V1_BIL

6 Discussion

The present study is the first to conduct Dynamical Causal Modeling (DCM) on fMRI data with visual attention task to explore differences in effective brain connectivity within the cortico-cerebellar visual attention network between typical readers and children with developmental dyslexia (DD). DD is a complex neurodevelopmental disorder with a broad range of symptoms (Smirni et al., 2020). Previous studies have established impairments in both visual and attention networks (Stein, 2003; Freedman et al., 2020), as well as in the cerebellum (Nicolson et al., 2001) shedding new light on the underlying processes of DD. However, the causal roles of the cerebellum in the DD have not yet been firmly established (Ashburn et al., 2020), and therefore, studying causal connections between these networks can have great importance for a better understanding of which mechanisms drive the symptoms of this disorder. To investigate these connections, previously published study by Mascheretti et al.,2021 was used with the participants performed a coherent motion sensitivity detection task, which assesses motion sensitivity (Cornelissen et al., 1998), a skill often impaired in individuals with DD (Stein, 2022). Specifically, this study defined a cortico-cerebellar visual attention network comprising seven nodes of interest: bilateral primary visual cortex (V1_BIL), left and right middle temporal areas (V5_L and V5_R), left and right middle frontal gyrus (MFG_L and MFG_R), and left and right crus I of the cerebellum (CRUSI_L and CRUSI_R). We aimed to reveal potential differences in causal connectivity patterns between those regions in the DD and TR groups. Thus, four models, each representing a specific hypothesis and architecture of effective connectivity were created based on current knowledge and assumptions of functioning in the visual attention networks, as well as the nature of connectivity between the cerebellum and cerebrum.

The results of the current study revealed that distinct models with different architectures best explain the data for the DD and TR groups. In the TR group, Model 3, representing the right-lateralized ventral attention network (VAN) was selected as the most probable among the four defined models. This finding aligns with existing literature that emphasizes the importance of right-hemispheric regions in visual attention processes (Corbetta & Shulman, 2002). The dominance of this model suggests that typical readers might rely more heavily on a right-lateralized network for tasks involving visual attention. In contrast, Model 1, featuring bidirectional connections between visual and cerebellar areas, was found to be the most explanatory in the DD group. This model suggests that children with DD have a different

neural strategy in visual and attentional processing. Our results are consistent with previous functional connectivity studies which identified significant differences in brain region activation and connectivity patterns between children with DD and TR (Fin et al., 2014; Mascheretti et al., 2021; Schurz et al., 2015). However, unlike prior studies that focused on functional connectivity without directional specificity, this study implicates the causal relationships between regions providing a deeper understanding of impairments in the connectivity in DD.

Moreover, the involvement of both the left and right middle frontal gyrus (MFG_L and MFG_R) in Model 1 for children with DD might suggest that those individuals utilize both hemispheres to compensate for deficits in visual and attentional processing. The middle frontal gyrus (MFG) plays a crucial role in higher cognitive functions, including working memory, attention, and executive control (Japee et al., 2015). This bilateral involvement could indicate that the DD group requires additional neural resources to achieve similar levels of performance as the typical readers, a phenomenon supported by previous research showing that individuals with DD often engage compensatory neural mechanisms (Shaywitz & Shaywitz, 2008).

Additionally, Model 3 captures direct bidirectional connections between V1 and MFG_R, despite the absence of established anatomical connections between these regions. This finding underscores that effective connectivity does not necessarily reflect direct anatomical pathways. In contrast, the DD group's winning model, Model 1, lacks these direct causal connections, suggesting impaired or altered functional integration. This absence might reflect that children with DD may rely on more complex and distributed networks for processing visual information. Instead of a direct pathway, these children might engage additional regions and pathways to compensate for their visual processing deficits. This complexity can be necessary due to the inefficiencies or deficits in their primary visual processing areas, requiring additional neural resources to support attention functions as supported by the literature (Everatt, et al., 1999; Bacon et al.,2010; Heiervang, et al., 2003).

Further, the direct connection between the cerebellum and MFG_R in Model 3 reflects the cerebellum's role in cognitive functions, such as attention and language (Schmahmann& Caplan, 2006), supporting the findings that the cerebellum is involved in the cognitive processes contributing to efficient visual attention and task performance (Brissenden & Somers, 2019). On the other hand, the lack of those connections in the winning model for the

DD group implies different involvement and impairment of the cerebellum in DD supporting the cerebellar deficit theory (Nicolson and Fawcett 1990).

The important point to be mentioned is the lower posterior evidence of the winning model in the DD group and disperse results among all four models. The greater heterogeneity observed in the DD group's model selection indicates a less consistent pattern of effective connectivity compared to the TR group. This variability could point to individual differences in how children with DD process visual information (Ziegler et al., 2008). The lack of a dominant model suggests that a single neural pathway or strategy might not characterize developmental dyslexia. Instead, it highlights the possibility of multiple underlying neural mechanisms contributing to the disorder in line with the previous studies proposing the multifactorial etiology of DD (Pennington, 2006).

Additionally, Bayesian Model Averaging (BMA) results revealed weaker excitatory connections originating from V1 in the DD group compared to the TR group, even within the winning model for DD. This finding reveals an impaired visual pathway, potentially supporting the magnocellular theory of DD. The magnocellular pathway, which projects to V1, is crucial for visual processing and thus can affect the functioning of V1. Therefore, weaker connections coming from V1 align with previous research that has established the impaired functions of magnocellular pathways in individuals with DD (Stein, 2003; Stein, 2018). Since brain's dynamic connectivity is influenced by transcriptional heterogeneity, suggesting that regional variations in gene expression contribute to the distinct dynamic behaviors of different brain areas (Deco et al., 2021a). Thus the possible differential gene expression and the transcriptional heterogeneity associated with DD could underline the observed weaker excitatory connections from V1, as regional gene expression profiles might affect the development and function of the magnocellular pathways. Furthermore, other connections appear to be stronger in the DD group, indicating compensatory mechanisms that may be employed to overcome the deficits in the connections originating from V1. The establishment of directional relationships, as emphasized by Deco et al. (2021b), underscores the causal role of impaired excitatory connections in disrupting the hierarchical organization of the brain's global workspace. Effective connectivity highlights how changes in one region can causally influence another, revealing adaptive mechanisms that might not be apparent in structural or functional connectivity. In DD, this suggests that while structural and functional connectivity is altered, the brain dynamically reorganizes its effective connectivity to

compensate for these deficits, supporting the idea of a flexible neural network adapting to impairments in specific pathways.

Advantages of the study

The current study has two main advantages:

(a) Employing DCM on fMRI in DD;

(b) Inclusion of cerebellum in the analysis.

(a) *Employing DCM on fMRI in DD.* Even though DD is well researched and there is a growing body of functional connectivity studies in this field, current DD literature comprises only a few studies employing effective connectivity and DCM. The available literature on DD that employs DCM is summarized in Table 6.1. Therefore, the present study is a step forward to a more comprehensive understanding of the connectivity process in DD. Furthermore, the present study provided an in-depth exploration of the specific nature of connections by employing BMA, allowing a comparison of the strengths of connectivity between TR and DD groups in the selected winning models.

Study	Task	Subjects	Nodes
Cao et al., 2008	Rhyming task	12 DD (2 females), 12 TR (4 females)	Bilateral medial frontal gyrus Left fusiform gyrus, inferior frontal gyrus, and inferior parietal lobule
Morken et al.,2017	Picture recognition Literacy tasks (logographic processing, alphabetic processing, orthographic processing, and sentence processing)	Longitudinal study Age 6: 6 DD (5 females), 12 TR (5 females) Age 8: 10 DD (5 females), 20 TR(8 females) Age 12: 10 DD (6 females), 17 TR (8 females)	Inferior frontal gyrus, precentral gyrus, superior temporal gyrus, inferior parietal lobule, and occipito-temporal cortex
Di Pietro et al., 2023	Phonological lexical decision task	83 TR (40 females), 49 DD (23 females)	Inferior frontal gyrus, precentral gyrus, inferior parietal lobule, visual word form area, primary visual cortex
Turker et al., 2023	Reading task	28 TR (13 females), 26 DD (17 females)	left inferior frontal gyrus left dorsal temporo-parietal cortex, left and right ventral occipito-temporal cortex, left supramarginal gyrus, bilateral lingual gyri, right cerebellum

Table 6.1 ***DD DCM Literature.***

(b) *Inclusion of cerebellum in the analysis*. An important advantage of the present study is the inclusion of the cerebellum (specifically the Crus I region) in the DCM analysis. As shown in Table 6.1, previous research has not incorporated this specific brain region nor utilized visual attention tasks in the context of DD. Thus, our approach provides valuable new insights. Particularly the incorporation of Crus I, allowed us to directly investigate the cerebellar deficit

theory of DD, and examine how cerebellar dysfunction impacts the broader neural network involved in reading and visual attention.

Potential Limitations and Considerations

The first aim of the study was to include two visual attention tasks: The full-field sinusoidal grating task and the coherent motion sensitivity detection task. However, due to the passive nature of the full-field sinusoidal grating task and the young age of the participants, maintaining their full engagement and attention to the task proved to be challenging. Consequently, participants were not consistently focused on the task, leading to lower neural activations. This further resulted in challenges in VOI extraction and therefore challenges in implementation of the DCM analysis, thus the task was excluded from the study. Including both tasks would have allowed for a more comprehensive examination of the visual attention network. The full-field sinusoidal grating task, and more specifically the magnocellular condition of this task could have provided more direct insights into the function of the magnocellular visual pathway. Moreover, the inclusion of both tasks could have highlighted the distinct and overlapping neural circuits involved in processing different types of visual stimuli, and therefore exclusion of the full-field sinusoidal grating task represents one of the limitations of the current study.

Further, although DCM is a promising methodology for exploiting causal relations of brain activations, its limitations must be considered. Firstly, as Seghier & Friston (2013) suggested DCM can reliably infer effective connectivity for models involving fewer than eight regions of interest due to the limitation of computational demands. Therefore, DCM may struggle to reliably infer effective connectivity in networks comprising more than a few regions of interest, limiting its application in exploring large-scale brain networks where interactions among numerous regions are crucial (Lohmann et al., 2020). Current study included seven regions of interest and further study should consider including large-scale network models that infer the effective (directed) connectivity among neuronal populations from neuroimaging data such as regression DCM (rDCM) (Frässle et al., 2017). Further, even though BMS accounts for the model complexity when computing the probabilities of the given models, the common bias towards the fully connected models (Stephan et al., 2007) should be kept in mind. For this reason, the current study excluded the fully connected model from analysis, preventing the selection of the model with the seemingly best fit but with limited generalization properties. Moreover, Lohmann and Couleges (2012) critique the

interpretability of DCM results, emphasizing the challenge of translating complex neuroimaging data into meaningful insights about neural interactions. They highlight that DCM assumptions may not always align with the true complexity of brain function, raising doubts about the validity of inferred connectivity patterns. Additionally, the limitations of model selection should be mentioned. Since DCM is a hypothesis-based approach, the model space is created by specifying several plausible models (Stephan et al., 2010), thus limitations in interpreting the model structure arise from how the model space is defined. Given the complexity of the pathology of DD, as well as the functioning of visual attention networks in healthy populations, the predefined model space makes it unlikely that the absolute optimal model for explaining the data will be found. Therefore, when referring to a "best", "winning" or "optimal" model in DCM, one has to be aware of the possibility that models outside the considered model space could better explain the given data. In conclusion, interactions among brain regions are still not fully understood (Lohmann et al.,2012), therefore there is still no method that can provide an entirely satisfactory approach in studying effective connectivity. However, despite its described limitations, DCM is a valuable tool that offers a robust framework for modeling and inferring the directional influences between brain regions, providing insights for advancing our understanding of neural dynamics in both healthy populations and pathology.

Future Studies

The present study provided valuable new insights into the neural patterns of DD; however, more studies are needed to achieve a full understanding of this neurodevelopmental disorder. Future studies could correlate clinical assessments of reading ability, attentional capacity, and other cognitive functions with the effective connectivity patterns identified through DCM, to identify more clear neural biomarkers of DD. This could further allow the development of new and more effective interventions for DD.

Conclusions

The present research was the first one to explore effective brain connectivity by using visual attentive task with fMRI protocol, including the regions of visual attention networks such as middle frontal gyrus and cerebellum in developmental dyslexia. The study provided insights into the impaired patterns of causal connectivity of this neurodevelopmental disorder, deepening the knowledge of previous functional connectivity studies. By employing Dynamical Causal Modeling on fMRI data, we were able to identify and compare the distinct neural strategies and connectivity patterns between children with developmental dyslexia and typical readers.

The study's results highlighted differences in neural strategies and connectivity patterns between the two groups. We revealed aberrant involvement of the cerebellum, as well as the compensatory involvement of the left middle frontal gyrus in developmental dyslexia compared to the control group, aligning with attention deficit, cerebellar deficit, and magnocellular theories of developmental dyslexia.

By advancing our understanding of the causal connectivity patterns within the cortico-cerebellar visual attention network, this research offers a deeper comprehension of the underlying mechanisms of developmental dyslexia and provides a base for further research and the potential development of new interventions.

References

Aguirre, G. K., Zarahn, E., &D'Esposito, M. (1998). The variability of human, BOLD hemodynamic responses. *Neuroimage*, *8*(4), 360-369

Allen, G., Buxton, R. B., Wong, E. C., & Courchesne, E. (1997). Attentional activation of the cerebellum independent of motor involvement. *Science*, *275*(5308), 1940-1943.

Amaro Jr, E., & Barker, G. J. (2006). Study design in fMRI: basic principles. *Brain and cognition*, *60*(3), 220-232.

Amunts, K., Mohlberg, H., Bludau, S., & Zilles, K. (2020). Julich-Brain: A 3D probabilistic atlas of the human brain's cytoarchitecture. *Science*, *369*(6506), 988-992.

Arina, S., Iervolino, I., & Stella, G. (2013). Prima raccolta di datinormativi per la valutazionedelladislessiaevolutivanegliadolescentisu un campione di scuolasecondaria di secondo grado. *Dislessia*, *10*(1), 9-38.

Ashburner, J., Barnes, G., Chen, C. C., Daunizeau, J., Flandin, G., Friston, K., ... & Penny, W. (2014). SPM12 manual. *Wellcome Trust Centre for Neuroimaging, London, UK*, *2464*(4).

Ashburn, S. M., Flowers, D. L., Napoliello, E. M., & Eden, G. F. (2020). Cerebellar function in children with and without dyslexia during single word processing. *Human brain mapping*, *41*(1), 120-138.

Bandettini, P. A. (2020). *Fmri*. MIT Press.

Bacon, A. M., & Handley, S. J. (2010). Dyslexia and reasoning: The importance of visual processes. *British Journal of Psychology*, *101*(3), 433-452.

Bertelli, B., &Bilancia, G. (2006). Batterie per la Valutazionedell'AttenzioneUditiva e della Memoria di LavoroFonologicanell'EtàEvolutiva-VAUMeLF. *Giunti Psychometric Edition, Florence*.

Bertoni, S., Franceschini, S., Ronconi, L., Gori, S., &Facoetti, A. (2019). Is excessive visual crowding causally linked to developmental dyslexia?.*Neuropsychologia*, *130*, 107-117.

Bießmann, F., Murayama, Y., Logothetis, N. K., Müller, K. R., & Meinecke, F. C. (2012). Improved decoding of neural activity from fMRI signals using non-separable spatiotemporal deconvolutions. *NeuroImage*, *61*(4), 1031-1042.

Briggs, G. G., &Nebes, R. D. (1975). Patterns of hand preference in a student population. *Cortex*, *11*(3), 230-238.

Brissenden, J. A., & Somers, D. C. (2019). Cortico–cerebellar networks for visual attention and working memory. Current opinion in psychology, 29, 239-247

Brown, M. A., &Semelka, R. C. (2011). *MRI: basic principles and applications*. John Wiley & Sons.

Brown, R. W., Cheng, Y. C. N., Haacke, E. M., Thompson, M. R., & Venkatesan, R. (2014). Magnetic resonance imaging: physical principles and sequence design. John Wiley & Sons.

Caballero-Gaudes, C., & Reynolds, R. C. (2017). Methods for cleaning the BOLD fMRI signal. *Neuroimage*, *154*, 128-149.

Cao, F., Bitan, T., & Booth, J. R. (2008). Effective brain connectivity in children with reading difficulties during phonological processing. *Brain and language*, *107*(2), 91-101.

Casey, B. J., Giedd, J. N., & Thomas, K. M. (2000). Structural and functional brain development and its relation to cognitive development. *Biological psychology*, *54*(1-3), 241-257.

Cattinelli, I., Borghese, N. A., Gallucci, M., &Paulesu, E. (2013). Reading the reading brain: a new meta-analysis of functional imaging data on reading. *Journal of neurolinguistics*, *26*(1), 214-238.

Caverly, R. H. (2015). MRI fundamentals: RF aspects of magnetic resonance imaging (MRI). *IEEE Microwave Magazine*, *16*(6), 20-33.

Cercignani, M., Dowell, N. G., &Tofts, P. S. (2018). *Quantitative MRI of the brain: principles of physical measurement*.

Chen, J. E., & Glover, G. H. (2015). Functional magnetic resonance imaging methods. *Neuropsychology review*, *25*, 289-313.

Christidis, P., Reynolds, R.(2004). Stimulus Timing Design. AFNI HowTo's. Retrieved from https://afni.nimh.nih.gov/pub/dist/HOWTO/howto/ht03_stim/html/stim_background.html

Corbetta, M., & Shulman, G. L. (2002). Control of goal-directed and stimulus-driven attention in the brain. *Nature reviews neuroscience*, *3*(3), 201-215.

Cornelissen, P. L., Hansen, P. C., Gilchrist, I. D., Cormack, F., Essex, J., & Frankish, C. (1998). Coherent motion detection and letter position encoding. *Vision research*, *38*(14), 2181-2191.

Cornoldi, C., &Colpo, G. (1995). Prove di lettura MT, nuove prove di lettura MT per la scuola media inferiore [Test for reading assessment in the lower secondary school]. *Firenze, Italy: Giunti OS*.

Cornoldi, C., &Colpo, G. (1998). *Prove di lettura MT per la scuolaelementare. 2: manuale*. OS.

Conners, C. K. (1990). *Manual for Conner's rating scales*. Multi-Health Systems, Incorporated.

Conners, C. K., Sitarenios, G., Parker, J. D., & Epstein, J. N. (1998). The revised Conners' Parent Rating Scale (CPRS-R): factor structure, reliability, and criterion validity. *Journal of abnormal child psychology*, *26*, 257-268.

Courchesne, E., Townsend, J., Akshoomoff, N. A., Saitoh, O., Yeung-Courchesne, R., Lincoln, A. J., ... & Lau, L. (1994). Impairment in shifting attention in autistic and cerebellar patients. Behavioral neuroscience, 108(5), 848.

D'Angelo, E. (2011). Neural circuits of the cerebellum: Hypothesis for function. *Journal of Integrative Neuroscience, 10*(3), 317–352.

Deco, G., Kringelbach, M. L., Arnatkeviciute, A., Oldham, S., Sabaroedin, K., Rogasch, N. C., ... &Fornito, A. (2021a). Dynamical consequences of regional heterogeneity in the brain's transcriptional landscape. *Science Advances*, *7*(29), eabf4752.

Deco, G., Vidaurre, D., & Kringelbach, M. L. (2021b). Revisiting the global workspace orchestrating the hierarchical organization of the human brain. *Nature human behaviour*, *5*(4), 497-511.

Deichmann, R. (2016). Principles of MRI and Functional MRI. *fMRI Techniques and Protocols*, 3-28.

Démonet, J. F., Taylor, M. J., &Chaix, Y. (2004). Developmental dyslexia. *The Lancet*, *363*(9419), 1451-1460.

Desikan, R. S., Ségonne, F., Fischl, B., Quinn, B. T., Dickerson, B. C., Blacker, D., ... &Killiany, R. J. (2006). An automated labeling system for subdividing the human cerebral cortex on MRI scans into gyral based regions of interest. *Neuroimage*, *31*(3), 968-980.

Dietrich, O., Raya, J. G., Reeder, S. B., Reiser, M. F., & Schoenberg, S. O. (2007). Measurement of signal-to-noise ratios in MR images: influence of multichannel coils, parallel imaging, and reconstruction filters. *Journal of Magnetic Resonance Imaging: An Official Journal of the International Society for Magnetic Resonance in Medicine*, *26*(2), 375-385.

Di Pietro, S. V., Willinger, D., Frei, N., Lutz, C., Coraj, S., Schneider, C., ... &Brem, S. (2023). Disentangling influences of dyslexia, development, and reading experience on effective brain connectivity in children. *NeuroImage*, *268*, 119869.

Dimoka, A. (2012). How to conduct a functional magnetic resonance (fMRI) study in social science research. *MIS quarterly*, 811-840.

Diedrichsen, J., Balsters, J. H., Flavell, J., Cussans, E., & Ramnani, N. (2009). A probabilistic MR atlas of the human cerebellum. *neuroimage*, *46*(1), 39-46.

Donaldson, D. I. (2004). Parsing brain activity with fMRI and mixed designs: what kind of a state is neuroimaging in?.*Trends in neurosciences*, *27*(8), 442-444.

Eden, G. F., VanMeter, J. W., Rumsey, J. M., Maisog, J. M., Woods, R. P., &Zeffiro, T. A. (1996). Abnormal processing of visual motion in dyslexia revealed by functional brain imaging. *Nature*, *382*(6586), 66-69.

Esteban, O., Markiewicz, C. J., Blair, R. W., Moodie, C. A., Isik, A. I., Erramuzpe, A., ... &Gorgolewski, K. J. (2019). fMRIPrep: a robust preprocessing pipeline for functional MRI. *Nature methods*, *16*(1), 111-116.

Everatt, J., Bradshaw, M. F., & Hibbard, P. B. (1999). Visual processing and dyslexia. *Perception*, *28*(2), 243-254.

Finn, E. S., Shen, X., Holahan, J. M., Scheinost, D., Lacadie, C., Papademetris, X., ... & Constable, R. T. (2014). Disruption of functional networks in dyslexia: a whole-brain, data-driven analysis of connectivity. *Biological psychiatry*, *76*(5), 397-404.

Fisher, S. E., &DeFries, J. C. (2002). Developmental dyslexia: genetic dissection of a complex cognitive trait. *Nature Reviews Neuroscience*, *3*(10), 767-780.

Franceschini, S., Gori, S., Ruffino, M., Pedrolli, K., &Facoetti, A. (2012). A causal link between visual spatial attention and reading acquisition. *Current biology*, *22*(9), 814-819.

Frazier, J. A., Chiu, S., Breeze, J. L., Makris, N., Lange, N., Kennedy, D. N., ... & Biederman, J. (2005). Structural brain magnetic resonance imaging of limbic and thalamic volumes in pediatric bipolar disorder. *American Journal of Psychiatry*, *162*(7), 1256-1265.

Frässle, S., Lomakina, E. I., Razi, A., Friston, K. J., Buhmann, J. M., & Stephan, K. E. (2017). Regression DCM for fMRI. *NeuroImage*, *155*, 406-421.

Freedman, L., Zivan, M., Farah, R., & Horowitz-Kraus, T. (2020). Greater functional connectivity within the cingulo-opercular and ventral attention networks is related to better fluent reading: A resting-state functional connectivity study. *NeuroImage: Clinical*, *26*, 102214.

Friston, K. J. (1994). *Functional and effective connectivity in neuroimaging: A synthesis. Human Brain Mapping, 2(1-2), 56–78.*

Gori, S., &Facoetti, A. (2015). How the visual aspects can be crucial in reading acquisition: The intriguing case of crowding and developmental dyslexia. *Journal of vision*, *15*(1), 8-8.

Gallagher, T. A., Nemeth, A. J., &Hacein-Bey, L. (2008). An introduction to the Fourier transforms: relationship to MRI. *American journal of roentgenology*, *190*(5), 1396-1405.

Ganzetti, M., Wenderoth, N., &Mantini, D. (2015). Mapping pathological changes in brain structure by combining T1-and T2-weighted MR imaging data. *Neuroradiology*, *57*, 917-928.

Gibby, W. A. (2005). Basic principles of magnetic resonance imaging. *Neurosurgery Clinics*, *16*(1), 1-64.

Glover, G. H. (2011). Overview of functional magnetic resonance imaging. *Neurosurgery Clinics*, *22*(2), 133-139.

Goense, J., Logothetis, N. K., Ullsperger, M., &Debener, S. (2010). Physiological basis of the BOLD signal. *Simultaneous EEG and fMRI: Recording, analysis, and application*, 21-46.

Goldstein, J. M., Seidman, L. J., Makris, N., Ahern, T., O'Brien, L. M., Caviness Jr, V. S., ... &Tsuang, M. T. (2007). Hypothalamic abnormalities in schizophrenia: sex effects and genetic vulnerability. *Biological psychiatry*, *61*(8), 935-945.

Heeger, D. J., &Ress, D. (2002). *What does fMRI tell us about neuronal activity? Nature Reviews Neuroscience, 3(2), 142–151.*

Heiervang, E., & Hugdahl, K. (2003). Impaired visual attention in children with dyslexia. *Journal of learning disabilities*, *36*(1), 68-73.

Henson, R. N. A., & Penny, W. D. (2003). ANOVAs and SPM. *Wellcome Department of Imaging Neuroscience, London, UK*.

Honey, Christopher J., Rolf Kötter, Michael Breakspear, and Olaf Sporns. "Network structure of cerebral cortex shapes functional connectivity on multiple time scales." *Proceedings of the National Academy of Sciences* 104, no. 24 (2007): 10240-10245.

Japee, S., Holiday, K., Satyshur, M. D., Mukai, I., & Ungerleider, L. G. (2015). A role of right middle frontal gyrus in reorienting of attention: a case study. *Frontiers in systems neuroscience*, *9*, 23.

Jenkinson, M., & Smith, S. (2001). A global optimisation method for robust affine registration of brain images. *Medical image analysis*, *5*(2), 143-156.

Jenkinson, M., Bannister, P., Brady, M., & Smith, S. (2002). Improved optimization for the robust and accurate linear registration and motion correction of brain images. *Neuroimage*, *17*(2), 825-841.

Jenkinson, M., Beckmann, C. F., Behrens, T. E., Woolrich, M. W., & Smith, S. M. (2012). Fsl. *Neuroimage*, *62*(2), 782-790.

Kahan, J., &Foltynie, T. (2013). Understanding DCM: ten simple rules for the clinician. *Neuroimage*, *83*, 542-549.

Khanna, N., Altmeyer, W., Zhuo, J., & Steven, A. (2015). Functional neuroimaging: fundamental principles and clinical applications. *The neuroradiology journal*, *28*(2), 87-96.

Kuerten, A. B., Mota, M. B., &Segaert, K. (2020). Developmental dyslexia: a condensed review of literature. *Ilha do Desterro*, *72*, 249-270.

Lindgren, S. D., De Renzi, E., & Richman, L. C. (1985). Cross-national comparisons of developmental dyslexia in Italy and the United States. *Child development*, 1404-1417.

Lerch, J. P., Van Der Kouwe, A. J., Raznahan, A., Paus, T., Johansen-Berg, H., Miller, K. L., ... & Sotiropoulos, S. N. (2017). Studying neuroanatomy using MRI. *Nature neuroscience*, *20*(3), 314-326.

Lindgren, S. D., De Renzi, E., & Richman, L. C. (1985). Cross-national comparisons of developmental dyslexia in Italy and the United States. *Child development*, 1404-1417.

Lohmann, G., Erfurth, K., Müller, K., & Turner, R. (2012). Critical comments on dynamic causal modelling. *Neuroimage*, *59*(3), 2322-2329.

Mascheretti, S., Peruzzo, D., Andreola, C., Villa, M., Ciceri, T., Trezzi, V., ... & Arrigoni, F. (2021). Selecting the most relevant brain regions to classify children with developmental dyslexia and typical readers by using complex magnocellular stimuli and multiple kernel learning. *Brain Sciences*, *11*(6), 722.

Mascheretti, S., De Luca, A., Trezzi, V. *et al.* Neurogenetics of developmental dyslexia: from genes to behavior through brain neuroimaging and cognitive and sensorial mechanisms. *Transl Psychiatry* 7, e987 (2017).

Makris, N., Goldstein, J. M., Kennedy, D., Hodge, S. M., Caviness, V. S., Faraone, S. V., ... & Seidman, L. J. (2006). Decreased volume of left and total anterior insular lobule in schizophrenia. *Schizophrenia research*, *83*(2-3), 155-171.

Mariën, P., &Borgatti, R. (2018). Language and the cerebellum. *Handbook of clinical neurology*, *154*, 181-202.

Marreiros, A. C., Stephan, K. E., & Friston, K. J. (2010). *Dynamic causal modeling. Scholarpedia, 5(7), 9568.*

Mazziotta, J. C., Toga, A. W., Evans, A., Fox, P., & Lancaster, J. (1995). A probabilistic atlas of the human brain: theory and rationale for its development. *Neuroimage*, *2*(2), 89-101.

McCarthy, P. (2024). FSLeyes (1.11.0). Zenodo. https://doi.org/10.5281/zenodo.11047709

McRobbie, D. W. (2005). *MRI from picture to proton*. Cambridge University Press.

Morken, F., Helland, T., Hugdahl, K., & Specht, K. (2017). Reading in dyslexia across literacy development: A longitudinal study of effective connectivity. *Neuroimage*, *144*, 92-100.

Monti, M. M. (2011). Statistical analysis of fMRI time-series: a critical review of the GLM approach. *Frontiers in human neuroscience*, *5*, 28.

Moratal, D., Vallés-Luch, A., Martí-Bonmatí, L., & Brummer, M. E. (2008). k-Space tutorial: an MRI educational tool for a better understanding of k-space. *Biomedical imaging and intervention journal*, *4*(1).

Nicolson, R. I., Fawcett, A. J., & Dean, P. (2001). Developmental dyslexia: the cerebellar deficit hypothesis. *Trends in neurosciences*, *24*(9), 508-511.

Nicolson, R. I., & Fawcett, A. J. (1990). Automaticity: A new framework for dyslexia research?.*Cognition*, *35*(2), 159-182.

Nobile, M., Alberti, B., &Zuddas, A. (2007). *CRS-R. Conners' Rating Scales. Revised. Manuale*. GiuntiEditore.

Norton, E. S., & Wolf, M. (2012). Rapid automatized naming (RAN) and reading fluency: Implications for understanding and treatment of reading disabilities. *Annual review of psychology*, *63*, 427-452.

Parker, D. B., &Razlighi, Q. R. (2019). The Benefit of Slice Timing Correction in Common fMRI Preprocessing Pipelines. *Frontiers in Neuroscience*, *13*.

Peelle, J. (2019). Using SPM's CheckReg tool to compare images. Retrieved fromhttp://jpeelle.net/mri/misc/checkreg.html#ref-checkreg

Pellicano, E., & Gibson, L. Y. (2008). Investigating the functional integrity of the dorsal visual pathway in autism and dyslexia. *Neuropsychologia*, *46*(10), 2593-2596.

Pennington, B. F. (2006). From single to multiple deficit models of developmental disorders. *Cognition*, *101*(2), 385-413.

Penny, W. D., Stephan, K. E., Daunizeau, J., Rosa, M. J., Friston, K. J., Schofield, T. M., &Leff, A. P. (2010). Comparing families of dynamic causal models.*PLoS computational biology,* 6(3), e1000709.

Penny, W. D., Friston, K. J., Ashburner, J. T., Kiebel, S. J., & Nichols, T. E. (Eds.). (2011). *Statistical parametric mapping: the analysis of functional brain images*. Elsevier.

Peterson, R. L., & Pennington, B. F. (2012). Developmental dyslexia. *The lancet*, *379*(9830), 1997-2007.

Peterson, R. L., & Pennington, B. F. (2015). Developmental dyslexia. *Annual review of clinical psychology*, *11*, 283-307.

Petersen, S. E., & Posner, M. I. (2012). The attention system of the human brain: 20 years after. *Annual review of neuroscience*, *35*, 73-89.

Poldrack, R. A., Mumford, J. A., & Nichols, T. E. (2011). *Handbook of functional MRI data analysis*. Cambridge University Press.

Popescu, V., Battaglini, M., Hoogstrate, W. S., Verfaillie, S. C., Sluimer, I. C., van Schijndel, R. A., ... & MAGNIMS Study Group. (2012). Optimizing parameter choice for FSL-Brain Extraction Tool (BET) on 3D T1 images in multiple sclerosis. *Neuroimage*, *61*(4), 1484-1494.

Price, C. J., & Friston, K. J. (1997). Cognitive conjunction: a new approach to brain activation experiments. *Neuroimage*, *5*(4), 261-270.

Rajapakse, J. C., & Zhou, J. (2007). Learning effective brain connectivity with dynamic Bayesian networks. *Neuroimage*, *37*(3), 749-760.

Rajan, S. S. (1998). MRI: a conceptual overview.

Reynolds, C. R., & Bigler, E. D. (1994). *Test of memory and learning: Examiner's manual*. Pro-ed.

Riva, V., Mozzi, A., Forni, D., Trezzi, V., Giorda, R., Riva, S., ... & Mascheretti, S. (2019). The influence of DCDC2 risk genetic variants on reading: Testing main and haplotypic effects. *Neuropsychologia*, *130*, 52-58.

Robert-Jan M. van Geuns; Piotr A. Wielopolski; Hein G. de Bruin; Benno J. Rensing; Peter M.A. van Ooijen; Marc Hulshoff; Matthijs Oudkerk; Pim J. de Feyter (1999). *Basic principles of magnetic resonance imaging. , 42(2), 149–156.*

Roostaei, T., Nazeri, A., Sahraian, M. A., &Minagar, A. (2014). The human cerebellum. *Neurologic clinics*, *32*(4), 859-869.

Rubinov, M., &Sporns, O. (2010). Complex network measures of brain connectivity: uses and interpretations. *Neuroimage*, *52*(3), 1059-1069.

Rykhlevskaia, E., Gratton, G., &Fabiani, M. (2008). Combining structural and functional neuroimaging data for studying brain connectivity: a review. *Psychophysiology*, *45*(2), 173-187.

Schmahmann, J. D., & Caplan, D. (2006). Cognition, emotion and the cerebellum. *Brain*, *129*(2), 290-292.

Smirni, P., Vetri, L., Misuraca, E., Cappadonna, M., Operto, F. F., Pastorino, G. M. G., & Marotta, R. (2020). Misunderstandings about developmental dyslexia: A historical overview. *Pediatric Reports*, *12*(2), 8505.

Sands, M. J., & Levitin, A. (2004, June). Basics of magnetic resonance imaging. In *Seminars in vascular surgery* (Vol. 17, No. 2, pp. 66-82). WB Saunders.

Sandrone, S., Bacigaluppi, M., Galloni, M. R., Cappa, S. F., Moro, A., Catani, M., ... & Martino, G. (2014). Weighing brain activity with the balance: Angelo Mosso's original manuscripts come to light. *Brain*, *137*(2), 621-633.

Sartori, G., Job, R., &Tressoldi, P. E. (1995). *Batteria per la valutazionedelladislessia e delladisortografiaevolotiva: manuale*. OrganizzazioniSpeciali.

Scerri, T. S., & Schulte-Körne, G. (2010). Genetics of developmental dyslexia. *European child & adolescent psychiatry*, *19*, 179-197.

Schurz, M., Wimmer, H., Richlan, F., Ludersdorfer, P., Klackl, J., &Kronbichler, M. (2015). Resting-state and task-based functional brain connectivity in developmental dyslexia. *Cerebral Cortex*, *25*(10), 3502-3514.

Seghier, M. L., & Friston, K. J. (2013). Network discovery with large DCMs. *Neuroimage*, *68*, 181-191.

Sharma, H. A. (2009). MRI physics–basic principles. *Acta Neuropsychiatrica*, *21*(4), 200-201.

Shaywitz, S. E., &Shaywitz, B. A. (2008). Paying attention to reading: The neurobiology of reading and dyslexia. *Development and psychopathology*, *20*(4), 1329-1349.

Shaywitz, S. E., &Shaywitz, B. A. (2005). Dyslexia (specific reading disability). *Biological psychiatry*, *57*(11), 1301-1309.

Smith, S. M. (2002). Fast robust automated brain extraction. *Human brain mapping*, *17*(3), 143-155.

Smith, S. M. (2004). Overview of fMRI analysis. *The British Journal of Radiology*, *77*(suppl_2), S167-S175.

Smith, S. M., Jenkinson, M., Woolrich, M. W., Beckmann, C. F., Behrens, T. E., Johansen-Berg, H., ... & Matthews, P. M. (2004). Advances in functional and structural MR image analysis and implementation as FSL. *Neuroimage*, *23*, S208-S219.

Smitha, K. A., Akhil Raja, K., Arun, K. M., Rajesh, P. G., Thomas, B., Kapilamoorthy, T. R., &Kesavadas, C. (2017). Resting state fMRI: A review on methods in resting state

connectivity analysis and resting state networks. *The neuroradiology journal*, *30*(4), 305-317.

Sporns, O. (2007). Brain connectivity. *Scholarpedia*, *2*(10), 4695.

Sporns, O., Tononi, G., &Kötter, R. (2005). The human connectome: a structural description of the human brain. *PLoS computational biology*, *1*(4), e42.

Stein, J. (2023). Theories about developmental dyslexia. *Brain sciences*, *13*(2), 208.

Stein, J. (2022). The visual basis of reading and reading difficulties. *Frontiers in Neuroscience*, *16*, 1004027.

Stein, J. (2018a). What is developmental dyslexia?.*Brain sciences*, *8*(2), 26.

Stein, J. (2018b). The magnocellular theory of developmental dyslexia. *Reading and dyslexia: From basic functions to higher order cognition*, 103-134.

Stein, J. (2003). Visual motion sensitivity and reading. *Neuropsychologia*, *41*(13), 1785-1793.

Stephan, K. E., Penny, W. D., Moran, R. J., den Ouden, H. E., Daunizeau, J., & Friston, K. J. (2010). Ten simple rules for dynamic causal modeling. *Neuroimage*, *49*(4), 3099-3109.

Stephan, K. E., Penny, W. D., Daunizeau, J., Moran, R. J., & Friston, K. J. (2009). Bayesian model selection for group studies. *Neuroimage*, *46*(4), 1004-1017.

Stephan, K. E., Harrison, L. M., Kiebel, S. J., David, O., Penny, W. D., & Friston, K. J. (2007). Dynamic causal models of neural system dynamics: current state and future extensions. *Journal of biosciences*, *32*, 129-144.

Stephan, K. E., Weiskopf, N., Drysdale, P. M., Robinson, P. A., & Friston, K. J. (2007). Comparing hemodynamic models with DCM. *Neuroimage*, *38*(3), 387-401.

Talcott, J. B., Hansen, P. C., Assoku, E. L., & Stein, J. F. (2000). Visual motion sensitivity in dyslexia: evidence for temporal and energy integration deficits. *Neuropsychologia*, *38*(7), 935-943.

The MathWorks Inc. (2022). MATLAB version: 9.13.0 (R2022b), Natick, Massachusetts: The MathWorks Inc. https://www.mathworks.com

Tononi, G., Sporns, O., & Edelman, G. M. (1994). A measure for brain complexity: relating functional segregation and integration in the nervous system. *Proceedings of the National Academy of Sciences*, *91*(11), 5033-5037.

Turker, S., Kuhnke, P., Jiang, Z., &Hartwigsen, G. (2023). Disrupted network interactions serve as a neural marker of dyslexia. *Communications Biology*, *6*(1), 1114.

Tsougos, I. (2017). *Advanced MR neuroimaging: from theory to clinical practice*. CRC Press.

Van Geuns, R. J. M., Wielopolski, P. A., de Bruin, H. G., Rensing, B. J., Van Ooijen, P. M., Hulshoff, M., ... & de Feyter, P. J. (1999). Basic principles of magnetic resonance imaging. *Progress in cardiovascular diseases*, *42*(2), 149-156.

Valdois, S., Roulin, J. L., &Bosse, M. L. (2019). Visual attention modulates reading acquisition. *Vision research*, *165*, 152-161.

Vellutino, F. R., Fletcher, J. M., Snowling, M. J., & Scanlon, D. M. (2004). Specific reading disability (dyslexia): What have we learned in the past four decades?.*Journal of child psychology and psychiatry*, *45*(1), 2-40.

Vidyasagar, T. R., &Pammer, K. (2010). Dyslexia: a deficit in visuo-spatial attention, not in phonological processing. *Trends in cognitive sciences*, *14*(2), 57-63.

Vossel, S., Geng, J. J., & Fink, G. R. (2014). Dorsal and ventral attention systems: distinct neural circuits but collaborative roles. *The Neuroscientist*, *20*(2), 150-159.

Warnke, A., Schulte-Körne, G., & Ise, E. (2012). Developmental dyslexia. *IACAPAP book series. The working with children and adolescents series*, *19*, 173-198.

Weishaupt, D., Köchli, V. D., Marincek, B., Froehlich, J. M., Nanz, D., &Pruessmann, K. P. (2006). *How does MRI work?: an introduction to the physics and function of magnetic resonance imaging* (Vol. 2). Berlin: Springer.

Wechsler, D. Wechsler Intelligence Scale for Children, 3rd ed.; OrganizzazioniSpeciali: Firenze, Italy, 2006.

Woolrich, M. W., Jbabdi, S., Patenaude, B., Chappell, M., Makni, S., Behrens, T., ... & Smith, S. M. (2009). Bayesian analysis of neuroimaging data in FSL. *Neuroimage*, *45*(1), S173-S186.

Yoshioka, T. (2012). Physical aspects of medical science. *The Kaohsiung journal of medical sciences*, *28*(2), S26-S32.

Zamanian, A., & Hardiman, C. J. H. F. E. (2005). Electromagnetic radiation and human health: A review of sources and effects. *High Frequency Electronics*, *4*(3), 16-26.

Zeidman, P., Jafarian, A., Corbin, N., Seghier, M. L., Razi, A., Price, C. J., & Friston, K. J. (2019a). A guide to group effective connectivity analysis, part 1: First level analysis with DCM for fMRI. *Neuroimage*, *200*, 174-190.

Zeidman, P., Jafarian, A., Seghier, M. L., Litvak, V., Cagnan, H., Price, C. J., & Friston, K. J. (2019b). A guide to group effective connectivity analysis, part 2: Second level analysis with PEB. *Neuroimage*, *200*, 12-25.

Ziegler, J. C., Castel, C., Pech-Georgel, C., George, F., Alario, F. X., & Perry, C. (2008). Developmental dyslexia and the dual route model of reading: Simulating individual differences and subtypes. *Cognition*, *107*(1), 151-178.

Zafar, R., Malik, A. S., Kamel, N., & Dass, S. C. (2015, October). Importance of realignment parameters in fMRI data analysis. In *2015 IEEE International Conference on Signal and Image Processing Applications (ICSIPA)* (pp. 546-550). IEEE.

Zhang, Y.; Brady, M.; Smith, S. (2001). *Segmentation of brain MR images through a hidden Markov random field model and the expectation-maximization algorithm. , 20(1), 45–57.*

Appendix

	Typical Readers					Developmental Dyslexia				
	Min	Max	Mean	Skewness	Kurtosis	Min	Max	Mean	Skewness	Kurtosis
IQ total	80	159	128.25	-0.95	1.37	80	131	104.05	0.11	-0.99
TR, accuracy	-0.13	1.42	0.62	0.06	0.85	-12.01	5.19	-3.98	-0.4	0.73
TR, speed	-1.00	1.18.	0.18	0.05	-0-63	-4.21	-0.09	-2.62	0.60	0.14
SWR, accuracy	-0.67	1.00	0.32	-0.13	-1.16	-10.00	0.33	-3.19	-0.98	0.68
SWR, speed	-1.11	0.83	0.01	-0.28	-0.88	-10.12	-0.14	-3.79	-1.48	2.49
SPWR, accuracy	-0.67	1.33	0.44	-0.24	0.12	-8.50	0.33	-2.54	-1.48	3.63
SPWR, speed	-1.03	1.15	0.20	-0.25	-0.89	-9.42	-0.67	-3.40	-1.38	1.08
SLFS	-1.35	1.35	0.16	-0.76	0.14	-2.30	0.65	-1-77	0.57	0.72
SLBS	-1.35	1.60	-0.06	0.67	-0.68	-2.2	1.35	-0.72	1.00	2.26
SDFS	-2.00	1.00	0.57	0.07	-0.27	-2.20	0.00	-1.38	0.49	0.22
SDBS	-1.40	2.00	0.57	0.98	-0.06	-1.35	0.65	-0.57	0.62	0.97
SNWR	-2.79	3.00	1.18	-1.40	1.85	-7.00	3.53	-1.63	-0.13	-0.53

Neuropsychological assessment scores for both typical readers and developmental dyslexia groups. TR: Text reading; SWR: single words reading; SPWR: single pseudo-words reading; SLFS: single letters forward span; SLBS: single letters backward span; SDFS: single digits forward span; SDBS: single digits backward span; SNWR: single non-word repetition.

Acknowledgements